(13)

Second-Order Steady Forces on Floating Bodies with Forward Speed

by

Marcos Donato Auler da Silva Ferreira

BS, Naval Architecture, Federal University of Rio de Janeiro, 1983
MS, Ocean Engineering, Federal University of Rio de Janeiro, 1989

Submitted to the Department of Ocean Engineering
in partial fulfillment of the requirements for the degree of

Doctor of Philosophy in Hydrodynamics

at the

MASSACHUSETTS INSTITUTE OF TECHNOLOGY

June 1997

Author .....
Department of Ocean Engineering
May 12th, 1997

Certified by .....
J. Nicholas Newman
Professor of Naval Architecture
Thesis Supervisor

Accepted by .....
J. Kim Vandiver
Chairman, Departmental Committee on Graduate Studies

Second-Order Steady Forces on Floating Bodies with Forward Speed

by

Marcos Donato Auler da Silva Ferreira

Submitted to the Department of Ocean Engineering
on May 12^{th}, 1997, in partial fulfillment of the
requirements for the degree of
Doctor of Philosophy in Hydrodynamics

Abstract

In this thesis a numerical solution is developed for the computation of the second-order steady-forces acting on a ship with forward speed in the presence of incident waves under the Neumann-Kelvin flow assumption.

The computation of these forces is achieved by integration of pressures over the ship hull and also through the use of momentum-flux relations, in the frequency domain.

The solution of the first-order problem is obtained through the use of an existing time-domain computer program, where the computation of the velocities and the velocity potential in points in the fluid region using the source formulation was implemented as part of this work. Global and local quantities are Fourier-transformed to the frequency-domain, and the second-order steady-forces coming from first-order quantities computed.

The boundary-value problem for the second-order Neumann-Kelvin steady potential is formulated and a solution attempted for the diffraction case under the low-speed assumption. The contribution coming from this second-order steady potential is found not to be significant for the computation of the total second-order steady force, in the cases analyzed. In connection with the momentum-flux approach, it can be seen that there will be no contribution coming from the second-order steady potential to the second-order steady horizontal forces.

Results are presented for the Wigley hull, a hemisphere and a shallow circular cylinder. Comparisons are made with other theories and data from other publications.

Thesis Supervisor: J. Nicholas Newman
Title: Professor of Naval Architecture

Acknowledgments

I wish to thank my wife, Christiane and my sons, Guilherme and Eduardo, for being willing to modify their lives to accommodate my dreams. I hope, as a result, they have had as many good experiences as I did.

Professor Newman was always available to share all his experience and knowledge in so many aspects of the hydrodynamic theory. His patience in the reading and correcting of my notes was always remarkable.

My thanks also to Dr. Korsmeyer, always available to help me with the time domain codes, as well as to Dr. Bingham, for the many explanations and illuminating emails. Dr. Chang-Ho Lee was also very friendly, and his great expertise with the frequency domain formulation was of great help.

My thesis committee, besides Professor Newman and Dr. Korsmeyer, always gave strong feedback in a multitude of ways. Professor Ogilvie raising the more fundamental hydrodynamic issues, Professor Nielsen lending his experience and many observations, and Professor Faltinsen with his sharp questioning.

My thanks to the folks of the Computational Hydrodynamics Facility, for the friendly environment and nice discussions.

Having my company, PETROBRÁS S.A., supporting me during the time I was at M.I.T. was a great benefit to my career and I am very grateful. Special thanks to Dr. Álvaro M. da Costa, Luiz A. P. Levy, José A. de Figueiredo, Dr. Antônio C. Fernandez, Enrique and Raquel C. Gonzalez, my parents and parents-in-law for the constant encouragement and help with many issues.

Contents

List of Figures

Chapter 1

Introduction

1.1 Background

The use of vessels for the transportation of goods, or the exploration of the sea floor in the search for minerals or other scientific purposes, requires a good understanding of the forces acting on them and the consequent behavior of these floating bodies, while operating in the sea with or without the presence of incident waves.

In quantifying the resistance force ships have to overcome when trying to speed through the oceans, the use of the Froude hypothesis, separating the total resistance in two components, the flat-plate drag and the residual drag, gave great insight to this problem, and was latter justified by Prandtl's boundary layer theory.

The flat-plate drag represents friction effects between the hull and the sea water and is supposed to be a function only of the Reynolds number R. The residual drag encompasses the viscous form drag, which is related to the change in the flow and pressure field due to the action of viscosity, and the steady wave force associated with the energy transferred from the ship to the fluid, in order to sustain the steady wave pattern created by this uniform velocity forward motion. The residual drag under this hypothesis is supposed to be a function of F (Froude number) alone. This is not true for the viscous form drag but for actual prototype and model scales and shapes used today this approximation gives a satisfactory correlation.

The effect of uniform currents always can be modeled as a change of the vessel

constant velocity. Other forces are generated by the action of the wind, which was earlier used to power the ships but now (unless in some leisure sailboats) has to be overcome by thrusters power or mooring forces (depending on the particular concept).

The action of incident waves have the most obvious effect of generating oscillatory forces and motions, but also acts in more subtle ways, giving rise to forces proportional to higher and lower harmonics and steady drift forces, that may cause trouble in the station keeping of research vessels as well as affecting the steady resistance drag acting over vessels with forward constant velocity.

Flat-plate friction forces are not hard to compute, and empirical methods based on the ship wetted area and Reynolds number are known to give very good results. Viscous pressure forces drives a lot of effort in search of solutions (mainly computer intensive numerical approaches) for the Navier-Stokes equations, and reasonable engineering solutions are still in demand. The same approaches can be used for frictional and viscous-pressure wind forces.

The steady wave problem has been studied in connection with the ideal-fluid assumption, leading to the solution of the linear Laplace equation in the fluid domain with mathematically nonlinear boundary conditions on the water and body surfaces. Engineering solutions valid for all body shapes and forward velocities are still elusive, and indeed contradicts the main assumption of ideal flow, as we will have strong viscous effects with boundary-layer separation. Over this steady incident flow (or some approximation of it) we may linearize the boundary conditions and get approximate solutions for the unsteady wave velocity and pressure fields and consequent forces, including the steady ones. This is our goal on this thesis, where many assumptions will be made in pursuing a workable solution.

The study of steady wave forces over stationary structures is not recent, going back to the work of Maruo [23] in 1960 computing the horizontal forces over a stationary floating body using momentum-flux relations. In 1967 Newman [27] extended this momentum approach to include the yaw moment.

Over the last decade, the use of the panel method (also known as boundary element method or integral equation method) for solving three-dimensional zero-velocity wave-

body problems has drawn the attention of many researchers, and we may cite the work of Korsmeyer et all [18] as a good representative of the work that has been made. The related computer programs that were developed typically solved the first order linear hydrodynamics problem and made it possible to get wave velocities and pressures on points over the body surface and in the fluid domain due to the unsteady wave potentials, more specifically diffracted and radiated waves generated by the presence of a fixed- or free-floating body with arbitrary geometry.

Introducing wave nonlinearity in the Stokes perturbation scheme that the wave amplitude is of order ε but the wavelength and the body characteristic dimension is of order one, we can compute second order steady forces integrating the second order steady pressures over the bodies and adding the corrections to the first order steady pressures due to first order motions of the boundaries and bodies around their mean positions. This turned out to be a very attractive approach (see Lee and Newman [20] and Pinkster [38]) as it enables the computation of all steady forces and moments acting over the bodies. The use of more panels than the momentum approach in order to achieve convergence of the results is in general a rule.

The momentum approach may also be extended to the case when the control surface is a compact one around the floating body, and in this context the six second order steady forces components may be computed evaluating the momentum flux over this surface (Zhao and Faltinsen [43] and Ferreira and Lee [7]). This method at first seems to retain the best of the two previous ones, because we achieve the convergence of results as fast as using the momentum approach and may compute the six loads as with the pressure integration method. Its main drawback is when you need to compute potentials and velocities at too many points on the compact control surface to achieve convergence, because it can get computationally expensive.

The ship with finite forward velocity problem, associated with incident, scattered and radiated waves is in general approached with assumptions about the slenderness of the floating body. The steady wave flow may be approximated by the Neumann-Kelvin flow (see Bingham [2]), in conjunction with the use of a Green function satisfying the free-surface boundary condition. Another option is the so called double-body

flow approach (as in Nakos [26]), in combination with the Rankine Green function.

Special concepts of vessels for the exploration and production of hydrocarbons at large depths, like semisubmersibles, T.L.P. or spar-buoy platforms, having motion resonances out of the frequency range of the oscillatory wave forces are commonplace in today's oil industry. These platforms may have resonances close to the sum or difference frequency of sinusoidal incoming waves, creating the necessity of a better understanding of this nonlinear waves interaction mechanism. As the difference frequency excitation may induce large excursions, it is reasonable to assume the motion as equivalent to a small forward velocity, and the corresponding damping force, which will be proportional to the square of this forward velocity, will be negligible. On the other hand, following Grue & Palm (1993), we can say that for realistic ocean structures a forward velocity of 1 m/s may change the magnitude of the drift force on the order of 50% compared to the zero forward velocity case, and therefore it is necessary to quantify the influence of this small drift velocity on the steady forces.

This interaction between very small forward speed (or steady current in the opposite direction) and waves has been studied by Grue & Palm [8] [9] [11] (1985, 1986, 1993), Nossen et all [34] (1991), Zhao & Faltinsen [41] [42] [43] (1988, 1988, 1989), and Wu & Eatock Taylor [40] (1990). Also this problem has been studied by Agnon & Mei [1] (1985) and Newman [33](1993), by using two different time scales associated with first and second order motions.

One also may note that those are not exhaustive situations. Blunt (offshore structures type) bodies in the presence of not so small currents adding up to its own horizontal velocities will require special treatment or a compromised solution, when one will have to check (in a model experiment for example) when the slender assumption or the small velocity approach is more appropriate or even if none of the above will hold and a more comprehensive view of the problem will be required.

1.2 Overview

Our goal is the computation of the second-order steady forces acting on a ship with forward speed under the Neumann-Kelvin hypothesis. We will also discuss the equations for an arbitrary choice of incident basis flow, and some specific choices such as the double-body approach. This is not only for a comparison with the Neumann-Kelvin approach but also for a discussion of the difficulties involved in implementing these different approaches in connection to the strategy we will use to solve the hydrodynamic problem.

In Chapter 2, the hydrodynamic problem is presented. We start by introducing the problem of a ship advancing with forward speed and the coordinate systems we are going to use in the formulation of the mathematical problem. This problem, as most things in nature, is nonlinear. Many assumptions will be needed in order to achieve a solution for the problem, from the nature of the fluid (inviscid, incompressible, without important surface-tension effects) to the amplitude of the subsequent wave height and unsteady ship motions.

A solution based on a velocity potential will be developed, and this potential expanded as a series with terms in powers of a small parameter ε. Different linearizations of the first-order linear problem are discussed, with the difference consisting of the choice of how the steady flow around the ship due to its forward speed is treated.

Chapter 3 contains the discussion of the solutions to the hydrodynamic problems. The first-order linear solution is obtained using the approach previously proposed by Bingham [2] and Korsmeyer [17]. The transient integral equation approach used is described as well as the potential decomposition, when the hydrodynamic problem is subdivided in the incident plane-waves problem, the scattered-waves problem and the problem of the radiated waves. The sum and composition of all solutions obtained will define the total potential of velocities.

The definition of the equation of motions will be the next step, which will be required for the computation of the amplitudes of the linear ship motions in its six degrees of freedom. All those computations are carried out in the time domain, as

a way to avoid the difficulties inherent to the numerical computation of the Green function representing a periodically pulsating and steadily-translating source. The second-order steady force will be computed in the frequency domain, enabling us to know the contribution that will come from each wave component with distinct periods of oscillation. With this information, the designers of floating structures may look for hull shapes that will perform best in a certain range of wave periods, which in turn will be chosen as the ones which carry most of the energy of the sea where the floating structure is going to operate.

We Fourier transform integrated quantities such as added mass or exciting forces to the frequency domain, as well as local quantities like velocity potentials or fluid velocities, which will be needed for the computation of the second-order steady forces.

Then we will establish the Neumann-Kelvin second-order steady potential problem, using the integral-equation formulation as defined in Appendix A. Each wave frequency will generate different body and free-surface boundary conditions. The solution of this steady problem will come in the time domain, as the large time asymptotic of the transient problem with constant in time boundary conditions.

Chapter 4 contains the formulation of the frequency domain second-order steady force using two different approaches, namely by the integration of the pressures over the floating structure hull and through the computation of the momentum flux over a compact surface surrounding the hull and a region of the water surface.

In Chapter 5 we will show the results obtained by our approach and how it compares with results obtained using other linearizations and different ways of solving the hydrodynamic problem. In doing that we will begin the comparisons with the Wigley hull, which is a slender, mathematically defined, surface-piercing hull geometry. We compare results for zero speed with the well tested WAMIT code, to show that the Fourier-transform approach used is able to give good results for second-order quantities computed in the frequency domain. For higher Froude numbers we compare the results with another extensively tested program, the SWAN code, described by [26]. Comparisons using non-slender bodies such as a circular sphere and cylinder were carried against results obtained by Zhao and Faltinsen [43] using the low-speed

double-body approach.

Chapter 6 contains a discussion about the work developed and the results obtained, as well as some concluding remarks and a suggestion of possible improvements.

Chapter 2

The Hydrodynamic Problem

2.1 Introduction

Throughout this work we will disregard the compressibility and surface tension of the fluid as well as viscous effects. The former assumptions are easy to justify in as much as our analysis is restricted to Mach numbers much smaller than one and wavelengths much bigger than a few inches (see Lighthill [21]), but the latter assumption depends on other flow characteristics. In general if we are looking at a slender and smooth ship hull at moderate speeds, this hypotheses will be true and viscous effects may be disregarded.

General blunt bodies moving with finite forward speed in the presence of arbitrarily chosen waves will certainly cause the viscous effects not to be confined to a small boundary layer close to the hull, but the detachment of this boundary layer from the hull surface with global consequences for the flow itself and the distribution of pressures. Zhao and Faltinsen [42] have made some experimental work for the half-sphere case and showed that for Keulegan-Carpenter numbers less than 3 or 2 and no currents the boundary layer does not separate. As they increased the current the flow separation will occur for smaller Keulegan-Carpenter numbers until $U/U_m = 1$, U_m being the maximum wave orbital velocity, when separation will always take place. So the hull geometry, the Keulegan-Carpenter number and the ratio between U and U_m will be important parameters for this assumption. They also tried to quantify the

influence of the non-dimensional frequency $\omega_e\sqrt{D/g}$, D being the body characteristic length (diameter for the sphere case) and g the acceleration due to the gravity, on the flow separation phenomena. They could not quantify it, seeming from their experiment that it does not played an important role. A simple statement that can be made is that the blunter the body, the smaller the Froude number should be in order that viscosity may be ignored.

We are going to approach the hydrodynamic problem by first stating the nonlinear boundary-value problem and then making some assumptions in order to linearize this problem. We follow the development presented on Newman [30], but we will present the final equations for different basis-flow cases and show the expansion of the potentials in terms of a small parameter.

2.2 The Coordinate Systems and Fluid Domain Region

We will use three Cartesian coordinate systems: $\vec{x}_0 = (x_0, y_0, z_0)$ is fixed in space and defined as having $z_0 = 0$ on the mean free surface with the x_0 and y_0 axis lying in this plane; $\vec{x}_s = (x_s, y_s, z_s)$ is fixed on the ship at all times; and $\vec{x} = (x, y, z)$ moves with the same mean forward velocity U as the ship. The $\vec{x}$ coordinate system is equal to $\vec{x}_0$ at the beginning of the motion and has the x component in the same direction as the ship mean forward velocity.

The fluid domain region is confined by the free surface S_f, which is defined by $\eta_0(\vec{x}_0, t) - z_0 = 0$, $\eta_0(\vec{x}_0, t)$ being the wave elevation; the instantaneous ship position S_b; and S_∞ defined by $R = \sqrt{x_0^2 + y_0^2 + z_0^2} \to \infty$ and which bounds the lower half space up to S_f.

The three coordinate systems and the problem boundaries are shown in Figure 2-1 with the presence of a ship hull on its actual position (S_b) and on its mean position (S_{bm}). We also should note that when the independent variables ($\vec{x}_0$, $\vec{x}_s$, $\vec{x}$ and t representing time) appear as subscripts, partial differentiation is implied. The free-

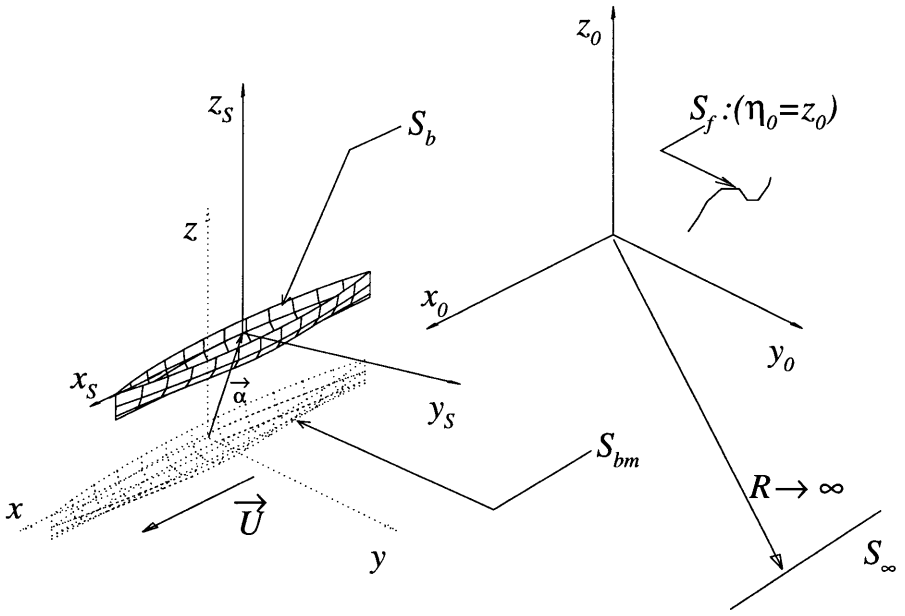

Figure 2-1: The three coordinate systems, the problem boundaries and the ship hull on the mean (dotted lines) and actual (solid lines) positions.

surface boundary condition and fluid pressure are better defined on the fixed reference frame $\vec{x}_0$ and this is where we are going to define the nonlinear hydrodynamic problem. The Cartesian coordinate $\vec{x}_s$ is ideal for representing the ship geometry, the boundary conditions on the ship surface and also to compute pressures over the hull. $\vec{x}$ is a coordinate system that, if we make the assumption that the motions of the ship besides its forward displacement are small, remains close to $\vec{x}_s$ at all times, having the advantage over $\vec{x}_s$ of being an inertial reference frame. It is easy to see that when we linearize the problem and under a "small motions" assumption, we will be able to transfer boundary conditions and hydrodynamic quantities from $\vec{x}_s$ (where we defined S_b) to $\vec{x}$ (where we defined S_{bm}), and through the use of Taylor expansions make the necessary corrections up to the order we want, as long as S_b is a smooth surface. This approach will be taken when we will linearize the problem.

2.3 The Nonlinear Problem

Under the previous assumptions we will define a velocity potential in the fixed referential frame given by $\Phi(\vec{x}_0, t)$, where t denotes time, and the velocity vector as $\vec{V}(\vec{x}_0, t) = \nabla\Phi(\vec{x}_0, t)$ which obeys the continuity equation, so Laplace equation

$$\nabla^2\Phi = 0 \tag{2.1}$$

governs the velocity potential in the fluid domain for all times, according to Kelvin's theorem for ideal fluids under conservative fields (see Newman [29]).

The pressure will be defined using the alternative form of the Bernoulli equation, which is valid for unsteady irrotational flows, with the potential redefined in order to eliminate the function of time that may appear on the right hand side but has no influence on the velocity vector,

$$(p - p_a) = -\rho\left(\Phi_t + \frac{1}{2}\nabla\Phi \cdot \nabla\Phi + g\, z_0\right). \tag{2.2}$$

Where $p(\vec{x}_0, t)$ is the fluid pressure, p_a is the atmospheric pressure, ρ is the fluid density and g is the acceleration due to gravity.

The boundary condition on the submerged ship hull surface will be given by

$$\nabla\Phi \cdot \vec{n} = \vec{V}_{S_b} \cdot \vec{n} \qquad \text{on } S_b \tag{2.3}$$

where $\vec{n}$ is the normal vector, pointing out of the fluid domain, and $\vec{V}_{S_b}$ is the instantaneous velocity of the actual submerged hull surface.

From 2.2, knowing that $p = p_a$ on $\eta_0(\vec{x}_0, t) = z_0$, we will have

$$\eta_0 = -\frac{1}{g}\left(\Phi_t + \frac{|\nabla\Phi|^2}{2}\right) \qquad \text{on } z_0 = \eta_0. \tag{2.4}$$

Imposing the pressure from (2.2) to remain constant over the free surface, we will

have

$$\frac{D}{Dt}\left(\frac{\Phi_t}{g}+\frac{|\nabla\Phi|^2}{2g}+z_0\right)=0 \qquad \text{on } z_0=\eta_0 \tag{2.5}$$

or:

$$\Phi_{tt}+2\nabla\Phi\cdot\nabla\Phi_t+\frac{1}{2}\nabla\Phi\cdot\nabla(\nabla\Phi\cdot\nabla\Phi)+g\Phi_{z_0}=0 \qquad \text{on } z_0=\eta_0. \tag{2.6}$$

We should point out that S_f is not known a priori. Now we need to impose a boundary condition on the surface at infinity or, in the time domain, to impose two initial conditions. Calling the starting time of the fluid motion as t_0, which will be taken to be zero for the radiation problem and negative infinity for the diffraction problem, they will be given by the fluid initially at rest conditions, which determine that for $t \leq t_0$,

$$\begin{aligned}\Phi &= 0\\ \Phi_t &= 0 \qquad \text{on } z_0=0.\end{aligned} \tag{2.7}$$

The translation of these initial conditions into the frequency domain give the radiation conditions. This states that besides the incident wave there will only be disturbances made by the presence of the body, so the waves generated in the radiation or scattering problems will always propagate outwards.

2.4 Velocity Potential Decomposition

The problem defined in the previous section, despite the assumptions made regarding the flow being inviscid and incompressible, presents great difficulties because of the nonlinear terms in equation (2.6) and of the moving boundaries S_b and S_f.

Knowing that the ship forward velocity (or the incident current velocity) is a finite quantity, without further assumptions it will only make sense to think about linearizing the perturbation potentials about this flow, which will be steady in the moving $\vec{x}$ frame.

Redefining the potential in the steadily-moving referential frame $\vec{x}$, we may write

$$\Phi(\vec{x}_0, t) = \Phi(\vec{x} + U\hat{\imath}, t) \equiv \phi(\vec{x}, t). \tag{2.8}$$

As $\vec{x}$ represents a reference system moving with constant forward speed $U\hat{\imath}$, we will also have that the partial time derivative taken in $\vec{x}_0$ will be translated as

$$\frac{\partial \Phi(\vec{x}_0, t)}{\partial t} = \left(\frac{\partial}{\partial t} - U \frac{\partial}{\partial x} \right) \phi(\vec{x}, t). \tag{2.9}$$

We will consider the total potential as being composed of the sum of an unsteady potential $\varphi(\vec{x}, t)$, representing a linear perturbation, on top of a possible nonlinear steady basis flow $\overline{\phi}_B(\vec{x})$. In most cases this basis flow is only an approximation to the actual solution of the steady problem, since its computation presents mathematical and numerical difficulties due to its nonlinear free-surface boundary conditions. We will define $\overline{\phi}(\vec{x})$ as a linear steady potential that will correct our basis flow choice $\overline{\phi}_B(\vec{x})$. In this work a solution for this problem will not be sought, but this can be found in Bingham [2] for the Neumann-Kelvin flow or Nakos [26] for the double-body flow. As this correction is considered to be small, unlike the basis flow $\overline{\phi}_B(\vec{x})$, it will not affect the boundary conditions for the unsteady potentials.

So will have the total potential decomposed as

$$\begin{aligned} \phi(\vec{x}, t) \quad &= \overline{\phi}_B(\vec{x}) + \overline{\phi}(\vec{x}) + \varphi(\vec{x}, t) \\ &= \overline{\phi}_B(\vec{x}) + \overline{\phi}(\vec{x}) + \sum_{i=1}^{6} \phi_k(\vec{x}, t) + \phi_S(\vec{x}, t) + \phi_I(\vec{x}, t) \end{aligned} \tag{2.10}$$

in the moving reference frame $\vec{x}$. $\phi_k(\vec{x}, t)$ is one of the six components of the *radiation potential*, each component representing the waves generated by the ship as it moves in one of the six possible rigid body degrees of freedom. $\phi_I(\vec{x}, t)$ is the *incident wave potential* and $\phi_S(\vec{x}, t)$ is the *scattered wave potential*, generated by the presence of the body as the incident wave passes by. The sum $\phi_D(\vec{x}, t) = \phi_I(\vec{x}, t) + \phi_S(\vec{x}, t)$ will be referred as the *diffraction wave potential*, and $\varphi(\vec{x}, t)$ represents the sum of all unsteady potentials.

Throughout this work we will choose to treat this problem as having solutions in terms of series expansions in powers of a small parameter ε. This approach enables us to include nonlinear effects proportional to powers of the wave amplitude without really solving a nonlinear equation.

As stated by Wehausen and Laitone [39], this parameter should be defined in such a way that this expansion will give us some insight into the nature of our problem and as $\varepsilon \to 0$, the solution will approach in some sense a known solution. Here as in the classical Stokes perturbation scheme ε will be the ratio between wave height and wavelength. It is also true that once the mathematical form of the solution is defined, the physical meaning of ε will bear no consequence on the algebra. The velocity potential and wave elevation will have the following power series expansion in terms of ε:

$$\begin{aligned} \varphi &= \varepsilon\varphi^{(1)} + \varepsilon^2\varphi^{(2)} + \varepsilon^3\varphi^{(3)} + \dots \\ \eta &= \eta^{(0)} + \varepsilon\eta^{(1)} + \varepsilon^2\eta^{(2)} + \dots \end{aligned} \tag{2.11}$$

and now we are ready to linearize the problem presented in the previous section. We will then be able to solve the problem for $\varphi^{(1)}$ as all other terms will be multiplied by higher ε factors and will be negligible in comparison to $\varphi^{(1)}$. Going to the next order, $\varphi^{(2)}$ will be solved by disregarding all terms of order equal or greater than ε^3, and substituting the solution for $\varphi^{(1)}$ in the problem, since this is already known. We will then arrive to a inhomogeneous linear equation for $\varphi^{(2)}$, although the whole problem is nonlinear. By doing that recursively we may get higher order solutions that will represent corrections to the previous solutions obtained. In practice going beyond the first order solution takes great effort, as Ogilvie [36] pointed out.

When we do not use the superscripts (1), (2),..., it is clear that we refer to the whole series (2.11), but most of the time only the first term will be included, all others giving contributions to higher order terms that are implicitly being disregarded.

We will define $\overline{\phi}$ also as expandable in powers of a small parameter δ, but the

definition of δ will come with the proper choice of the basis flow. Then we will have

$$\overline{\phi} = \delta\overline{\phi}^{(1)} + \delta^2\overline{\phi}^{(2)} + \delta^3\overline{\phi}^{(3)} + \ldots. \tag{2.12}$$

2.5 Linearized Free-surface Boundary Condition

2.5.1 Plane incident wave

The total potential in the moving coordinate system $\vec{x}$ will be given by $\phi(\vec{x},t) = \overline{\phi}_B(\vec{x}) + \phi_I(\vec{x},t)$, knowing that $\overline{\phi}_B(\vec{x}) = -Ux$ is the exact solution so $\overline{\phi}(\vec{x}) = 0$. As we do not have the presence of a floating body, $\phi_k(\vec{x},t) = 0$ and $\phi_S(\vec{x},t) = 0$. Under the assumption of small ε we will Taylor expand the free surface condition (2.6) and enforce it on the plane $z_0 = 0$ instead of on the actual free-surface elevation. Retaining only first order terms, we will use (2.9) to get

$$\phi_{I\,tt} - 2U\phi_{I\,xt} + U^2\phi_{I\,xx} + g\phi_{I\,z} + O(\varepsilon^2) = 0 \qquad \text{on } z = 0 \tag{2.13}$$

in the moving reference frame $\vec{x}$. The first-order solution (which in this particular case also satisfies the second-order problem) to this boundary-value problem will be given by

$$\phi_I^{(1)} = \frac{igA}{\omega_0}\exp[K_0(z - ix\cos\beta - iy\sin\beta) + i\omega_e t] \tag{2.14}$$

where ϕ_I is the first-order incident wave potential, $i = \sqrt{-1}$, A is the wave amplitude, K_0 the wave number or $K_0 = 2\pi/\lambda$, λ being the wave length, ω_0 is the wave frequency in the space-fixed reference frame $\vec{x}_0$, ω_e is the wave frequency in the moving reference frame $\vec{x}$, and β is the angle between the direction of wave propagation and the x_0 or x axis. K_0 and ω_0 are related through the infinite depth dispersion relation

$$K_0 = \frac{\omega_0^2}{g}, \tag{2.15}$$

and ω_0, K_0, and ω_e, the "encounter frequency", are related by

$$\omega_e = \omega_0 - K_0 U \cos\beta. \tag{2.16}$$

2.5.2 General Basis Flow

Now we are going to consider the presence of a floating body moving with mean velocity $U\ \hat{\imath}_0$, or in the presence of a current with velocity $-U\ \hat{\imath}$, which is equivalent. We are going to assume that the total potential in the moving reference system $\vec{x}$ will be given as

$$\phi(\vec{x},t) = \overline{\phi}_B(\vec{x}) + \varphi(\vec{x},t), \tag{2.17}$$

where $\varphi(\vec{x},t)$ stands for the sum of all unsteady potentials.

We can not linearize the steady flow over the $z = 0$ plane because U is finite and there is no reason to suppose the wave elevation not to be of $O(1)$. Using Bernoulli (2.2) we will have the steady wave elevation in the moving reference frame as

$$\overline{\eta}(x,y) = -\frac{1}{2g}\left(|\nabla\overline{\phi}_B|^2 - U^2\right) \qquad \text{on } z = \overline{\eta}, \tag{2.18}$$

and the steady nonlinear free-surface condition, from (2.6), will be

$$\nabla\overline{\phi}_B \cdot \nabla(\nabla\overline{\phi}_B \cdot \nabla\overline{\phi}_B) + g\overline{\phi}_{B\,z} = 0 \qquad \text{on } z = \overline{\eta}. \tag{2.19}$$

Considering also the unsteady potentials we will have the total wave elevation given by

$$\eta(x,y) = -\frac{1}{g}\left[\varphi_t + \frac{1}{2}\left(|\nabla\overline{\phi}_B|^2 - U^2 + \nabla\varphi\cdot\nabla\varphi + \nabla\overline{\phi}_B\cdot\nabla\varphi\right)\right] \qquad \text{on } z = \eta, \tag{2.20}$$

and by using $D/Dt(p) = 0$ on $z = \eta(x,y)$, we will get the new nonlinear free-surface

condition as

$$\begin{aligned}\varphi_{tt} \quad & +2\nabla\overline{\phi}_B \cdot \nabla\varphi_t + \nabla\overline{\phi}_B \cdot \nabla(\nabla\overline{\phi}_B \cdot \nabla\varphi) + \frac{1}{2}\nabla(\nabla\overline{\phi}_B \cdot \nabla\overline{\phi}_B) \cdot \nabla\varphi + \\ & g\overline{\phi}_{B\,z} + \frac{1}{2}\nabla(\nabla\overline{\phi}_B \cdot \nabla\overline{\phi}_B) \cdot \nabla\overline{\phi}_B + g\varphi_z, \qquad \text{on } z = \eta. \end{aligned} \tag{2.21}$$

Now we are ready to linearize our unsteady potential over the mean steady wave elevation $\overline{\eta}(x, y)$, since we have that $(\eta(x, y) - \overline{\eta}(x, y))$ will be $O(\varphi)$. So we will get

$$\begin{aligned}\varphi_{tt} \quad & +2\nabla\overline{\phi}_B \cdot \nabla\varphi_t + \nabla\overline{\phi}_B \cdot \nabla(\nabla\overline{\phi}_B \cdot \nabla\varphi) + \frac{1}{2}\nabla(\nabla\overline{\phi}_B \cdot \nabla\overline{\phi}_B) \cdot \nabla\varphi - \\ & \frac{\partial}{\partial z}\left(\frac{1}{2}\nabla\overline{\phi}_B \cdot \nabla(\nabla\overline{\phi}_B \cdot \nabla\overline{\phi}_B) + g\overline{\phi}_{B\,z}\right)\left(\frac{\varphi_t + \nabla\overline{\phi}_B \cdot \nabla\varphi}{g + \nabla\overline{\phi}_B \cdot \nabla\overline{\phi}_{B\,z}}\right) + \\ & g\overline{\phi}_{B\,z} + \frac{1}{2}\nabla(\nabla\overline{\phi}_B \cdot \nabla\overline{\phi}_B) \cdot \nabla\overline{\phi}_B + g\varphi_z + O(\varepsilon^2), \qquad \text{on } z = \overline{\eta}. \end{aligned} \tag{2.22}$$

It is not an easy task to satisfy this boundary condition on the mean free surface and indeed there is not a complete solution for this problem in general. The alternative problems that we can solve will come with the introduction of more assumptions and some compromises to this rather general approach.

2.5.3 Neumann-Kelvin Free-surface Condition

In 1898 Michell [25] proposed the thin-ship approximation, supposing that ships have the beam much smaller than draft and length, so the body boundary condition may be enforced on the center plane of the ship and the free-surface boundary condition (2.6) may be linearized about the incoming flow. The resulting linear free-surface condition is also known as the "Neumann-Kelvin" free surface condition. The Neumann-Kelvin formulation in the context of ship motions was proposed by Chang in 1977 [4] and actually suggests that we linearize the free-surface and body boundary conditions over the uniform incoming current but enforce the body boundary condition on the actual body surface.

Under the integral-equation method, we will have to perform integrations over all the boundary surfaces that define our problem, which in this case are the body

and the whole free surface. If we employ as the Green function the potential of a translating and pulsating source, we will be able to replace the integral over the free surface with an integral over the ship waterline plus a convolution in time, which can be advantageous. This is the approach used in the work of Liapis [15], Beck [16], Korsmeyer [17] and Bingham [2].

We will also follow along this line, so $\overline{\phi}_B = -Ux$, and $\overline{\phi}$ will be given by (2.12). In the work cited above Bingham showed that the steady potential under the Neumann-Kelvin assumption can be regarded as the limit as $t \to \infty$ of the unsteady impulsive surge potential. δ is considered to be small in the sense that it will not be a order one quantity and $\overline{\phi}$ can be disregarded by comparison to the basis flow. So the total first-order potential will be given by $\phi^{(1)} = \overline{\phi}^{(1)} + \varphi^{(1)}$ and will give the unsteady first-order free-surface condition, equivalent to (2.13):

$$\left(\frac{\partial}{\partial t} - U\frac{\partial}{\partial x}\right)^2 \varphi + g\varphi_z + O(\varepsilon^2) + O(\varepsilon\delta) = 0, \qquad \text{on } z = 0, \tag{2.23}$$

and the steady first-order free-surface condition as:

$$\frac{U^2}{g}\frac{\partial^2\overline{\phi}}{\partial x^2} + \frac{\partial\overline{\phi}}{\partial z} + O(\varepsilon^2) + O(\varepsilon\delta) = 0, \qquad \text{on } z = 0. \tag{2.24}$$

We can see that in this approximation, once we assume that the disturbance imposed by the presence of the body in the basis flow is an infinitesimal perturbation, no further assumptions need to be made. But this is a strong statement by itself and one should be aware of that when trying to generalize this approach to non-slender body shapes.

2.5.4 Double-body Free-surface Condition

Proposed first in connection with low Froude numbers, the idea here is to regard the double-body flow as the zeroth order approximation of the steady ship problem. Following this approach we can mention linearizations proposed by Ogilvie [35] in 1968, Newman [28] in 1976, and Maruo [24] in 1980. In 1977, Dawson [6] followed

the same path with a more pragmatic and less rigorous approach that, due to the easier numerical implementation received a lot of attention and gave promising results. Nakos [26] in 1990 made an exposition of the assumptions involved and got results for the unsteady and steady potentials in the frequency domain using the Rankine panel method.

Calling the double-body potential $\overline{\phi}_{DB}$, substituting $\overline{\phi}_B = \overline{\phi}_{DB}$ in (2.22), and noticing that at $z = 0$, $\overline{\phi}_{DB\,z} = 0$ we will have the free-surface boundary condition for the unsteady potential φ given as

$$\begin{aligned} \varphi_{tt} \quad & +2\nabla\overline{\phi}_{DB} \cdot \nabla\varphi_t + \nabla\overline{\phi}_{DB} \cdot \nabla(\nabla\overline{\phi}_{DB} \cdot \nabla\varphi) + \frac{1}{2}\nabla(\nabla\overline{\phi}_{DB} \cdot \nabla\overline{\phi}_{DB}) \cdot \nabla\varphi \\ & +g\varphi_z - \overline{\phi}_{DBzz}\left(\varphi_t + \nabla\overline{\phi}_{DB} \cdot \nabla\varphi\right) + O(\varepsilon^2) + O(\varepsilon\delta) = 0, \qquad \text{on } z = 0. \end{aligned} \tag{2.25}$$

Once again δ is considered to be small in the sense that it will not be an order one quantity and $\overline{\phi}$ will be disregarded by comparison to the basis flow. Still in connection with this approach we may ease the requirements on the body slenderness by assuming the floating body to possess very small forward velocity. As $U << 1$, the problem is also linearized with respect to the forward velocity, and terms proportional to $U^n, n > 1$ will be disregarded as higher order terms. Grue & Palm [8] [9] [11] (1985, 1986, 1993), Nossen, Grue & Palm [34] (1991) and Zhao & Faltinsen [41], [42], [43], (1988, 1988, 1989) followed this approach. The linearized free-surface condition will now be given as

$$\varphi_{tt} \quad +2\nabla\overline{\phi}_{DB} \cdot \nabla\varphi_t + g\varphi_z - \overline{\phi}_{DBzz}\varphi_t + O(\varepsilon^2) + O(\varepsilon\delta) + O(U^2) = 0, \qquad \text{on } z = 0, \tag{2.26}$$

which is similar to (2.25), without the quadratic double-body velocity terms. Here we will compare results obtained by Zhao & Faltinsen [43] for the circular cylinder case at very small forward velocity with our own results under the Neumann-Kelvin assumption, but we will not pursue this approach.

2.6 Linearized Body Boundary Condition

The steady body boundary condition will be given by

$$\frac{\partial \phi_B}{\partial n} = 0, \qquad \text{on } S_{bm}. \tag{2.27}$$

and it is with respect to this basis flow that the linearization will be made. We will linearize the body boundary condition (2.3) knowing that the unsteady linear motion of the ship will be proportional to the wave amplitude, of order ε. Defining this motions as

$$\vec{\alpha}(t) = \vec{\xi}(t) + \vec{\Omega}(t) \times \vec{x}_s, \tag{2.28}$$

where $\vec{\xi}(t)$ is the linear rigid body displacements (surge, sway and heave motions) and $\vec{\Omega}(t)$ is the angular rotations (roll, pitch and yaw motions). Transferring the boundary condition from S_b to S_{bm}, correcting for the gradients not being computed on $\vec{x}_s$ but on $\vec{x}$, collecting the first-order (proportional to ε) terms, and doing some vector algebra (see Newman [30]) we will arrive at

$$\begin{aligned} \frac{\partial \varphi}{\partial n} \quad &= \dot{\vec{\xi}} \cdot \vec{n} + \dot{\vec{\Omega}} \cdot (\vec{x} \times \vec{n}) + \\ &\vec{\xi} \cdot [-(\vec{n} \cdot \nabla) \nabla \phi_B] + \vec{\Omega} \cdot [-(\vec{n} \cdot \nabla)(\vec{x} \times \nabla \phi_B)] \qquad \text{on } S_{bm}. \end{aligned} \tag{2.29}$$

Following Ogilvie and Tuck [37], we will define the *m-terms* as

$$\begin{aligned} \{m_1, m_2, m_3\} &= -(\vec{n} \cdot \nabla) \nabla \phi_B \\ \{m_4, m_5, m_6\} &= -(\vec{n} \cdot \nabla)(\vec{x} \times \nabla \phi_B), \end{aligned} \tag{2.30}$$

$\xi_{i+3} = \Omega_i$, and $n_{i+3} = (\vec{x} \times \vec{n})_i$, where $i = 1, 2, 3$. Then we will finally be able to write

$$\frac{\partial \varphi_i}{\partial n} = \dot{\xi}_i \cdot n_i + \xi_i m_i \qquad i = 1, \ldots, 6 \qquad \text{on } S_{bm}. \tag{2.31}$$

This is the linear boundary condition to be used for all the different approaches.

Under the *Neumann-Kelvin* assumption $\phi_B = -U\,x$ and we will arrive at

$$\begin{aligned} m_1 &= m_2 = m_3 = m_4 = 0 \\ m_5 &= Un_3 \\ m_6 &= -Un_2, \end{aligned} \tag{2.32}$$

and using the *double-body* approach the *m-terms* will be given by (2.30), with ϕ_{DB} instead of ϕ_B.

Chapter 3

Solutions of the Hydrodynamic Problems

When we expand our problem as a set of linear problems of increasing orders in terms of a small parameter, results from lower order problems will enter as boundary conditions on the higher order problems. As we will see latter, we need the solution of the first-order problem not only to set the boundary conditions for the second-order steady problem but also because most of the terms of the second-order steady forces come from the first-order potentials and velocities. Indeed, for the zero forward velocity case, the second-order steady force will be a function of the first-order linear potential alone. For the computation of the first-order time-domain potentials we have used the low-order panel method[1] solution developed by Bingham [2], as a continuation of the work initiated by Korsmeyer [17], and which is incorporated in the FORTRAN code *TIMIT*.

We do not have an efficient and reliable procedure for the computation of the Green function equivalent to a pulsating and translating source in the presence of a free surface in the frequency domain, but we always can solve the linear problem in the time domain and transform to the frequency domain.

We will outline how the problem is solved in the time domain, under the Neumann-

[1] also known as boundary-element or integral-equation method

Kelvin assumption, using the code *TIMIT*. For the calculation of second-order steady forces in the frequency domain we will need to know some first-order quantities also in the frequency domain.

We will also show the importance of knowing the second-order steady potential when the ship has forward speed, and how to compute it. There will be a first-order inhomogeneous part on this problem (the forcing function) acting on the free surface which will be a function of the frequency, and so this second-order steady potential will also be frequency dependent. The form of this problem is similar to the steady first-order problem, and the approach to solve it is also based on computing the steady potential as time goes to infinity, with the only difference that now the problem has an inhomogeneous boundary condition on $z = 0$.

3.1 Integral Equations

Our low-order panel method uses a free-surface Green function, presented by Haskind in 1946 [13], as its fundamental solution which satisfies the initial boundary-value problem without the presence of a floating body, and is given by

$$G(\vec{x};\vec{\xi},t) = G^{(0)}(\vec{x};\vec{\xi}) + H(\vec{x};\vec{\xi},t), \tag{3.1}$$

where $G^{(0)}(\vec{x};\vec{\xi})$ is the Rankine part of the Green function with a mirror with respect to $z = 0$, and $H(\vec{x};\vec{\xi},t)$ is the unsteady part of the Green function, that gives the wave-like behavior.

They are defined as

$$\begin{aligned} G^{(0)}(\vec{x};\vec{\xi}) &= \left(\frac{1}{r}-\frac{1}{r'}\right), \\ H(\vec{x};\vec{\xi},t) &= 2\int_0^\infty dk\,\left[1-\cos(t\sqrt{gk})\right]\mathrm{e}^{\,kZ}J_0(kR), \end{aligned}$$

where

$$\begin{aligned} r &= \sqrt{(x-\xi)^2+(y-\eta)^2+(z-\zeta)^2}, \\ r' &= \sqrt{(x-\xi)^2+(y-\eta)^2+(z+\zeta)^2}, \\ R &= \sqrt{(x-\xi+U\,t)^2+(y-\eta)^2}, \\ Z &= (z+\zeta). \end{aligned}$$

One problem with this definition of the Green function is that its time-domain representation contains *all* frequencies and we will never be able to correctly represent this feature in time, since numerical algorithms are essentially discrete. Helping us to overcome this undesirable feature is a low-pass filter inherent to the low-order panel method being employed, which is regulated by the depth of the source Green function. Linear waves have an exponential decay and as the source point goes deeper less high frequency waves will be excited by its presence.

We can see this trend in Figure 3-1, where in the upper half of the picture we represent the steady potential due to a source point located at $Z = z/(U^2/g) = 0.1$, and the lower half plane represents the same steady source located at $Z = z/(U^2/g) = 0.01$. The steady-state Green function field was evaluated as suggested in Newman [31] following the classical analysis of ship waves by Lord Kelvin [14],

$$G_{st}(\vec{X}) = \lim_{T\to\infty}\int_{-T}^{0} G_\tau(X+\tau,Y,Z,-\tau)\,d\tau. \tag{3.2}$$

The waves move away from the source path, given by the line from $(-\infty,0,0)$ to $(0,0,0)$. We may see in the upper-half plane that up to a certain distance (which is a function of X and the Z-coordinate of the source), the diverging waves have been

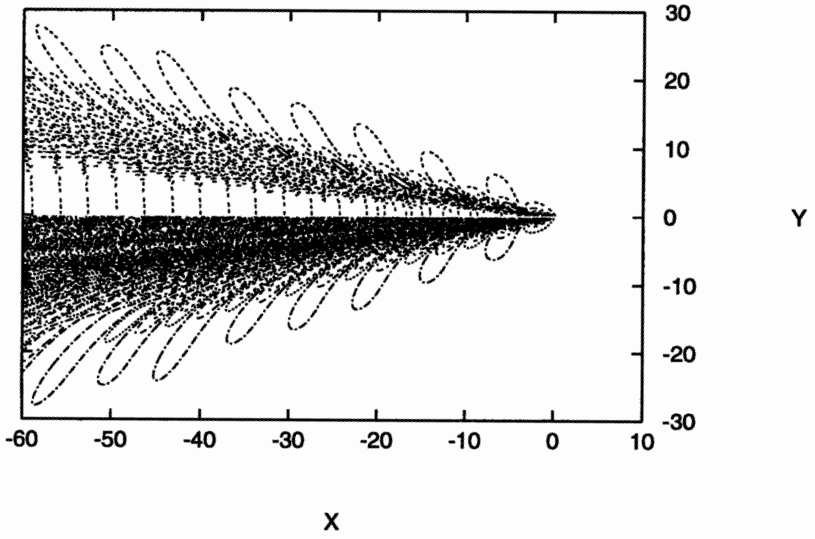

Figure 3-1: Translating steady-state Green function field. The coordinates X,Y and Z are nondimensionalized by U^2/g. In the upper half part of the plot the source point is submerged to $Z = -0.1$ and in the lower half part to $Z = -0.01$.

filtered out, while in the lower-half plane the short length, high-frequency waves are present throughout the sector up to very close to the centerline. This comparison can also be appreciated by making a transverse cut at $Y = 0.2$, which is shown in Figure 3-2. The three curves represent the steady Green function for a submergence of the source point equal to $Z = 0.01$, $Z = 0.05$ and $Z = 0.1$. Although getting closer to the free surface will let us have more information about the high-frequency content, it will require a finer discretization in time and space to avoid the aliasing phenomena as well as a good representation in space of the higher frequency wave components. We should observe that as the source points in the low-order version of the *TIMIT* code are located on the centroids of each panel, we are introducing this low-pass filter automatically.

We should note that using the so called "cosine spacing" when discretizing our floating body can introduce very shallow panels close to the free surface. This will

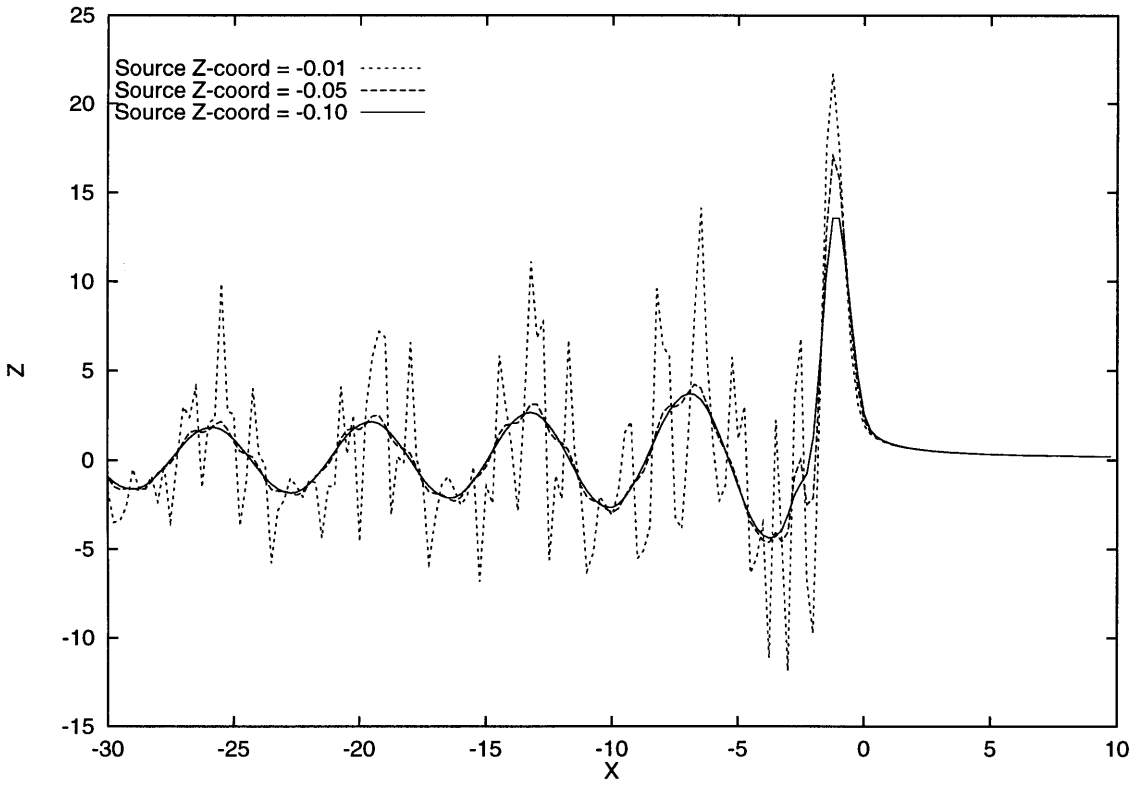

Figure 3-2: XZ-plane cut of the Green function field shown in Figure 3-1 for Y=0.2. We can see the high-frequency components being eliminated as the depth of the source is increased. The definitions given in Figure 3-1 also apply here.

bring high-frequency wave components that will not be filtered out and which may be not well resolved in time and with respect to the panels dimensions. This is not a problem in the zero-speed frequency-domain approach, because then we have absolute control over the range of the chosen frequencies and subsequent wavelengths, but in the time domain it will lead to numerical inaccuracies.

Knowing the mathematical definition of the impulsive, constant forward-speed free-surface Green function, and being able to efficiently evaluate it using the routines developed by Newman (1992) [32], we can define the first-order integral equation of our initial boundary-value problem following Bingham [2], applying Green theorem to the time derivative of the unsteady potential $\varphi(\vec{x}, \tau)$ and to the Green function and integrating over the time history.

After some manipulation we will arrive at

$$
\begin{aligned}
& 2\pi\varphi(\vec{x},t) + \iint_{S_{bm}} d\vec{\xi}\left(\varphi(\vec{\xi},t)G^{(0)}_{n_\xi}(\vec{x};\vec{\xi}) - G^{(0)}(\vec{x};\vec{\xi})\varphi_n(\vec{x},t)\right) \\
- & \int_{t_0}^{t} d\tau \iint_{S_{bm}} d\vec{\xi}\left(\varphi(\vec{\xi},\tau)G_{\tau n_\xi}(\vec{x};\vec{\xi},t-\tau) - G_\tau(\vec{x};\vec{\xi},t-\tau)\varphi_n(\vec{x},\tau)\right) \\
- & \frac{U}{g}\int_{t_0}^{t} d\tau \int_{\Gamma} dl(\vec{n}_{2D}\cdot\hat{\imath})\left[\varphi(\vec{\xi},\tau)\left(G_{\tau\tau}(\vec{x};\vec{\xi},t-\tau) - UG_{\tau\xi}(\vec{x};\vec{\xi},t-\tau)\right)\right] \\
& -G_{\tau\tau}(\vec{x};\vec{\xi},t-\tau)\left(\varphi_\tau(\vec{x},\tau) - U\varphi_\xi(\vec{x},\tau)\right) = 0. \qquad (3.3)
\end{aligned}
$$

Equation (3.3) is written in a form known as the *potential formulation* or *boundary element direct formulation.* To compute the second-order steady potential and the second-order steady forces, we need to calculate velocities and potentials over the body surface and in the fluid domain and this will be done using the integral equation.

When computing velocities using a low-order panel code, the use of the so called *source formulation* or *boundary element indirect formulation* is advisable, to avoid taking numeric spatial derivatives of the potential. We can derive the integral equation for the *source formulation* approach defining the source strength to be

$$\sigma = \frac{1}{4\,\pi}(\varphi - \varphi') \qquad (3.4)$$

where φ' is the potential that represents the solution of the flow in the region interior to the body, and has boundary conditions

$$
\begin{aligned}
\varphi'(\vec{x},t) &= \varphi(\vec{x},t) \qquad \text{on } S_{bm} \\
\left(\frac{\partial}{\partial t} - U\frac{\partial}{\partial x}\right)^2 \varphi' + g\frac{\partial}{\partial z}\varphi' &= 0 \qquad \text{on } S_f. \qquad (3.5)
\end{aligned}
$$

The difference in the integral equations representing φ and φ' is only with respect to the definition of the normal vector on the S_{bm} surface, which will point in the opposite direction.

Adding both integral equations we will get the *source formulation*

$$\begin{aligned}\varphi(\vec{x},t) &= \iint_{S_{bm}} d\vec{\xi}\,\left(G^{(0)}(\vec{x};\vec{\xi})\,\sigma(\vec{\xi},t)\right) + \int_{t_0}^{t} d\tau \iint_{S_{bm}} d\vec{\xi}\left(G_\tau(\vec{x};\vec{\xi},t-\tau)\sigma(\vec{\xi},\tau)\right) \\ &\quad -\frac{U^2}{g}\int_{t_0}^{t} d\tau \int_{\Gamma} dl\,(\vec{n}_{2D}\cdot\hat{\imath})^2\,\left(G_\tau(\vec{x};\vec{\xi},t-\tau)\,\sigma(\vec{\xi},\tau)\right). \qquad (3.6)\end{aligned}$$

We should change (3.6), which is a fine relation for computing the potential at any point in the fluid domain but not very useful for solving for the source strength, operating with $\vec{n}_x\cdot\nabla_x$, where the lower index x denotes the coordinate system where the normal and the derivatives will take place:

$$\begin{aligned}\vec{n}\cdot\nabla\varphi(\vec{x},t) &= 2\,\pi\,\sigma(\vec{\xi},t) + \iint_{S_{bm}} d\vec{\xi}\,\left(G^{(0)}_{n_x}(\vec{x};\vec{\xi})\,\sigma(\vec{\xi},t)\right) \\ &\quad + \int_{t_0}^{t} d\tau \iint_{S_{bm}} d\vec{\xi}\left(G_{n_x\tau}(\vec{x};\vec{\xi},t-\tau)\sigma(\vec{\xi},\tau)\right) \\ &\quad -\frac{U^2}{g}\int_{t_0}^{t} d\tau \int_{\Gamma} dl\,(\vec{n}_{2D}\cdot\hat{\imath})^2\,\left(G_{n_x\tau}(\vec{x};\vec{\xi},t-\tau)\,\sigma(\vec{\xi},\tau)\right). \qquad (3.7)\end{aligned}$$

Now the boundary S_{bm} should be discretized into a series of panels which in our case will be considered to be triangular or quadrilateral flat panels, but in the general case any surface made of interpolating functions consisting of polynomials, circular arcs, *etc* will do. By using the method of collocation, the discretized form of equation (3.3) or (3.7) will be applied to a number of particular nodes within each element where values of the potential and its normal (3.3) or values of the potential and the source strength (3.7) are associated. Integration over each panel is carried out analytically or numerically, depending on the integrand and interpolating functions used. Finally, imposing the prescribed boundary conditions, we will arrive at a system of linear algebraic equations, that can be solved using direct or iterative methods, to obtain the potential from (3.3) or the source strength from (3.7).

To compute the fluid velocities using the *source formulation* we can operate on (3.6) with ∇_x, and get an expression valid for any point in the fluid domain. Using the *potential formulation* would imply a similar operation in (3.3), but we would have to compute second space derivatives of the Green function which is not

desirable, and not robust numerically.

3.2 First-order Potentials

The discrete form of equations (3.3) and (3.7) can be solved for each time step to give the transient solution (unsteady potential or source strength) for each of the unsteady radiation and diffraction potentials, as well as the solution of the first-order steady potential, which will be the infinite-time limit of the radiation surge problem.

Depending if we are solving the *diffraction problem* or the *radiation problem* we will have not only different Neumann boundary conditions, but also the potentials will be decomposed in different ways and we will have to adopt specific forms of the integral equations for each potential. This subject is covered in detail for example in Liapis [15], King [16], Bingham *et al* [12], Bingham [2] and Korsmeyer *et al* [19].

For the solution of the diffraction problem, we have to solve equation (3.3) with the body boundary condition given in (2.3), or

$$\nabla\phi_S \cdot \vec{n} = -\nabla\phi_I \cdot \vec{n} \qquad \text{on } S_{bm}, \tag{3.8}$$

where in the moving reference system we can represent the first-order incident wave potential as an integral over the frequency range of the waves given in (2.14),

$$\phi_I(\vec{x},t) = \mathrm{Re} \int_{-\infty}^{\infty} d\omega_e \frac{ig}{\pi\,\omega_0} \exp[K_0(z - i\,x\cos\beta - iy\,\sin\beta) + i\,\omega_e t]. \tag{3.9}$$

The encounter frequency relation (2.16) may be written as

$$\omega_e = \omega_0 - \frac{\omega_0^2\,U}{g}\cos\beta, \tag{3.10}$$

and if we multiply this equation by $\frac{U}{g}\cos\beta$ and define the non-dimensional frequency as $\overline{\omega}_{=}\omega\left|\frac{U}{g}\cos\beta\right|$, we will have the non-dimensional encounter frequency

$$\overline{\omega}_e = \overline{\omega}_0 + \overline{\omega}_0^2 \qquad \text{for } \cos\beta < 0 \tag{3.11}$$

$$\overline{\omega}_e = \overline{\omega}_0 - \overline{\omega}_0^2 \qquad \text{for } \cos\beta > 0, \tag{3.12}$$

and for $\cos\beta = 0$, $\overline{\omega}_{=}\omega\frac{U}{g}$, so that

$$\overline{\omega}_e = \overline{\omega}_0 \qquad \text{for } \cos\beta = 0. \tag{3.13}$$

We can visualize the relation between the encounter frequency and the absolute frequency for the different wave headings in Figure 3-3.

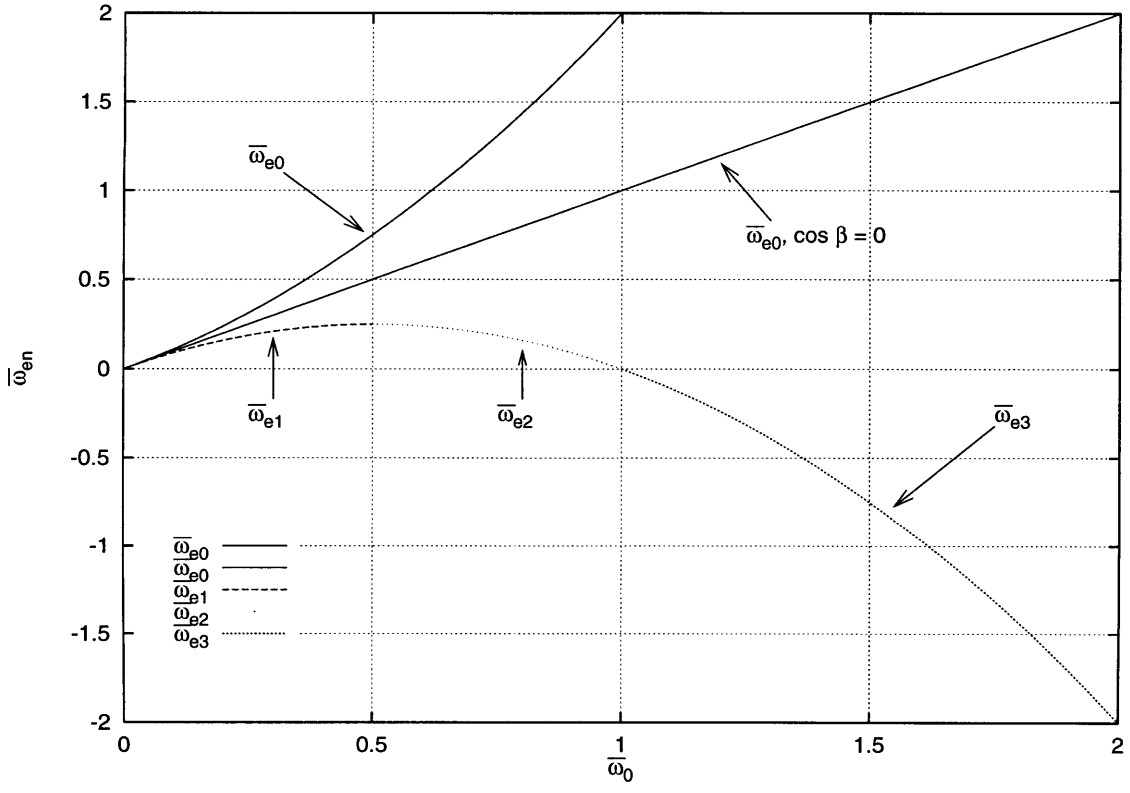

Figure 3-3: Relation between the non-dimensional absolute frequency $\overline{\omega}_0$ and the non-dimensional encounter frequencies $\overline{\omega}_{en}$, $n = 0, \ldots, 3$. The case $n = 0$ occurs when $\cos\beta < 0$. Cases $n = 1, 2$ or 3 represent the three possible encounter frequencies when $\cos\beta > 0$. When $\cos\beta = 0$ (beam seas), this relation becomes trivial and the solution is actually given by $\overline{\omega}_{e0} = \overline{\omega}_0$.

The curve representing $\overline{\omega}_{e0}(\overline{\omega}_0)$ is given by (3.11), and all waves with this encounter frequency $\overline{\omega}_{e0}(\overline{\omega}_0)$ will move in the direction given by the heading angle β with respect to the moving reference system.

The second curve $\overline{\omega}_{e1}(\overline{\omega}_0)$ is defined by equation (3.12) for $\overline{\omega}_0 < 1/2$. The waves having encounter frequency given by $\overline{\omega}_{e1}(\overline{\omega}_0)$ have phase velocity $C_e = \omega_e/K_e$ and group velocity $C_{eg} = \frac{\partial \omega_e}{\partial K_e}$ $(= \omega_e/(2\,K_e)$ for the deep water case) bigger than the ship speed U. In the moving reference system they will overtake the ship.

An interesting situation occurs with the encounter frequencies contained in $\overline{\omega}_{e2}(\overline{\omega}_0)$, which is also defined by equation (3.12), but for $\overline{\omega}_0$ in the range $1/2 < \overline{\omega}_0 < 1$. These waves have a phase velocity greater than the ship speed, which means that for someone on the ship reference frame it would look like these waves are overtaking the ship, but their group velocity is less than U, meaning that the ship moves faster than their energy. So if we look at a wave packet in this situation, it would be represented as undulations on the free surface that overtake the ship but are continuously disappearing as it moves faster than their energy. Simultaneously, new undulations will show up to take their place inside the space region moving with the group velocity of the wave packet.

Finally we have the waves with encounter frequency given by $\overline{\omega}_{e3}(\overline{\omega}_0)$, also defined by equation (3.12), and of group and phase velocities smaller than U. Those waves are being overtaken by the ship, and the negative frequency of encounter means that their phase velocity relative to the ship has changed sign, and they appear to be going in the $-\overline{x}$-direction. If we only compare the absolute value of the encounter frequency, we can see that the range of encounter frequencies covered by $\overline{\omega}_{e1}(\overline{\omega}_0)$ and $\overline{\omega}_{e2}(\overline{\omega}_0)$ will also be covered by $\overline{\omega}_{e3}(\overline{\omega}_0)$.

Figure 3-4 shows impulsive waves in a moving reference frame with speed given by a Froude number $Fr = U/\sqrt{L\,g} = 0.25$. The first three curves from the top represent the free-surface undulation of an impulsive incident wave with a heading angle $\beta = 180$ degrees. The three curves are for a non-dimensional time $\overline{t} = t\sqrt{g/l}$ equal to -20, 0 and 20. We can see in $\overline{t} = -20$ that as the higher frequency waves (smaller wavelengths) have smaller group velocity, they are organized closer to the

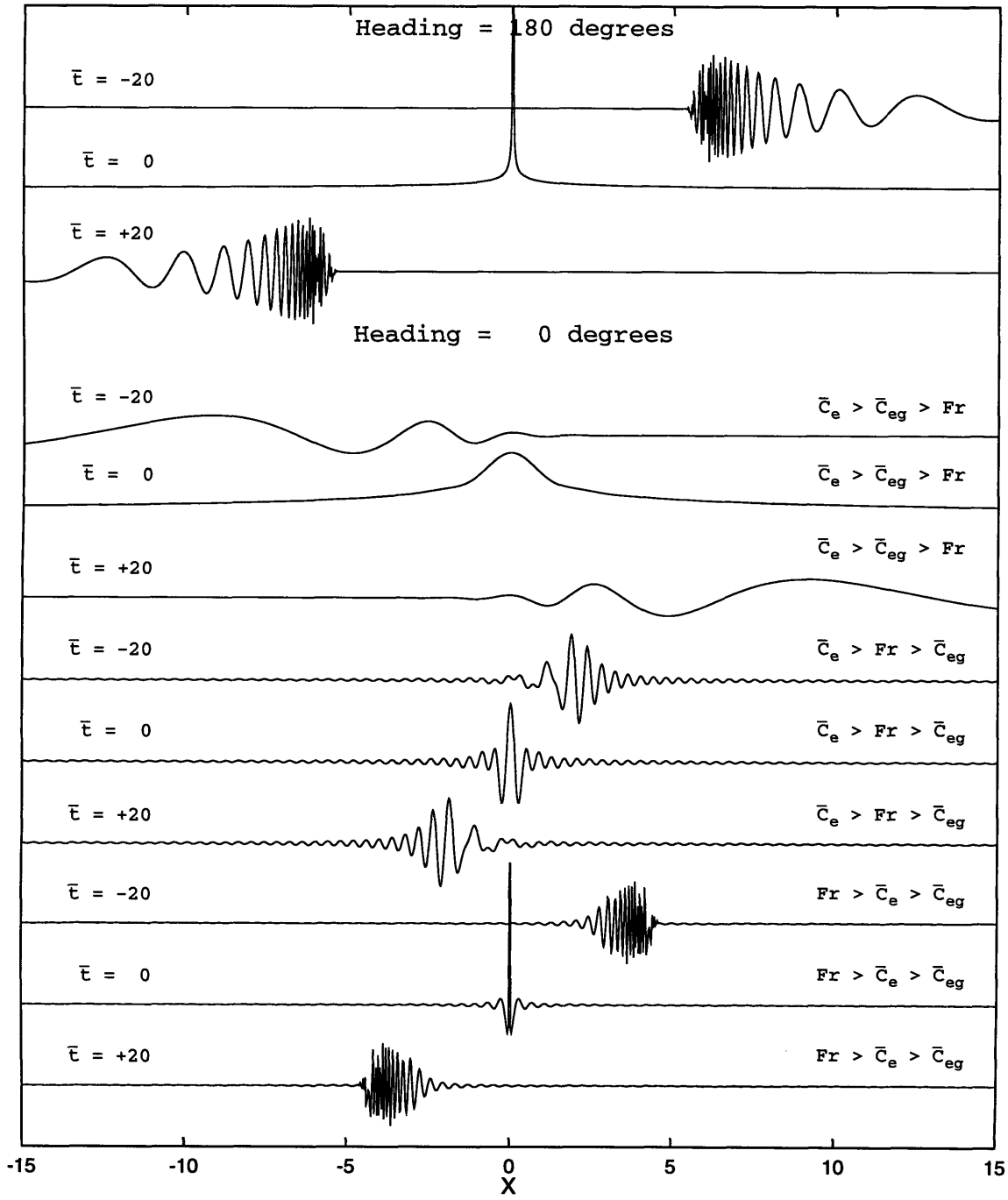

Figure 3-4: Impulsive incident wave elevations for head seas (first three plots), time equal to -20, 0 and 20. The following seas impulsive wave elevations come on the next nine curves, each set of three instantaneous shots for each component with different group and phase velocities relative to the ship speed, $Fr = 0.25$. The first three wave elevations are scaled by a factor of 5, and the last three by a factor of 4, with respect to the six waves in the middle.

point given by $\overline{x} = x/L = 5$, where the ship will reach in 20 units of time to encounter the impulsive wave, as shown in the second curve, and which it will soon leave behind, as we can see in the third curve.

The next three curves are the wave elevation for the waves with encounter frequency $\overline{\omega}_{e1}(\overline{\omega}_0)$, belonging to an impulsive incident wave with heading angle $\beta = 0$ degrees. The waves are clearly overtaking the ship.

The interesting $\overline{\omega}_{e2}(\overline{\omega}_0)$ case is represented by the next three curves and is clearly being overtaken by the ship, although it would seem otherwise for someone on the ship.

Finally the last three curves represent the waves with encounter frequency given by $\overline{\omega}_{e3}(\overline{\omega}_0)$ which will move much slower than the ship and the undulations on the free surface due to its presence.

Knowing the behavior of the incident wave in the moving reference frame and how we can get the same frequency of encounter for different waves representing distinct physical problems, we may define a better representation for the incident wave potential then (3.9), separating the following seas case from the head or beam seas ($n = 0$), and splitting it into the three regions numbered from 1 to 3:

a) $\cos\beta \leq 0$, $n = 0$:

$$\phi_I(\vec{x},t) = \mathrm{Re}\int_0^\infty d\omega_e \left[\frac{ig}{\pi\,\omega_0} \mathrm{e}^{\,K_0(z - i\,x\cos\beta - iy\,\sin\beta) + i\,\omega_e t}\right]. \tag{3.14}$$

b) $\cos\beta > 0$, $0 < \omega_0 \leq \frac{U\cos\beta}{2g}$, $n = 1$:

$$\begin{aligned}\phi_{I1}(\vec{x},t) \;=\; & \mathrm{Re}\int_0^{\frac{U\cos\beta}{2g}} d\omega_0 \left[\frac{ig}{\pi\,\omega_0}\left(1 - 2\,\omega_0\frac{U\,\cos\beta}{g}\right)\right. \\ & \left.\mathrm{e}^{\,K_0(z - i\,(x+U\,t)\cos\beta - iy\,\sin\beta) + i\,\omega_0 t}\right].\end{aligned} \tag{3.15}$$

c) $\cos\beta > 0$, $\frac{U\cos\beta}{2g} < \omega_0 \leq \frac{U\cos\beta}{g}$, $n = 2$:

$$\begin{aligned}\phi_{I2}(\vec{x},t) \;=\; & -\mathrm{Re}\int_{\frac{U\cos\beta}{2g}}^{\frac{U\cos\beta}{g}} d\omega_0 \left[\frac{ig}{\pi\,\omega_0}\left(1 - 2\,\omega_0\frac{U\,\cos\beta}{g}\right)\right. \\ & \left.\mathrm{e}^{\,K_0(z - i\,(x+U\,t)\cos\beta - iy\,\sin\beta) + i\,\omega_0 t}\right].\end{aligned} \tag{3.16}$$

d) $\cos\beta > 0$, $\frac{U\cos\beta}{g} < \omega_0 < \infty$, $n = 3$:

$$\begin{aligned}\phi_{I3}(\vec{x},t) &= -\mathrm{Re}\int_{\frac{U\cos\beta}{g}}^{\infty} d\omega_0 \left[\frac{ig}{\pi\,\omega_0}\left(1-2\,\omega_0\frac{U\,\cos\beta}{g}\right)\right. \\ &\left. \mathrm{e}^{\,K_0(z-i\,(x+U\,t)\cos\beta-iy\,\sin\beta)+i\,\omega_0 t}\right]. \end{aligned} \tag{3.17}$$

For $\cos\beta > 0$, the total incident wave potential is

$$\phi_I(\vec{x},t) = \sum_{n=1}^{3}\phi_{In}(\vec{x},t). \tag{3.18}$$

For the solution of the radiation problem we consider the ship to be advancing with mean forward speed U and moving impulsively in each mode k. $\varphi_k^{[n]}$ represents a set of canonical potentials due to an impulse in the n^{th} derivative of the ship impulsive motion in mode k. Here we will use $n = 2$, which defines an impulsive acceleration, but the choice of n is arbitrary. The body boundary condition will then be given as

$$\vec{n}\cdot\nabla\varphi_k^{[n]}(\vec{x},t) = n_k\dot{x}_k(t) + m_k x_k(t), \tag{3.19}$$

remembering that $\dot{x}_k$ and x_k are defined to match the impulsive motion applied to the body. For $n = 2$, impulsive acceleration, we will have $\ddot{x}_k = \delta(t)$,the Dirac delta function, so $\dot{x}_k = h(t)$, the Heaviside step function, and $x_k = r(t)$, the ramp function. We may decompose our canonical radiation potential as

$$\phi_k^{[n]}(\vec{x},t) = \mathcal{N}_k(\vec{x})\,\dot{x}_k(t) + \mathcal{M}_k(\vec{x})\,x_k(t) + \psi_k^{[n]}(\vec{x},t), \tag{3.20}$$

where $\mathcal{N}_k(\vec{x})$ and $\mathcal{M}_k(\vec{x})$ are waveless solutions independent of time, and $\psi_k^{[n]}(\vec{x},t)$ will give the transient behavior of the solution, or the *memory* of the *radiation problem.*

The boundary value problems for each of these auxiliary potentials can be obtained by applying the boundary conditions (2.13) to (3.19), and they will be given as

$$\begin{aligned} \nabla^2 \mathcal{N}_k &= 0 \qquad \text{in all the fluid region} \\ \mathcal{N}_k &= 0 \qquad \text{on } z = 0 \\ \vec{n} \cdot \nabla \mathcal{N}_k &= n_k \qquad \text{on } S_{bm}, \end{aligned} \tag{3.21}$$

and

$$\begin{aligned} \nabla^2 \mathcal{M}_k &= 0 \qquad \text{in all the fluid region} \\ \mathcal{M}_k &= 0 \qquad \text{on } z = 0 \\ \vec{n} \cdot \nabla \mathcal{M}_k &= m_k \qquad \text{on } S_{bm}, \end{aligned} \tag{3.22}$$

with the corresponding integral equations given as

$$2\pi \mathcal{N}_k + \iint_{S_{bm}} d\vec{\xi} \left(\mathcal{N}_k G^{(0)}_{n_\xi} - n_k G^{(0)} \right) = 0, \tag{3.23}$$

$$2\pi \mathcal{M}_k + \iint_{S_{bm}} d\vec{\xi} \left(\mathcal{M}_k G^{(0)}_{n_\xi} - m_k G^{(0)} \right) = 0. \tag{3.24}$$

The same substitution for the transient part of the radiation potential will lead to the following set of boundary conditions (exemplified for the impulsive acceleration):

$$\begin{aligned} \nabla^2 \psi_k^{[2]} &= 0 && \text{in all the fluid region} \\ \psi_k^{[2]} &= 0, \qquad \frac{\partial \psi_k^{[2]}}{\partial t} = 0 && \text{on } z = 0,\ t = 0 \\ \left(\frac{\partial}{\partial t} - U \frac{\partial}{\partial x} \right)^2 \psi_k^{[2]} &= -g \left(\frac{\partial \mathcal{N}_k}{\partial z} + \frac{\partial \mathcal{M}_k}{\partial z} t \right) && \text{on } z = 0,\ t > 0, \end{aligned} \tag{3.25}$$

with the integral equation for the memory potential coming from the substitution of the potential decomposition (3.20), boundary conditions for $\mathcal{N}_k(\vec{x})$, $\mathcal{M}_k(\vec{x})$ and

$\psi(\vec{x},t)$, and the integral equations of the auxiliary potentials (3.3). Thus

$$
\begin{aligned}
2\pi\psi(\vec{x},t) + \iint_{S_{bm}} d\vec{\xi}\left(\psi(\vec{\xi},t)G^{(0)}_{n_\xi}(\vec{x};\vec{\xi})\right) - \int_{t_0}^{t} d\tau \iint_{S_{bm}} d\vec{\xi}\left(\psi(\vec{\xi},\tau)G_{\tau n_\xi}(\vec{x};\vec{\xi},t-\tau)\right) \\
-\frac{U}{g}\int_{t_0}^{t} d\tau \int_{\Gamma} dl(\vec{n}_{2D}\cdot\hat{\imath})\left[\psi(\vec{\xi},\tau)\left(G_{\tau\tau}(\vec{x};\vec{\xi},t-\tau) - UG_{\tau\xi}(\vec{x};\vec{\xi},t-\tau)\right)\right] \\
-G_\tau(\vec{x};\vec{\xi},t-\tau)\left(\psi_\tau(\vec{x},\tau) - U\varphi_\xi(\vec{x},\tau)\right) = \\
-\iint_{S_{bm}} d\vec{\xi}\left(n_k\, H(\vec{x};\vec{\xi},t) - H_n(\vec{x};\vec{\xi},t)\mathcal{N}_k(\vec{x})\right) \\
-\int_{t_0}^{t} d\tau \iint_{S_{bm}} d\vec{\xi}\left(m_k\, H(\vec{x};\vec{\xi},t) - H_n(\vec{x};\vec{\xi},t)\mathcal{M}_k(\vec{x})\right)
\end{aligned}
\tag{3.26}
$$

3.3 First-order Equations of Motion

Applying Newton's law to the linear floating body problem whose hydrodynamic potentials were described in the last section will give

$$
\sum_{k=1}^{6} M_{jk}\,\ddot{x}_k = F_j \qquad j = 1,\ldots,6, \tag{3.27}
$$

where M_{jk} is the rigid body mass matrix of the floating body and F_j stands for the external forces. Assuming that the floating body is in hydrostatic equilibrium, which means that the volume forces (weight and buoyancy forces) are in balance[2], we will compute the first-order *impulsive* hydrodynamic surface forces under the assumption of ideal fluid laid down in Chapter 2, integrating the first-order terms of Bernoulli equation (2.2) over S_{bm}. So we will have for the diffraction potential the impulse-response function given as

$$
K_{jD}(t) = \iint_{S_{bm}} d\vec{x}\left(\frac{\partial}{\partial t} - U\frac{\partial}{\partial x}\right)\left(\phi_I(\vec{x},t) + \phi_S(\vec{x},t)\right)n_j \qquad j = 1,\ldots,6. \tag{3.28}
$$

As the ship performs small unsteady motions around its mean positions it will experience the reaction of the forces coming from the radiation potentials, which will be

[2]Actually we should say that the weight, buoyancy and any hydrodynamic steady forces will be considered to balance each other

given as

$$F_{I\,j} = \iint_{S_{bm}} d\vec{x} \left(\frac{\partial}{\partial t} - U \frac{\partial}{\partial x} \right) \left(\sum_{k=1}^{6} \phi_k \right) n_j \qquad j = 1, \ldots, 6, \tag{3.29}$$

and knowing that the radiation potential has been decomposed as in (3.20), we can define one term proportional to the acceleration as a_{jk}, one term proportional to the velocity as b_{jk} and the term proportional to the displacement as c_{jk} and also the radiation impulsive-response function K_{jk}:

$$\begin{aligned}
a_{jk} &= \rho \iint_{Sbm} d\vec{x}\, \mathcal{N}_k n_j \\
b_{jk} &= \rho \iint_{Sbm} d\vec{x} \left(\mathcal{M}_k - U \frac{\partial \mathcal{N}_k}{\partial x} \right) n_j \\
c_{jk} &= \rho \iint_{Sbm} d\vec{x} \left(\psi_k^{[n]}(0) - U \frac{\partial \mathcal{M}_k}{\partial x} \right) n_j \\
K_{jk}^{[n]}(t) &= \rho \iint_{Sbm} d\vec{x} \left(\frac{\partial \psi_k^{[n]}(t)}{\partial t} - U \frac{\partial \psi_k^{[n]}(t)}{\partial x} \right) n_j.
\end{aligned} \tag{3.30}$$

Defining C_{jk} as the linearized hydrostatic restoring matrix we will write (3.27) as

$$\begin{aligned}
&\sum_{k=1}^{6} (M_{jk} + a_{jk}) \ddot{x}_k + b_{jk} \dot{x}_k + (C_{jk} + c_{jk}) x_k + \int_{-\infty}^{t} d\tau\; K_{jk}^{[n]}(t-\tau) \frac{d^n x_k}{d\tau^n}(\tau) \\
&\qquad = \int_{-\infty}^{\infty} d\tau\; K_{jD}(t-\tau) \zeta(\tau), \qquad j = 1, \ldots, 6,
\end{aligned} \tag{3.31}$$

We can see that by defining $\zeta(t)$, we will define the excitation force through the convolution on the right hand side, and we will be able to compute the response $\ddot{x}_k(t)$, $\dot{x}_k(t)$ and $x_k(t)$.

3.4 Frequency-domain Representation

We want to compute the steady second-order forces in the frequency domain, and in order to accomplish that we need to have a lot of information from the first-order linear time-domain problem Fourier transformed to the frequency domain. Having solved the time-domain problem, we can get this information for an arbitrary number

of frequencies, as long as their range remains inside the range of frequencies that are well represented by our impulsive forcing functions and subsequent ship responses.

We will need to solve the equations of motion in the frequency domain and get the frequency-domain response amplitude operator (RAO), which will be the ship response to a unit amplitude incident wave inside the chosen range of frequencies. The quantities we need to Fourier transform in this step are added mass, potential damping and exciting force. Those quantities are computed for the ship as a whole and we will call them *integrated quantities* or *global quantities.*

To compute non-integrated quantities in the fluid region, like fluid velocities and pressure, which we will call *local quantities*, we will have to get their representation in the time domain and also transform them to the frequency domain, as we will do in the next subsections.

3.4.1 Global Quantities

We need to define the radiation and diffraction forces in the frequency domain before transforming them from the time domain. In the frequency domain our first-order equation of motions, here represented in the time domain in (3.27), would be written as its Fourier transform

$$\mathcal{F}\left[(M_{jk}+a_{jk})\ddot{x}_k + b_{jk}\dot{x}_k + (C_{jk}+c_{jk})x_k + \int_{-\infty}^{t} d\tau\; K_{jk}^{[n]}(t-\tau)\frac{d^n x_k}{d\tau^n}(\tau)\right] = \mathcal{F}\left[\int_{-\infty}^{\infty} d\tau\; K_{jD}(t-\tau)\,\zeta(\tau)\right] \tag{3.32}$$

or, calling the Fourier transform of x_k as $\tilde{x}_k$,

$$-\omega_e^2(M_{jk}+a_{jk})\,\tilde{x}_k(\omega_e) + i\,\omega_e\,b_{jk}\,\tilde{x}_k(\omega_e) + (C_{jk}+c_{jk})\tilde{x}_k(\omega_e) + \int_{-\infty}^{\infty} dt\;\int_{-\infty}^{t} d\tau\; K_{jk}^{[n]}(t-\tau)\frac{d^n x_k}{d\tau^n}(\tau)\,\mathrm{e}^{-i\,\omega_e\,t} = \int_{-\infty}^{\infty} dt\;\int_{-\infty}^{\infty} d\tau\; K_{jD}(t-\tau)\,\zeta(\tau)\,\mathrm{e}^{-i\,\omega_e\,t}.$$

Noting that $K_{jk}^{[n]}(t)$ is a causal function, changing variables defining $s = t - \tau$, we will be able to write

$$-\omega_e^2(M_{jk} + a_{jk})\,\tilde{x}_k(\omega_e) + i\,\omega_e\,b_{jk}\,\tilde{x}_k(\omega_e) + (C_{jk} + c_{jk})\tilde{x}_k(\omega_e) + \int_{-\infty}^{\infty} ds\; K_{jk}^{[n]}(s)\,\mathrm{e}^{-i\,\omega_e\,s} \int_{-\infty}^{\infty} d\tau\; \frac{d^n x_k}{d\tau^n}(\tau)\,\mathrm{e}^{-i\,\omega_e\,\tau} = \int_{-\infty}^{\infty} ds\; K_{jD}(s)\,\mathrm{e}^{-i\,\omega_e\,s} \int_{-\infty}^{\infty} d\tau\; \zeta(\tau)\,\mathrm{e}^{-i\,\omega_e\,t},$$

or, changing the variable s for t, and once again remembering the causality of $K_{jk}^{[n]}(t)$, and calling the Fourier transform of the incident wave elevation as the complex variable $A_I(\omega_e)$,

$$-\omega_e^2(M_{jk} + a_{jk})\,\tilde{x}_k(\omega_e) + i\,\omega_e\,b_{jk}\,\tilde{x}_k(\omega_e) + (C_{jk} + c_{jk})\tilde{x}_k(\omega_e) + (i\,\omega_e)^n \left(\int_0^{\infty} dt\; K_{jk}^{[n]}(t)\,\mathrm{e}^{-i\,\omega_e\,t}\right) \tilde{x}_k(\omega_e) = \left(\int_{-\infty}^{\infty} dt\; K_{jD}(t)\,\mathrm{e}^{-i\,\omega_e\,t}\right) A_I(\omega_e). \tag{3.33}$$

A desirable frequency domain representation of the equation of motions would be given as

$$\sum_{k=1}^{6} \left[-\omega_e^2(M_{jk} + A_{jk}(\omega_e)) + i\,\omega_e\,B_{jk}(\omega_e) + C_{jk}\right] \tilde{x}_k(\omega_e) = F_D(\omega_e)\,A_I(\omega_e), \qquad j = 1, \ldots, 6, \tag{3.34}$$

where $A_{jk}(\omega_e)$ is the frequency domain added mass, $B_{jk}(\omega_e)$ the frequency-domain potential damping and $F_D(\omega_e)$ is the diffraction exciting force. Equating the quantities in (3.33) and (3.34), we will be able to write

$$\begin{aligned} A_{jk}(\omega_e) &= a_{jk} - \frac{c_{jk}}{\omega_e^2} - \mathrm{Re}\left[\frac{(i\,\omega_e)^n}{\omega_e^2} \int_0^{\infty} dt\; K_{jk}^{[n]}(t)\,\mathrm{e}^{-i\,\omega_e\,t}\right] \\ B_{jk}(\omega_e) &= b_{jk} - \mathrm{Im}\left[\frac{i\,(i\,\omega_e)^n}{\omega_e} \int_0^{\infty} dt\; K_{jk}^{[n]}(t)\,\mathrm{e}^{-i\,\omega_e\,t}\right] \\ F_D(\omega_e) &= \int_{-\infty}^{\infty} dt\; K_{jD}(t)\,\mathrm{e}^{-i\,\omega_e\,t}. \end{aligned} \tag{3.35}$$

We could have included c_{jk} in the definition of a frequency-domain forward-speed restoring coefficient $C_{jk}^{(w)}$, but since the frequency-domain approach usually does not use this representation and we can always include this term with the added-mass coefficient, this was the final choice.

3.4.2 Local Quantities

As defined in (3.20), in the time domain we represent the radiation potential as

$$\phi_k(\vec{x},t) = \mathcal{N}_k(\vec{x})\dot{\vec{x}}(t) + \mathcal{M}_k(\vec{x})\vec{x}(t) + \int_{-\infty}^{\infty} d\tau\ \psi_k^{[n]}(\vec{x},t-\tau)\frac{d^n x_k}{d\tau^n}(\tau) \tag{3.36}$$

so its frequency-domain representation will be given as

$$\begin{aligned}\mathcal{F}\left(\phi_k(\vec{x},t)\right) &= \mathcal{F}\left(\mathcal{N}_k(\vec{x})\dot{\vec{x}}(t) + \mathcal{M}_k(\vec{x})\vec{x}(t)\right) + \\ &\int_{-\infty}^{\infty} dt \int_{-\infty}^{\infty} d\tau\ \psi_k^{[n]}(\vec{x},t-\tau)\frac{d^n x_k}{d\tau^n}(\tau)\,\mathrm{e}^{-i\,\omega_e\,t}\end{aligned} \tag{3.37}$$

Applying the Fourier transforms and changing variables in the same way as in the last section, we will have

$$\begin{aligned}\tilde{\phi}_k(\vec{x},\omega_e) &= i\,\omega_e\,\mathcal{N}_k(\vec{x})\,\tilde{x}_k(\omega_e) + \mathcal{M}_k(\vec{x})\,\tilde{x}_k(\omega_e) + \\ &(i\,\omega_e)^n\left(\int_0^{\infty} dt\ \psi_k^{[n]}(\vec{x},t)\,\mathrm{e}^{-i\,\omega_e\,t}\right)\tilde{x}_k(\omega_e).\end{aligned} \tag{3.38}$$

We can see a comparison of computed values for the radiation potential on the free surface in the frequency domain using the *TIMIT* and the *WAMIT* codes, in the six degrees of freedom, in figures (3-5) to (3-10). *TIMIT* results were computed for ship speed ranging from $Fr = 0$ to $Fr = 0.25$. The radiation velocity is evaluated by operating with ∇ in (3.36) and following the same development as for the radiation potential, so

$$\begin{aligned}\nabla\tilde{\phi}_k(\vec{x},\omega_e) &= i\,\omega_e\,\nabla\mathcal{N}_k(\vec{x})\,\tilde{x}_k(\omega_e) + \nabla\mathcal{M}_k(\vec{x})\,\tilde{x}_k(\omega_e) + \\ &(i\,\omega_e)^n\left(\int_0^{\infty} dt\ \nabla\psi_k^{[n]}(\vec{x},t)\,\mathrm{e}^{-i\,\omega_e\,t}\right)\tilde{x}_k(\omega_e).\end{aligned} \tag{3.39}$$

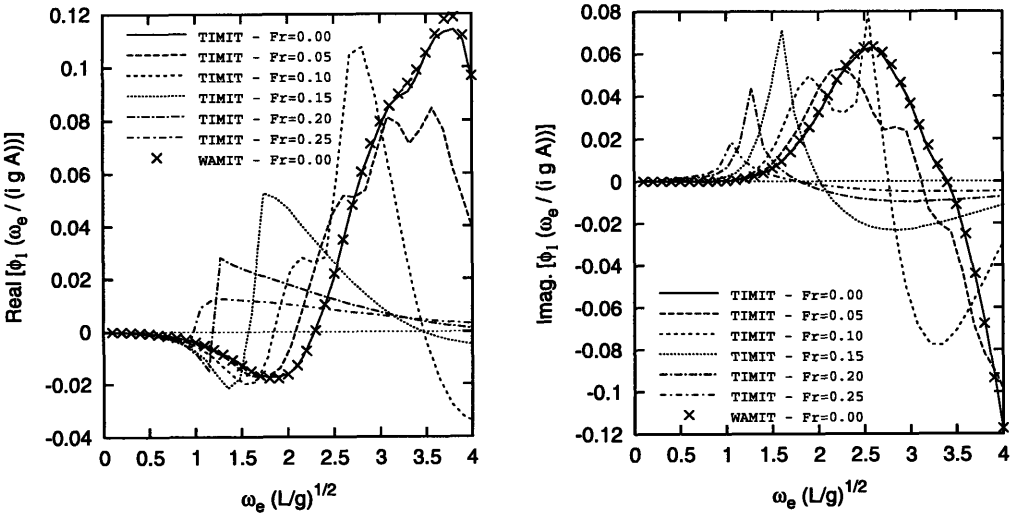

Figure 3-5: Non-Dimensional radiation surge potential at the point $\frac{x}{L} = 0.4$, $\frac{y}{L} = 0.2$ and $\frac{z}{L} = 0.0$. Results from *WAMIT* and *TIMIT* codes, $Fr = 0$ to $Fr = 0.25$.

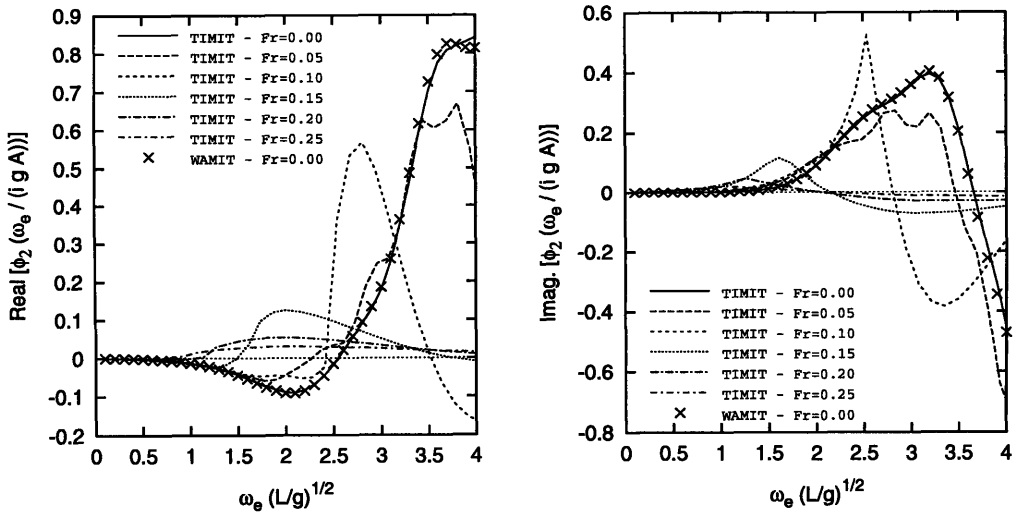

Figure 3-6: Non-Dimensional radiation sway potential at the point $\frac{x}{L} = 0.4$, $\frac{y}{L} = 0.2$ and $\frac{z}{L} = 0.0$. Results from *WAMIT* and *TIMIT* codes, $Fr = 0$ to $Fr = 0.25$.

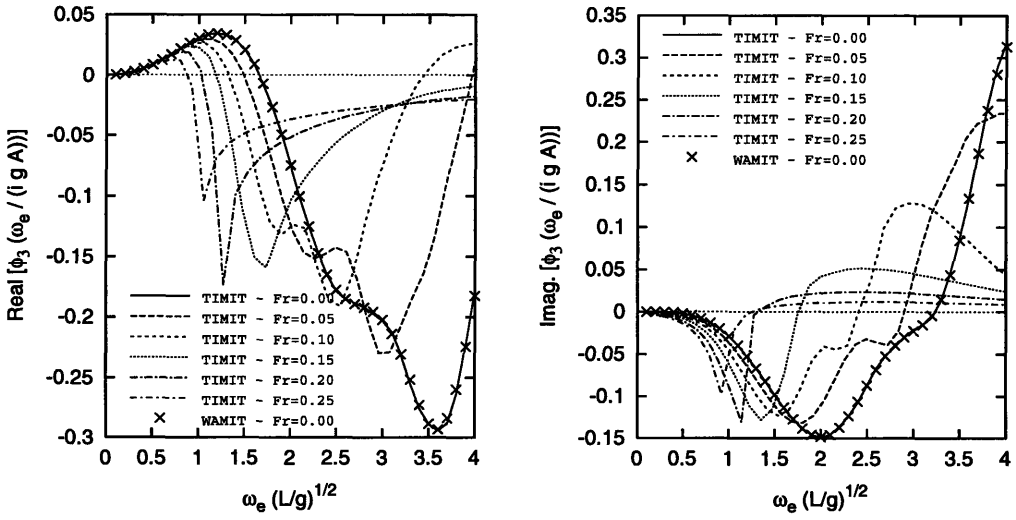

Figure 3-7: Non-Dimensional radiation heave potential at the point $\frac{x}{L} = 0.4$, $\frac{y}{L} = 0.2$ and $\frac{z}{L} = 0.0$. Results from *WAMIT* and *TIMIT* codes, $Fr = 0$ to $Fr = 0.25$.

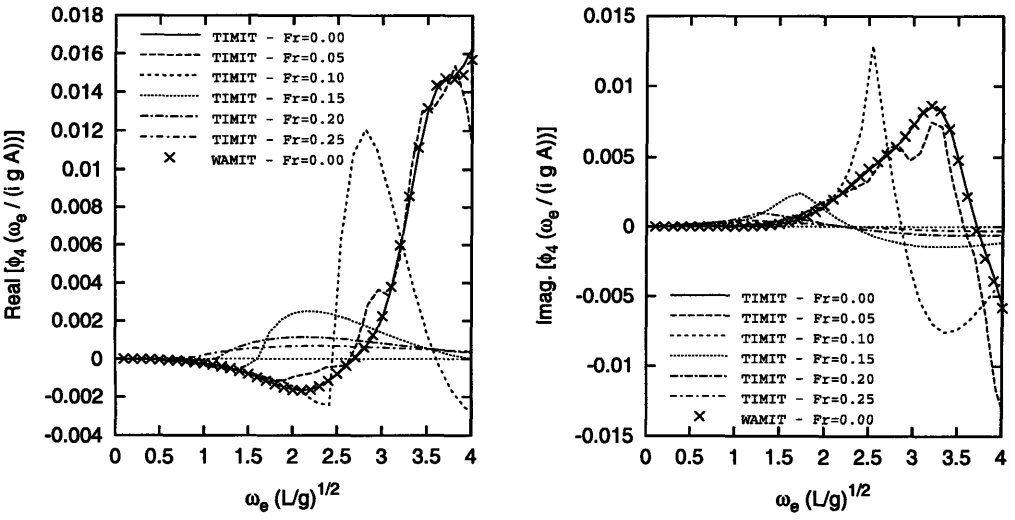

Figure 3-8: Non-Dimensional radiation roll potential at the point $\frac{x}{L} = 0.4$, $\frac{y}{L} = 0.2$ and $\frac{z}{L} = 0.0$. Results from *WAMIT* and *TIMIT* codes, $Fr = 0$ to $Fr = 0.25$.

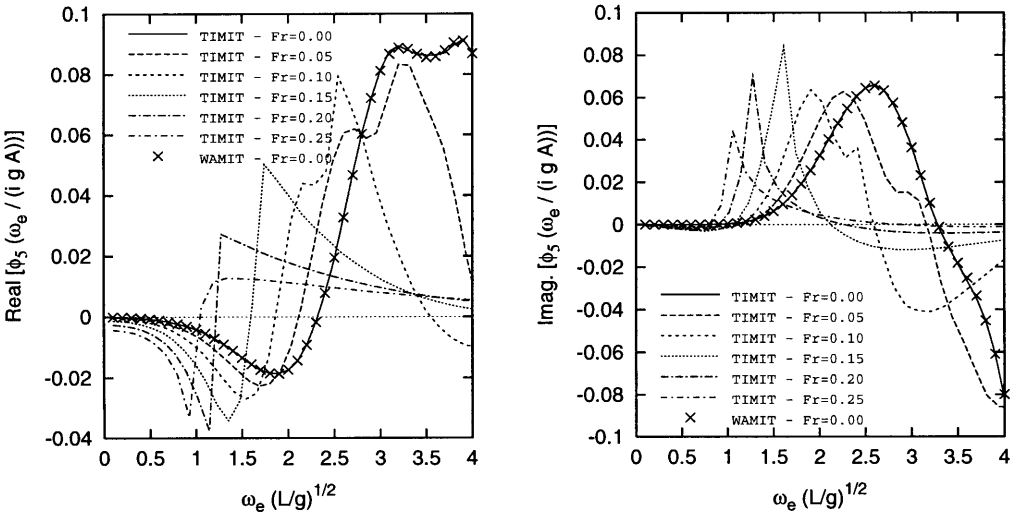

Figure 3-9: Non-Dimensional radiation pitch potential at the point $\frac{x}{L} = 0.4$, $\frac{y}{L} = 0.2$ and $\frac{z}{L} = 0.0$. Results from *WAMIT* and *TIMIT* codes, $Fr = 0$ to $Fr = 0.25$.

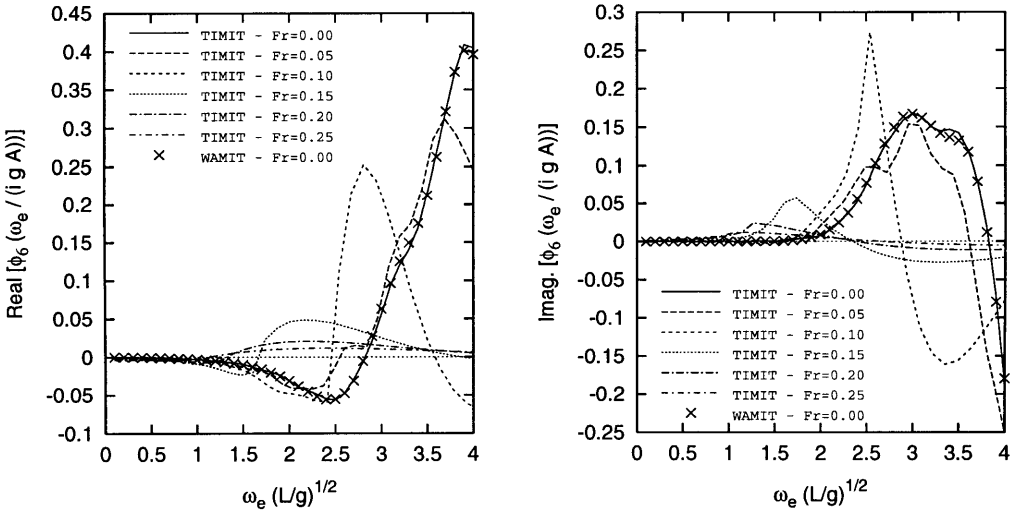

Figure 3-10: Non-Dimensional radiation yaw potential at the point $\frac{x}{L} = 0.4$, $\frac{y}{L} = 0.2$ and $\frac{z}{L} = 0.0$. Results from *WAMIT* and *TIMIT* codes, $Fr = 0$ to $Fr = 0.25$.

For the diffraction potential our frequency-domain representation will be given as

$$\mathcal{F}\left(\phi_S(\vec{x},t)+\phi_I(\vec{x},t)\right) = \int_{-\infty}^{\infty} dt \int_{-\infty}^{\infty} d\tau \ \left(\phi_S(\vec{x},t-\tau)+\phi_I(\vec{x},t-\tau)\right)\zeta(\tau)\,\mathrm{e}^{-i\omega_e t}, \quad (3.40)$$

but we know the closed form of the incident potential in the frequency domain, so there will be no need to compute its Fourier transform and the final representation will be given as

$$\tilde{\phi}_I(\vec{x},\omega_e) = \frac{igA}{\omega_0}\exp[K_0(z+-ix\cos\beta-iy\sin\beta)+i\omega_e t] \quad (3.41)$$

$$\tilde{\phi}_S(\vec{x},\omega_e) = \int_{-\infty}^{\infty} dt\ \phi_S(t)\,\mathrm{e}^{-i\omega_e t}, \quad (3.42)$$

and the scattered wave velocity as

$$\nabla\tilde{\phi}_S(\vec{x},\omega_e) = \int_{-\infty}^{\infty} dt\ \nabla\phi_S(t)\,\mathrm{e}^{-i\omega_e t}. \quad (3.43)$$

We can see that the potential representation in the frequency domain is smoother in the diffraction problem then in the radiation problem. This happens because (1) in the diffraction problem the incident wave potential, which is very smooth, will give the main contribution when compared to the scattered potential, and (2) in the radiation problem we will have that waves radiated from the body with group velocity less than the ship forward velocity will not reach the point where the potential is being computed. This means that waves with a nondimensional frequency greater than $w_e\sqrt{L/g} = 1/(4\mathrm{Fr})$ will never reach the point if they have to move against the current. This fact will contribute with some more spikes to the frequency domain representation of the radiation potential.

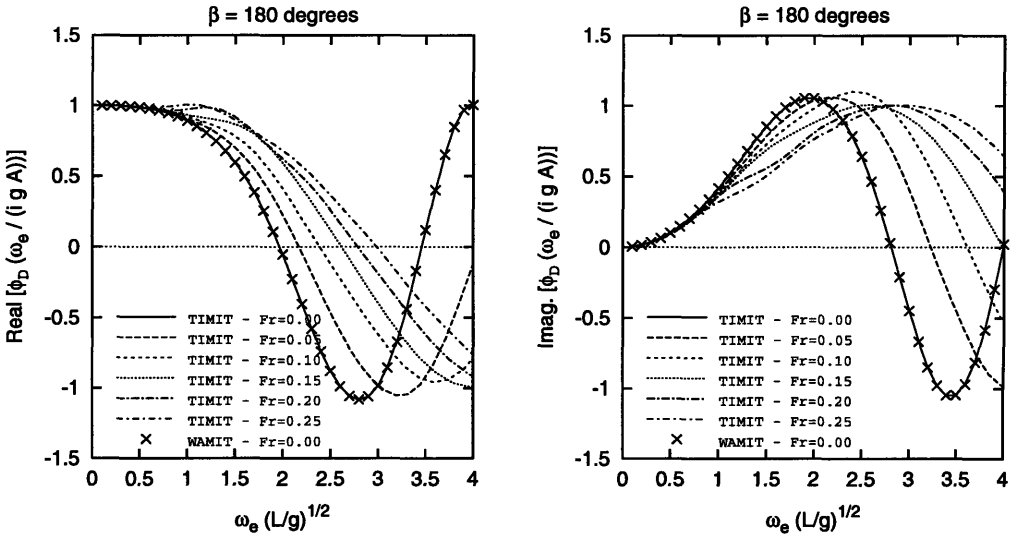

Figure 3-11: Non-Dimensional diffraction potential at the point $\frac{x}{L} = 0.4$, $\frac{y}{L} = 0.2$ and $\frac{z}{L} = 0.0$. Results from *WAMIT* and *TIMIT* codes, $Fr = 0$ to $Fr = 0.25$, incident waves heading equal to 180 degrees.

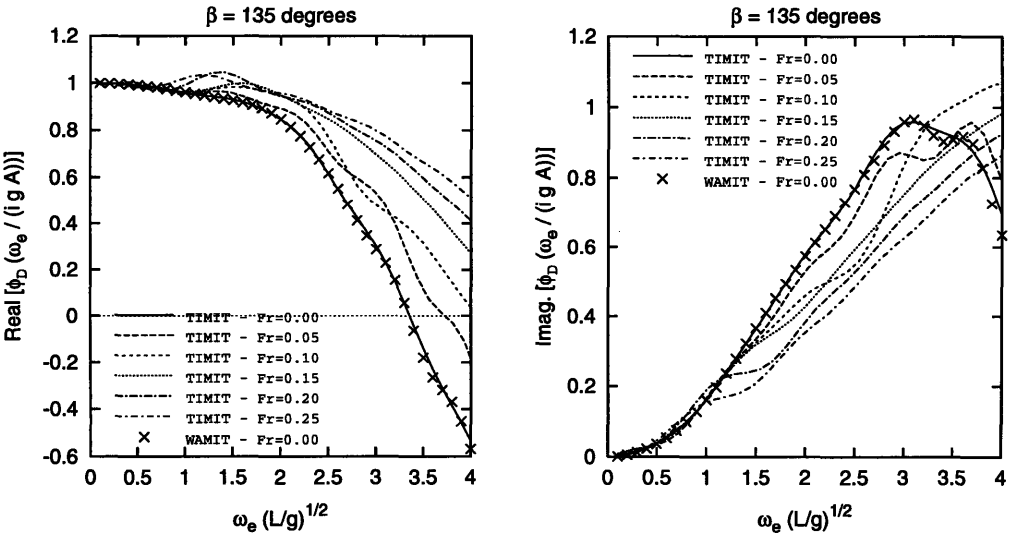

Figure 3-12: Non-Dimensional diffraction potential at the point $\frac{x}{L} = 0.4$, $\frac{y}{L} = 0.2$ and $\frac{z}{L} = 0.0$. Results from *WAMIT* and *TIMIT* codes, $Fr = 0$ to $Fr = 0.25$, incident waves heading equal to 135 degrees.

Chapter 4

Second-Order Steady Forces

4.1 Pressure Integration

Under the irrotational, ideal flow assumption, after obtaining the velocity potential that describes the flow around our body, the most natural way of computing hydrodynamic forces is by integrating the hydrodynamic pressure over its surface. This means taking an integral over the instantaneous wetted body surface (S_b). The transfer from this surface to the mean wetted surface (S_{bm}) will be made, using Taylor expansions under the small wave amplitude and small body-motions approach.

This approach will be followed, and the computation of forces by the integration of pressures will be outlined for the Neumann-Kelvin case, expanding Ogilvie's development [36] for the non-zero forward-velocity case.

Consistent with the Neumann-Kelvin approach, Bernoulli equation (2.2) will be given as

$$p = -\rho\left(\varphi_t + \frac{1}{2}\nabla\varphi\cdot\nabla\varphi - U\,\frac{\partial\varphi}{\partial x} + g\,z\right), \tag{4.1}$$

and we will have the wave elevation up to second order, under the Neumann-Kelvin flow and the small wave amplitude hypothesis, as

$$\begin{aligned}\eta(x,y,t) \;=\; & \varepsilon\left[-\frac{1}{g}\left(\varphi_t^{(1)} - U\,\varphi_x^{(1)}\right)\right] + \varepsilon^2\left\{-\frac{1}{g}\left(\frac{\nabla\varphi^{(1)}\cdot\nabla\varphi^{(1)}}{2} + \varphi_t^{(2)} - U\,\varphi_x^{(2)}\right)\right. \\ & \left. + \frac{1}{g^2}\left[\varphi_t^{(1)}\varphi_{zt}^{(1)} - U\left(\varphi_t^{(1)}\varphi_{xz}^{(1)} + \varphi_x^{(1)}\varphi_{zt}^{(1)}\right) + U^2\,\varphi_x^{(1)}\varphi_{xz}^{(1)}\right]\right\} \\ & + O(\varepsilon^3) \qquad\qquad \text{on } z = 0. \end{aligned} \tag{4.2}$$

We are going to define the first-order ship motions as

$$\begin{aligned}\vec{\xi} &= \{\xi_1,\xi_2,\xi_3\} = \{\text{surge},\text{sway},\text{heave}\} \\ &= \vec{\xi}^{(1)} + \vec{\xi}^{(2)} + \vec{\xi}^{(3)} + \ldots \\ \vec{\Omega} &= \{\xi_4,\xi_5,\xi_6\} = \{\text{roll},\text{pitch},\text{yaw}\} \\ &= \vec{\Omega}^{(1)} + \vec{\Omega}^{(2)} + \vec{\Omega}^{(3)} + \ldots, \end{aligned} \tag{4.3}$$

and, following Ogilvie [36], we see that we can relate the position vectors on $\vec{x}_s$ and $\vec{x}$ through

$$\vec{x} = \vec{x}_s + \varepsilon\left(\vec{\xi} + \vec{\Omega}\times\vec{x}_s\right) + \varepsilon^2\left(\mathbf{H}\,\vec{x}_s\right) + O(\varepsilon^3), \tag{4.4}$$

where $\mathbf{H}$ is a rotation matrix including second-order corrections to the vectorial product, first-order rotation, and is defined as

$$\mathbf{H} = -\frac{1}{2}\begin{bmatrix} (\xi_5^2\xi_6^2) & 0 & 0 \\ -2\xi_4\xi_5 & (\xi_4^2\xi_6^2) & 0 \\ -2\xi_4\xi_6 & -2\xi_5\xi_6 & (\xi_4^2\xi_5^2) \end{bmatrix}. \tag{4.5}$$

We can also relate the normal vectors, defined in the body fixed moving reference frame ($\vec{n}_s$) and in the steady moving reference frame ($\vec{n}$) through

$$\begin{aligned}
\vec{n} = \quad & \{n_1, n_2, n_3\} = \vec{n}_s + \varepsilon \left(\vec{\Omega} \times \vec{n}_s\right) + \varepsilon^2 \left(\mathbf{H}\, \vec{n}_s\right) + O(\varepsilon^3) \\
\vec{x} \times \vec{n} = \quad & \{n_4, n_5, n_6\} = \vec{x}_s \times \vec{n}_s + \varepsilon \left[\vec{\xi} \times \vec{n}_s + \vec{\Omega} \times (\vec{x}_s \times \vec{n}_s)\right] + \\
& \varepsilon^2 \left[\vec{\xi} \times \left(\vec{\Omega} \times \vec{n}_s\right) + \mathbf{H}\ (\vec{x}_s \times \vec{n}_s)\right] + O(\varepsilon^3).
\end{aligned} \tag{4.6}$$

Integrating the pressures over the hull surface we will get the total force acting on the floating body, which will be given as

$$\vec{F}(\omega_e) = \iint_{S_b} \vec{n}_s\, p\, dS. \tag{4.7}$$

We have already Fourier transformed the potentials and velocities from the time domain to the frequency domain, and we know that given two complex quantities A and B, with a time dependency as $\mathrm{e}^{\,iwt}$,

$$\mathrm{Re}\,(A\,\mathrm{e}^{\,iwt})\,\mathrm{Re}\,(B\,\mathrm{e}^{\,iwt}) \;=\; \frac{1}{2}\,\mathrm{Re}\,(A\,B\,\mathrm{e}^{\,i2wt} + A\,B^*), \tag{4.8}$$

where B^* denotes the complex conjugate of B, so it is easy to compute the steady part of the terms coming from the first-order solution. Here we will show the second-order terms contributing to the force and moment and it should be implicit that the second-order steady contribution is to be collected from the second-order force and moment using (4.8), and disregarding the contribution to the sum-frequency forces.

The integral in Equation (4.7) is to be taken over the instantaneous ship surface S_b, not known *a priori*, and we want to evaluate it on the known surface S_{bm}. We can use relations (4.4) and (4.6) to account for the proper relative positions of the surfaces. Equation (4.4) can be seen as a relation between the position vectors in $\vec{x}$ and $\vec{x}_s$ or as a function relating a point on the mean surface S_{bm} and the actual surface S_b. The same consideration goes for equation (4.6), with respect to the body normals $\vec{n}$ and $\vec{n}_s$. It is easy to see that in Figure 4-1, where $\vec{x}_s$ is a position vector in the frame of reference fixed on the ship.

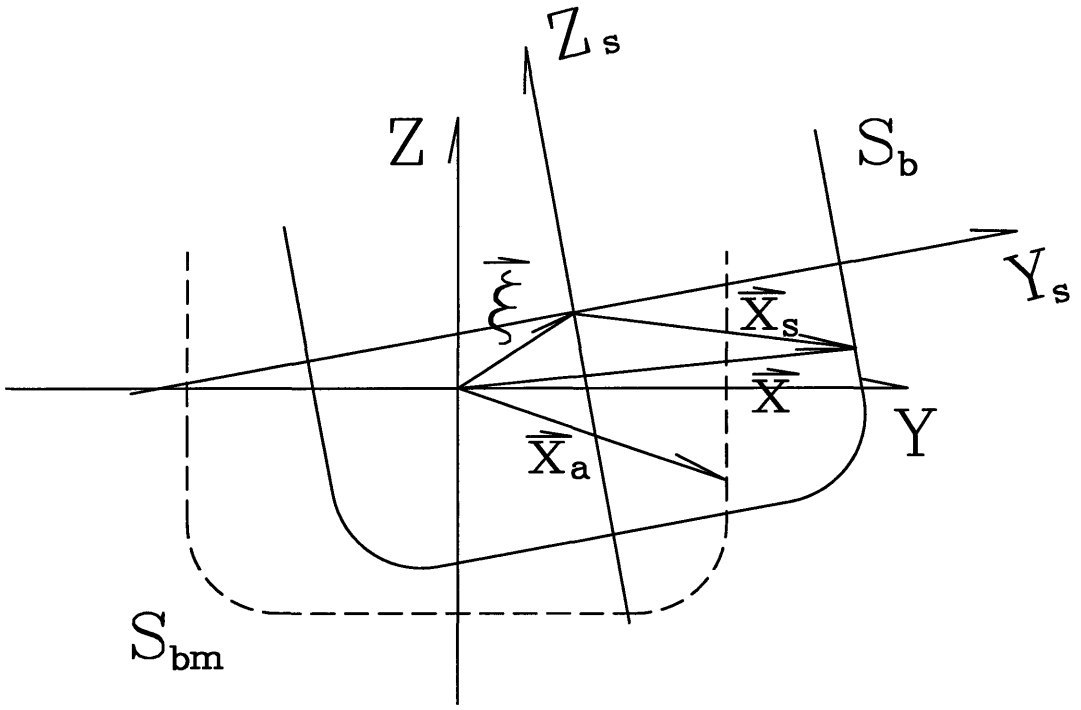

Figure 4-1: The two coordinate systems showing the two possible interpretations of equation (4.4).

Equation (4.4) can be interpreted as transforming $\vec{x}_s$ into $\vec{x}$ (up to second order), described in the moving reference frame with mean ship speed. The other interpretation of (4.4) is given when we look at $\vec{x}_a$ in the same figure, which will be a position vector over S_{bm} having the same coordinates in the mean ship speed reference frame as $\vec{x}_s$ in the body fixed reference frame. In this case the equation will transform a point on S_{bm} to its place over S_b, correct up to second order on φ. Both position vectors ($\vec{x}_a$ and $\vec{x}$) are described on the mean ship speed reference system. Our first-order pressure was computed with respect to the body mean position. Taylor expanding the pressure to the actual instantaneous position we will have

$$p|_{S_b} = p|_{S_{bm}} + (\vec{x} - \vec{x}_s) \cdot \nabla\, p|_{S_{bm}} + O(\varepsilon^3). \tag{4.9}$$

Substituting (4.1) and (4.4) in (4.9) we will get

$$\begin{aligned} p|_{S_b} &= -\rho\left[g\,z+\varepsilon\left(\varphi_t-U\,\frac{\partial\varphi}{\partial x}\right)+\varepsilon^2\,\frac{1}{2}\,|\nabla\varphi|^2+O(\varepsilon^3)\right] \\ &\quad -\rho\left[\varepsilon\left(\vec{\xi}+\vec{\Omega}\times\vec{x}_s\right)+\varepsilon^2\,(\mathbf{H}\,\vec{x}_s)+O(\varepsilon^3)\right]\cdot \\ &\quad \nabla\left[g\,z+\varepsilon\left(\varphi_t-U\,\frac{\partial\varphi}{\partial x}\right)+\varepsilon^2\,\frac{1}{2}\,|\nabla\varphi|^2+O(\varepsilon^3)\right], \end{aligned} \tag{4.10}$$

or looking at the order of each term, and dropping the s subscript of $\vec{x}_s$ as it is clear that our interpretation of (4.4) actually refers to a position vector over S_{bm} being transformed to S_b,

$$\begin{aligned} p|_{S_b} &= -\rho\,g\,z-\varepsilon\,\rho\left[\varphi_t^{(1)}-U\,\varphi_x^{(1)}+g\,(\xi_3+\xi_4\,y-\xi_5\,x)\right] \\ &\quad -\varepsilon^2\,\rho\left[\varphi_t^{(2)}-U\,\varphi_x^{(2)}+\frac{1}{2}\,|\nabla\varphi|^2+\left(\vec{\xi}+\vec{\Omega}\times\vec{x}\right)\cdot\nabla\left(\varphi_t^{(1)}-U\,\varphi_x^{(1)}\right)\right] \\ &\quad -\varepsilon^2\,\rho\,g\,\left(\mathbf{H}\,x\cdot\hat{k}\right)+O(\varepsilon^3). \end{aligned} \tag{4.11}$$

Substituting (4.6) and (4.11) in (4.7), also dropping the subscript s from $\vec{x}_s$ and the normal $\vec{n}_s$, and grouping the terms by order, we will have the force as

$$\begin{aligned} \vec{F}(\omega_e) &= \rho\iint_{S_{bm}} dS\,\left[\vec{n}+\varepsilon\left(\vec{\Omega}\times\vec{n}\right)+\varepsilon^2\,(\mathbf{H}\,\vec{n})\right] \\ &\quad \Big\{g\,z-\varepsilon\,\left[\varphi_t^{(1)}-U\,\varphi_x^{(1)}+g\,(\xi_3+\xi_4\,y-\xi_5\,x)\right] \\ &\quad -\varepsilon^2\,\left[\varphi_t^{(2)}-U\,\varphi_x^{(2)}+\frac{1}{2}\,|\nabla\varphi|^2+\left(\vec{\xi}+\vec{\Omega}\times\vec{x}\right)\cdot\nabla\left(\varphi_t^{(1)}-U\,\varphi_x^{(1)}\right)\right] \\ &\quad -\varepsilon^2\,g\,\left(\mathbf{H}\,x\cdot\hat{k}\right)\Big\}+\iint_{\Delta S_{bm}}\vec{n}\,p\,dS+O(\varepsilon^3), \end{aligned} \tag{4.12}$$

and the moments, using the definition of $\{n_4, n_5, n_6\}$ in (4.6), as

$$\begin{aligned}
\vec{M}(\omega_e) \;=\; & \rho \iint_{S_{bm}} dS \left\{ \vec{x} \times \vec{n} + \varepsilon \left[\vec{\xi} \times \vec{n} + \vec{\Omega} \times (\vec{x} \times \vec{n}) \right] \right. \\
& \left. + \varepsilon^2 \left[\vec{\xi} \times \left(\vec{\Omega} \times \vec{n} \right) + \mathbf{H} \; (\vec{x} \times \vec{n}) \right] \right\} \\
& \left\{ g\, z - \varepsilon \left[\varphi_t^{(1)} - U\, \varphi_x^{(1)} + g\, (\xi_3 + \xi_4\, y - \xi_5\, x) \right] \right. \\
& - \varepsilon^2 \left[\frac{1}{2} |\nabla \varphi|^2 + \left(\vec{\xi} + \vec{\Omega} \times \vec{x} \right) \cdot \nabla \left(\varphi_t^{(1)} - U\, \varphi_x^{(1)} \right) \right. \\
& \left. \left. - g \left(\mathbf{H}\, x \cdot \hat{k} \right) + \varphi_t^{(2)} - U\, \varphi_x^{(2)} \right] \right\} \\
& + \iint_{\Delta S_{bm}} (\vec{x} \times \vec{n})\; p\; dS + O(\varepsilon^3),
\end{aligned} \tag{4.13}$$

where the corrections $\iint_{\Delta S_{bm}} \vec{n}_s\, p\; d\vec{x}$ and $\iint_{\Delta S_{bm}} (\vec{x} \times \vec{n})\; p\; d\vec{x}$ stand for the integrals having to be taken over S_b, going up to where the water surface intersects the instantaneous body surface as we can see in Figure 4-2. Integrating only over S_{bm} makes our integrals stop at $z_s = 0$, not taking into account the $O(\varepsilon)$ missing part.

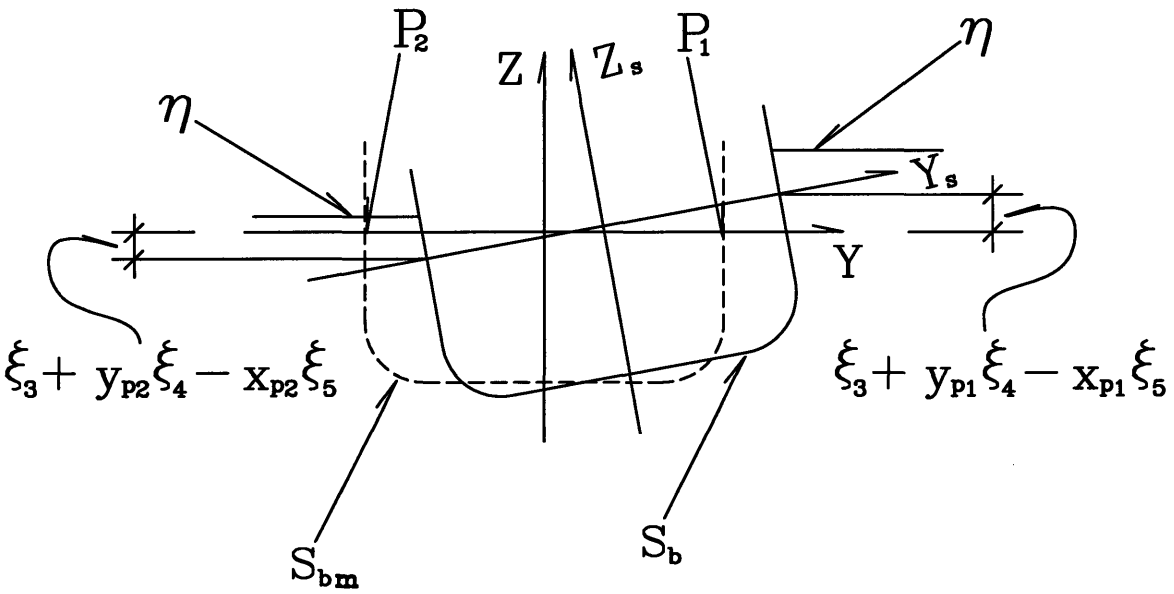

Figure 4-2: The two coordinate systems showing the differences on the boundary over the still waterline we should include on the integral over the mean wetted ship surface (dotted lines) to be mathematically equivalent to the actual (solid lines) position.

This correction is mathematically expressed as

$$\iint_{\Delta S_{bm}} \vec{n}\, p\, dS = -\rho \oint_{WL} dl \int_0^{\varepsilon(\eta-\xi_3-y\,\xi_4+x\,\xi_5)} dz \left[\vec{n} + \varepsilon\left(\vec{\Omega}\times\vec{n}\right) + O(\varepsilon^2)\right] \left\{g\,z + \varepsilon\, g\left[\varphi_t - U\,\frac{\partial\varphi}{\partial x} + (\xi_3 + \xi_4\, y - \xi_5\, x)\right] + O(\varepsilon^2)\right\} \quad (4.14)$$

and similarly, the correction for the moment,

$$\iint_{\Delta S_{bm}} (\vec{x}\times\vec{n})\, p\, dS = -\rho \oint_{WL} dl \int_0^{\varepsilon(\eta-\xi_3-y\,\xi_4+x\,\xi_5)} dz \left\{\vec{x}\times\vec{n} + \varepsilon\left[\vec{\xi}\times\vec{n} + \vec{\Omega}\times(\vec{x}\times\vec{n})\right] + O(\varepsilon^2)\right\} \left\{g\,z + \varepsilon\, g\left[\varphi_t - U\,\frac{\partial\varphi}{\partial x} + (\xi_3 + \xi_4\, y - \xi_5\, x)\right] + O(\varepsilon^2)\right\}. \quad (4.15)$$

The second-order terms coming from the line-integral corrections (4.14) and (4.15) that will contribute to the second-order steady force are

$$\iint_{\Delta S_{bm}} \vec{n}\, p\, dS = -\rho\, g \oint_{WL} dl\, \vec{n}\,(\eta - \xi_3 - y\xi_4 + x\xi_5)^2, \quad (4.16)$$

and

$$\iint_{\Delta S_{bm}} (\vec{x}\times\vec{n})\, p\, dS = -\rho\, g \oint_{WL} dl\, (\vec{x}\times\vec{n})\,(\eta - \xi_3 - y\xi_4 + x\xi_5)^2. \quad (4.17)$$

Inspecting (4.12) and (4.13), we can define the second-order hydrostatic forces to be

$$\vec{F}^{(2)}_{hst}(\omega_e) = -\rho\, g \iint_{S_{bm}} dS\, \vec{n}\left[\left(\mathbf{H}\, x\cdot\hat{k}\right) + \left(\vec{\Omega}\times\vec{n}\right)(\xi_3 + \xi_4\, y - \xi_5\, x) + (\mathbf{H}\,\vec{n})\, z\right] = -\hat{k}\,\rho\, g\,(\xi_4\xi_6 A_{wp} x_f + \xi_5\xi_6 A_{wp} y_f), \quad (4.18)$$

where A_{wp} is the waterplane area and x_f and y_f are the centers of flotation on the

waterline plane. For the moments we will have

$$\begin{aligned}
\vec{M}^{(2)}_{hst}(\omega_e) &= -\rho g \iint_{S_{bm}} dS \left[\vec{\xi}\times\vec{n}+\vec{\Omega}\times(\vec{x}\times\vec{n})\right](\xi_3+\xi_4 y-\xi_5 x) \\
&\quad -\rho g \iint_{S_{bm}} dS\ (\vec{x}\times\vec{n})\left(\mathbf{H}\,x\cdot\hat{k}\right) \\
&\quad -\rho g \iint_{S_{bm}} dS \left[\mathbf{H}\ (\vec{x}\times\vec{n})+\vec{\xi}\times\left(\vec{\Omega}\times\vec{n}\right)\right] z \\
&= \hat{\imath}\,\rho g\left\{\mathcal{V}\left[-\frac{y_b}{2}(\xi_4^2+\xi_6^2)+x_b\xi_4\xi_5\right]+[(L_{11}-L_{22})\xi_5\xi_6\right. \\
&\quad \left.-2L_{12}\xi_4\xi_6+A_{wp}(\,\xi_2\xi_5-x_f\xi_3\xi_6\,)-A_{wp}\xi_3\xi_2-A_{wp}y_f\xi_2\xi_4]\right\} \\
&\quad +\hat{\jmath}\,\rho g\left\{\mathcal{V}\frac{x_b}{2}(\xi_5^2+\xi_6^2)+[(L_{11}-L_{22})\xi_4\xi_6+2L_{12}\xi_5\xi_6\right. \\
&\quad \left.+A_{wp}\xi_3\xi_1+A_{wp}y_f\,(\xi_1\xi_4-\xi_3\xi_6)-A_{wp}x_f\xi_1\xi_5]\right\} \\
&\quad +\hat{k}\,\rho g\left[-(L_{11}-L_{22})\xi_4\xi_5+L_{12}(\xi_4^2-\xi_5^2)\right. \\
&\quad \left.+A_{wp}x_f\xi_3\xi_4+A_{wp}y_f\xi_3\xi_5\right], \qquad (4.19)
\end{aligned}$$

where $\mathcal{V}$ stands for the displaced volume, x_b, y_b and z_b as the coordinates of the center of buoyancy, and L_{ij} as the integral $\iint_{Awp} x_i x_j\ dS$. Now we can represent the second-order terms contributing to the total steady force as

$$\begin{aligned}
\vec{F}^{(2)}(\omega_e) &= \rho\iint_{S_{bm}}\vec{n}\left(U\,\varphi_x^{(2)}\right)\,dS-\rho\iint_{S_{bm}}\vec{n}\left(\frac{1}{2}\left|\nabla\varphi^{(1)}\right|^2\right)\,dS \\
&\quad -\rho\iint_{S_{bm}}\vec{n}\left[\left(\vec{\xi}+\vec{\Omega}\times\vec{x}\right)\cdot\nabla\left(\varphi_t^{(1)}-U\,\varphi_x^{(1)}\right)\right]\,dS \\
&\quad -\rho\iint_{S_{bm}}\left\{\left(\vec{\Omega}\times\vec{n}\right)\cdot\left[\varphi_t^{(1)}-U\,\varphi_x^{(1)}+g\ (\xi_3+\xi_4 y-\xi_5 x)\right]\right\}\,dS \\
&\quad -\rho g\oint_{WL}\vec{n}\,(\eta-\xi_3-y\xi_4+x\xi_5)^2\ dl+\vec{F}^{(2)}_{hst}(\omega_e), \qquad (4.20)
\end{aligned}$$

and to the second-order steady moments as

$$\begin{aligned}
\vec{M}^{(2)}(\omega_e) &= \rho\iint_{S_{bm}}(\vec{x}\times\vec{n})\left(U\,\varphi_x^{(2)}\right)\,dS-\rho\iint_{S_{bm}}(\vec{x}\times\vec{n})\left(\frac{1}{2}\left|\nabla\varphi^{(1)}\right|^2\right)\,dS \\
&\quad -\rho\iint_{S_{bm}}(\vec{x}\times\vec{n})\left[\left(\vec{\xi}+\vec{\Omega}\times\vec{x}\right)\cdot\nabla\left(\varphi_t^{(1)}-U\,\varphi_x^{(1)}\right)\right]\,dS \\
&\quad -\rho\iint_{S_{bm}}\left[\vec{\xi}\times\vec{n}+\vec{\Omega}\times(\vec{x}\times\vec{n})\right]\left[\varphi_t^{(1)}-U\,\varphi_x^{(1)}+g\ (\xi_3+\xi_4 y-\xi_5 x)\right]\,dS \\
&\quad -\rho g\oint_{WL}(\vec{x}\times\vec{n})\,(\eta-\xi_3-y\xi_4+x\xi_5)^2\ dl+\vec{M}^{(2)}_{hst}(\omega_e) \qquad (4.21)
\end{aligned}$$

Another way to display the second-order forces and moments is by using the definition of the first-order forces and moments, enabling us not to recompute some terms that have already been evaluated when solving the first-order problem. Substituting (4.6) and (4.11) in (4.7) it is easy to collect the terms contributing to the first-order forces,

$$\begin{aligned}\vec{F}^{(1)}(\omega_e) &= -\rho \iint_{S_{bm}} \vec{n}\left[\varphi_t^{(1)} - U\,\varphi_x^{(1)} + g\,(\xi_3 + \xi_4\,y - \xi_5\,x)\right]\,dS \\ &\quad -\rho\,g \iint_{S_{bm}} z\,\left(\vec{\Omega}\times\vec{n}\right)\,dS, \end{aligned} \tag{4.22}$$

letting us state that

$$\begin{aligned}-\rho \iint_{S_{bm}} &\left(\vec{\Omega}\times\vec{n}\right)\left[\varphi_t^{(1)} - U\,\varphi_x^{(1)} + g\,(\xi_3 + \xi_4\,y - \xi_5\,x)\right]\,dS = \\ &\vec{\Omega}\times\vec{F}^{(1)} - \rho\,g\,\vec{\Omega}\times\iint_{S_{bm}} z\,\left(\vec{\Omega}\times\vec{n}\right)\,dS = \\ &\vec{\Omega}\times\vec{F}^{(1)} - \rho\,g\,\mathcal{V}\,\left[-\xi_4\,\xi_6\hat{\imath} - \xi_5\,\xi_6\hat{\jmath} + (\xi_4^2 + \xi_6^2)\hat{k}\right], \end{aligned} \tag{4.23}$$

to finally get an alternate way of representing the second-order steady forces as

$$\begin{aligned}\vec{F}^{(2)}(\omega_e) &= \rho\iint_{S_{bm}} \vec{n}\left(U\,\varphi_x^{(2)}\right)\,dS - \rho\iint_{S_{bm}} \vec{n}\left(\frac{1}{2}\left|\nabla\varphi^{(1)}\right|^2\right)\,dS \\ &\quad -\rho\iint_{S_{bm}} \vec{n}\left[\left(\vec{\xi} + \vec{\Omega}\times\vec{x}\right)\cdot\nabla\left(\varphi_t^{(1)} - U\,\varphi_x^{(1)}\right)\right]\,dS \\ &\quad -\rho\,g\oint_{WL} \vec{n}\,(\eta - \xi_3 - y\xi_4 + x\xi_5)^2\,dl \\ &\quad +\vec{\Omega}\times\vec{F}^{(1)} - \rho\,g\,A_{wp}\,(\xi_4\,\xi_6\,x_f + \xi_5\,\xi_6\,y_f)\,\hat{k}. \end{aligned} \tag{4.24}$$

The second-order steady moments can be redefined following the same lines. Noting that the first-order moment is given as

$$\begin{aligned}\vec{M}^{(1)}(\omega_e) &= -\rho\iint_{S_{bm}} (\vec{x}\times\vec{n})\left[\varphi_t^{(1)} - U\,\varphi_x^{(1)} + g\,(\xi_3 + \xi_4\,y - \xi_5\,x)\right]\,dS \\ &\quad -\rho\,g\iint_{S_{bm}} \left\{\left(\vec{\xi}\times\vec{n}\right)\,z + \left[\vec{\Omega}\times(\vec{x}\times\vec{n})\right]\,z\right\}\,dS, \end{aligned} \tag{4.25}$$

which will enable us to get the relation

$$
\begin{aligned}
-\rho \iint_{S_{bm}} \vec{\Omega} \times (\vec{x} \times \vec{n}) \left[\varphi_t^{(1)} - U\,\varphi_x^{(1)} + g\,(\xi_3 + \xi_4\,y - \xi_5\,x)\right]\,dS \\
&= \vec{\Omega}^{(1)} \times \vec{M}^{(1)} - \rho\,g\,\vec{\Omega} \times \iint_{S_{bm}} \left[\left(\vec{\xi} \times \vec{n}\right)\,z + \vec{\Omega} \times (\vec{x} \times \vec{n})\,z\right]\,dS \\
&= \vec{\Omega}^{(1)} \times \vec{M}^{(1)} - \rho\,g\,\mathcal{V}\,\vec{\Omega} \times \left[\vec{\Omega} \times (y_b\hat{\imath} - x_b\hat{\jmath}) + \left(\vec{\xi} \times \hat{k}\right)\right]. \qquad (4.26)
\end{aligned}
$$

Using the expression (4.22) for the first-order forces we will also be able to write the relation

$$
\begin{aligned}
\vec{\xi}^{(1)} \times \vec{F}^{(1)} \;=\; & -\rho \iint_{S_{bm}} \left(\vec{\xi} \times \vec{n}\right) \left[\varphi_t^{(1)} - U\,\varphi_x^{(1)} + g\,(\xi_3 + \xi_4\,y - \xi_5\,x)\right]\,dS \\
& -\rho\,g \iint_{S_{bm}} \vec{\xi} \times \left(\vec{\Omega} \times \vec{n}\right)\,z\,dS. \qquad (4.27)
\end{aligned}
$$

Finally, using (4.26)and (4.27) we may rewrite the second-order steady moments (4.21) as

$$
\begin{aligned}
\vec{M}^{(2)}(\omega_e) \;=\; & \rho \iint_{S_{bm}} (\vec{x} \times \vec{n}) \left(U\,\varphi_x^{(2)}\right)\,dS - \rho \iint_{S_{bm}} (\vec{x} \times \vec{n}) \left(\frac{1}{2}\left|\nabla\varphi^{(1)}\right|^2\right)\,dS \\
& -\rho \iint_{S_{bm}} (\vec{x} \times \vec{n}) \left[\left(\vec{\xi} + \vec{\Omega} \times \vec{x}\right) \cdot \nabla \left(\varphi_t^{(1)} - U\,\varphi_x^{(1)}\right)\right]\,dS \\
& -\rho\,g \oint_{WL} (\vec{x} \times \vec{n})\,(\eta - \xi_3 - y\xi_4 + x\xi_5)^2\,dl \\
& +\vec{\xi}^{(1)} \times \vec{F}^{(1)} + \vec{\Omega}^{(1)} \times \vec{M}^{(1)} \\
& +\rho\,g \left[-\mathcal{V}\xi_1\xi_6 + \mathcal{V}\xi_4\xi_5 x_b - \mathcal{V}\xi_5\xi_6 z_b - \frac{\mathcal{V}}{2}\left(\xi_4^2 - \xi_6^2\right) y_b - L_{12}\xi_4\xi_6 - L_{22}\xi_5\xi_6\right]\,\hat{\imath} \\
& +\rho\,g \left[-\mathcal{V}\xi_2\xi_6 + \mathcal{V}\xi_4\xi_6 z_b + \frac{\mathcal{V}}{2}\left(\xi_5^2 - \xi_6^2\right) x_b + L_{11}\xi_4\xi_6 + L_{12}\xi_5\xi_6\right]\,\hat{\jmath} \\
& +\rho\,g\,(\mathcal{V}\xi_1\xi_4 + \mathcal{V}\xi_2\xi_5 + \mathcal{V}\xi_5\xi_6 x_b - \mathcal{V}\xi_4\xi_6 y_b)\,\hat{k}. \qquad (4.28)
\end{aligned}
$$

4.2 Momentum Flux

An alternate approach for integrating pressures over the ship wetted surface is to use momentum conservation relations over a control surface encompassing the ship and moving with its same mean forward speed. By computing the momentum flux through this control surface we will be able to tell the steady forces and moments.

As we said in the first chapter, early work using this approach was restricted to information about the planar forces and yaw moment. At that time there were no general solutions for the unsteady flow close to the floating body, but asymptotic computation of the potential and fluid velocities far from the ship were possible, so defining a control surface at great distances from the body was the way of choice. The planar forces and yaw moments have in common the fact that some integrals over the mean free surface that show up when we employ this approach will not contribute for those components, and we can avoid the computation of hydrodynamic quantities in the near field.

Under our approach, the evaluation of the potential or fluid velocities far from the body is not an advantage, because we are computing first order quantities in the time domain to subsequently Fourier transform them to the frequency domain. Higher frequency waves, which travel with small group velocities, will require the solution of long transient problems to reach our control surface making this whole idea computationally too expensive.

Defining a compact surface close to the floating body and using the momentum flux relations over it in order to compute steady second-order forces and moments is much more feasible. This approach, which we have already used (Ferreira and Lee [7]) in connection with the WAMIT program, gave convergence of the drift forces faster than using the pressure integration method with equivalent number of panels over the body surface. To be fair in this comparison we have to remember that each field point on the control surface will be roughly as computationally expensive as an extra body panel, and a proper balance between the number of panels and number of field points should be found in order that this method becomes attractive.

The required number of control points over the outer surface was found to be approximately of the same order of magnitude than the number of panels over the body. Although theoretically we may refine the number of points on the outer surface just by computing the time history of the potential and velocities on new chosen control points, improving our numerical quadratures in the same computer run, this is not numerically an easy task, and has not yet been implemented. Each outer surface refinement requires a new run of the simulation program.

In Figure 4-3 below we show the body consisting of a half sphere inside the compact surface, which is defined as the sum of S_o, the surface defining an outer region bellow and around the body up to the actual free surface S_f, and S_f itself, the actual free surface that goes up to the body instantaneous surface S_b. We should note that the compact surface is represented as a "mesh" only for visualization purposes, being actually a set of chosen points where some quadratures will be performed, and which do not play any role in the solution of the potentials. The definition of those quadratures will be the development of this section.

The total linear momentum of the fluid inside the compact surface is given by

$$\vec{M}(t) = \rho \iiint_V \nabla\varphi \, dV, \tag{4.29}$$

where V is the fluid volume contained between the compact surface and the ship hull, and the total angular momentum is

$$\vec{A}(t) = \rho \iiint_V \vec{x} \times \nabla\varphi \, dV. \tag{4.30}$$

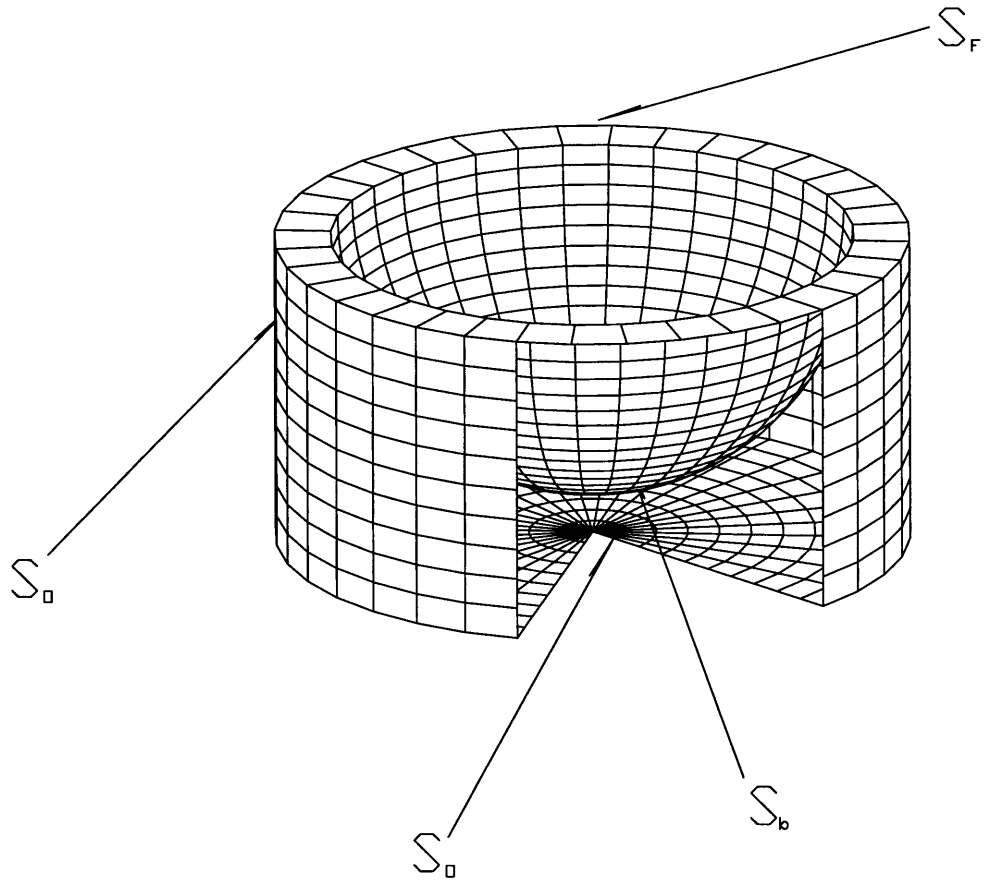

Figure 4-3: The compact surface ($S_o + S_f = S_{fo}$) surrounding the floating body S_{bm} (here a half sphere), without a 30 degrees sector on S_o for better visualization.

Using the transport theorem to compute the rate of change of the total momentum in the moving coordinate system, we will have

$$\frac{d\vec{M}(t)}{dt} = \rho \iiint_V \nabla\varphi_t \, dV + \rho \iint_{S_{fob}} \nabla\varphi \, U_{n_S} \, dS, \tag{4.31}$$

and

$$\frac{d\vec{A}(t)}{dt} = \rho \iiint_V \vec{x} \times \nabla\varphi_t \, dV + \rho \iint_{S_{fob}} \vec{x} \times \nabla\varphi \, U_{n_S} \, dS, \tag{4.32}$$

where U_{n_S} is the normal component of the surface $S_{fob} = S_f + S_o + S_b$ velocity, *in the moving reference frame.* We can refer to Euler equation in the moving reference

frame $\vec{x}$ to get

$$\rho\nabla\varphi_t + \rho\left[(\nabla\varphi - U\,\hat{\imath})\cdot\nabla\right]\nabla\varphi = -\nabla\left(p + \rho\,g\,z\right), \tag{4.33}$$

letting us write

$$\begin{aligned}\frac{d\vec{M}(t)}{dt} &= -\rho\iiint_V \left((\nabla\varphi - U\,\hat{\imath})\cdot\nabla\right)\nabla\varphi + \nabla\left(\frac{p}{\rho} + g\,z\right)\,dV \\ &\quad +\rho\iint_{S_{fob}} \nabla\varphi\,U_{n_S}\,dS,\end{aligned} \tag{4.34}$$

and

$$\begin{aligned}\frac{d\vec{A}(t)}{dt} &= -\rho\iiint_V \left(\vec{x}\times(\nabla\varphi - U\,\hat{\imath})\cdot\nabla\right)\nabla\varphi + \vec{x}\times\nabla\left(\frac{p}{\rho} + g\,z\right)\,dV \\ &\quad +\rho\iint_{S_{fob}} \vec{x}\times\nabla\varphi\,U_{n_S}\,dS.\end{aligned} \tag{4.35}$$

Observing that

$$\begin{aligned}\left((\nabla\varphi - U\hat{\imath})\cdot\nabla\right)\nabla\varphi &= \nabla\left(\frac{\partial\varphi}{\partial x}\right)\cdot(\nabla\varphi - U\,\hat{\imath})\,\hat{\imath} + \nabla\left(\frac{\partial\varphi}{\partial y}\right)\cdot(\nabla\varphi - U\,\hat{\imath})\,\hat{\jmath} \\ &\quad +\nabla\left(\frac{\partial\varphi}{\partial z}\right)\cdot(\nabla\varphi - U\,\hat{\imath})\,\hat{k},\end{aligned}$$

we will be able to rewrite (4.34), using the Gauss theorem, as

$$\begin{aligned}\frac{d\vec{M}(t)}{dt} &= -\rho\iint_{S_{fob}} \vec{n}\cdot(\nabla\varphi - U\,\hat{\imath})\left(\frac{\partial\varphi}{\partial x}\right)\,\hat{\imath} + \vec{n}\cdot(\nabla\varphi - U\,\hat{\imath})\left(\frac{\partial\varphi}{\partial y}\right)\,\hat{\jmath} \\ &\quad +\vec{n}\cdot(\nabla\varphi - U\,\hat{\imath})\left(\frac{\partial\varphi}{\partial z}\right)\,\hat{k} - \nabla\varphi\,U_{n_S} + \vec{n}\left(\frac{p}{\rho} + g\,z\right)\,dS \\ &= -\rho\iint_{S_{fob}} \nabla\varphi\,(\vec{n}\cdot\nabla\varphi - \vec{n}\cdot U\,\hat{\imath} - U_{n_S}) + \vec{n}\left(\frac{p}{\rho} + g\,z\right)\,dS \\ &= -\rho\iint_{S_{fob}} \nabla\varphi\,(\vec{n}\cdot\nabla\varphi - U_n) + \vec{n}\left(\frac{p}{\rho} + g\,z\right)\,dS,\end{aligned} \tag{4.36}$$

where $U_n = \vec{n}\cdot U\,\hat{\imath} + U_{n_S}$ is the normal velocity due to the motion of the moving reference system combined with the normal velocity relative to this system. This is

the normal velocity of the surfaces with respect to the fixed reference system, and we can see that the same result would have been obtained in case we had derived the momentum time rate in the fixed reference system. By analogy, the angular momentum time rate will be given as

$$\frac{d\vec{A}(t)}{dt} = -\rho \iint_{S_{fob}} (\vec{x} \times \nabla\varphi)\,(\vec{n} \cdot \nabla\varphi - U_n) + (\vec{x} \times \vec{n}) \left(\frac{p}{\rho} + g\,z\right)\, dS. \qquad (4.37)$$

For periodic incident waves we should observe that $\frac{d\vec{M}(t)}{dt}$ and $\frac{d\vec{A}(t)}{dt}$ will have zero mean over one period, as Ogilvie [36] pointed out, because any different result would reflect on an infinite amount of momentum inside our control volume as time goes to plus or minus infinity. Defining the forces and moments acting over the actual body hull as

$$\begin{aligned} \vec{F}_b &= \iint_{S_b} \vec{n}\, p\, dS \\ \vec{A}_b &= \iint_{S_b} (\vec{x} \times \vec{n})\, p\, dS, \end{aligned} \qquad (4.38)$$

knowing that the pressure on the free surface is equal to the atmospheric pressure, which we define arbitrarily to be zero, disregarding the hydrostatic term on the outer integral because it will give no net contribution, and also that $U_n = \vec{n} \cdot \nabla\varphi$ over S_f and S_b, we may rewrite (4.36) and (4.37) as

$$\vec{F}_b = -\rho\, g \iint_{S_{bf}} \vec{n}\, z\, dS - \rho \iint_{S_o} \left[\vec{n} \left(\frac{p}{\rho}\right) + \nabla\varphi \left(\frac{\partial\varphi}{\partial\vec{n}} - U_n\right)\right] dS, \qquad (4.39)$$

and

$$\begin{aligned} \vec{A}_b = & -\rho\, g \iint_{S_{bf}} (\vec{x} \times \vec{n})\, z\, dS \\ & -\rho \iint_{S_o} \left[(\vec{x} \times \vec{n}) \left(\frac{p}{\rho}\right) + (\vec{x} \times \nabla\varphi) \left(\frac{\partial\varphi}{\partial\vec{n}} - U_n\right)\right] dS. \end{aligned} \qquad (4.40)$$

The first integral in (4.39) and (4.40) is to be taken over the actual hull surface S_b and free-surface elevation S_f. Once more we do not want to do that, and the transfer

of this integral from S_b to S_{bm} and from S_f to the mean free surface S_{fm} is desired. Taylor expanding z over the hull from S_{bm} to S_b, we will get

$$z|_{S_b} = z|_{S_{bm}} + (\vec{x} - \vec{x}_s) \cdot \nabla\, z|_{S_{bm}}\,. \tag{4.41}$$

Substituting (4.4) in (4.41),

$$z|_{S_b} \;=\; z|_{S_{bm}} + \left[\varepsilon\left(\vec{\xi} + \vec{\Omega} \times \vec{x}_s\right) + \varepsilon^2\,(\mathbf{H}\,\vec{x}_s) + O(\varepsilon^3)\right] \cdot \hat{k}. \tag{4.42}$$

Now, using also (4.6), we can relate the integral of the z-term over S_b and S_{bm} with the hydrostatic force $\vec{F}_{hst}(\omega_e)$ as

$$\begin{aligned}
\vec{F}_{hst} \;&=\; -\rho\, g \iint_{S_b} \vec{n}\, z\; dS \\
&=\; -\rho\, g \iint_{S_{bm}} dS\;\; (\vec{n} z) - \varepsilon\, \rho\, g \iint_{S_{bm}} dS\;\; \left[\vec{n}\,(\xi_3 + \xi_4\, y - \xi_5\, x) + (\vec{\Omega} \times \vec{n}) z\right] \\
&\quad -\varepsilon^2\, \rho\, g \iint_{S_{bm}} dS\; \vec{n}\left[\left(\mathbf{H}\, x \cdot \hat{k}\right) + \left(\vec{\Omega} \times \vec{n}\right)\,(\xi_3 + \xi_4\, y - \xi_5\, x) + \right. \\
&\quad \left. (\mathbf{H}\,\vec{n})\; z\right] + O(\varepsilon^3),
\end{aligned} \tag{4.43}$$

and collect the second-order terms that contribute to the steady problem. Writing (4.43) as

$$\vec{F}_{hst} \;=\; \vec{F}^{(0)}_{hst} + \varepsilon\, \vec{F}^{(1)}_{hst} + \varepsilon^2 \vec{F}^{(2)}_{hst} + O(\varepsilon^3), \tag{4.44}$$

and for the moments

$$\vec{M}_b \;=\; \vec{M}^{(0)}_{bm} + \varepsilon\, \vec{M}^{(1)}_{bm} + \varepsilon^2 \vec{M}^{(2)}_{hst} + O(\varepsilon^3), \tag{4.45}$$

we will have those terms as $\vec{F}^{(2)}_{hst}$, given by (4.18), and $\vec{M}^{(2)}_{hst}$, given by (4.19).

The next step is the transfer of the integrals over S_f to S_{fm}. We have that

$$\begin{aligned}
z|_{S_f} \;&=\; z|_{S_{fm}} + \eta|_{S_{fm}}\; \left.\frac{\partial\, z}{\partial z}\right|_{S_{fm}} \\
&=\; \eta|_{S_{fm}}\,,
\end{aligned} \tag{4.46}$$

and we know $\eta|_{S_{fm}}$ from (4.2). The integration over the mean free surface will only contribute to the vertical force, as well as roll and pitch moments. We may now rewrite the integral over the free surface as

$$\begin{aligned} -\rho g \iint_{S_f} \vec{n} z \, dS &= -\rho \iint_{S_{fm}} dS \, \vec{n} \left(\varphi_t - U \varphi_x + \frac{|\nabla \varphi|^2}{2} \right) \\ &\quad -\rho \iint_{S_{fm}} dS \, \frac{\vec{n}}{g} \left[\varphi_t \varphi_{zt} + U^2 \varphi_x \varphi_{xz} \right. \\ &\quad \left. -U \left(\varphi_t \varphi_{xz} + \varphi_x \varphi_{zt} \right) \right] \\ &\quad + \iint_{\Delta S_{fm}} dS \, \vec{n} \left(\varphi_t - U \varphi_x \right), \end{aligned} \tag{4.47}$$

or

$$\begin{aligned} -\rho g \iint_{S_f} \vec{n} z \, dS &= -\rho \hat{k} \iint_{S_{fm}} dS \left(\varphi_t - U \varphi_x + \frac{|\nabla \varphi|^2}{2} \right) \\ &\quad + \rho \hat{k} \iint_{S_{fm}} dS \, \left[\eta \left(\varphi_{zt} - U \varphi_{xz} \right) \right] + \hat{k} \iint_{\Delta S_{fm}} dS \, \left(\varphi_t - U \varphi_x \right). \end{aligned} \tag{4.48}$$

Similarly we will have for the moments contributions given by

$$\begin{aligned} -\rho g \iint_{S_f} (\vec{x} \times \vec{n}) \, z \, dS &= -\rho \iint_{S_{fm}} dS \, (\vec{x} \times \vec{n}) \left(\varphi_t - U \varphi_x + \frac{|\nabla \varphi|^2}{2} \right) \\ + \rho \hat{k} \iint_{S_{fm}} dS \, (\vec{x} \times \vec{n}) \left[\eta \left(\varphi_{zt} - U \varphi_{xz} \right) \right] &+ \iint_{\Delta S_{fm}} dS \, (\vec{x} \times \vec{n}) \left(\varphi_t - U \varphi_x \right), \end{aligned} \tag{4.49}$$

The integrals over ΔS_{fm} stand as correction terms on the integrals over the mean free surface due to the lateral motions of the ship, as can be seen in Figure 4-4, and which will be given as

$$\vec{I}_{F_{S_{fm}}} = \rho \oint_{\Gamma} dl \left[\vec{n} \cdot (\vec{\xi} + \vec{\alpha} \times \vec{x}) (\varphi_t - U \varphi_x) \right], \tag{4.50}$$

for the forces and, for the moments, as

$$\vec{I}_{M_{S_{fm}}} = \rho \oint_{\Gamma} dl \left[(\vec{x} \times \vec{n}) \cdot (\vec{\xi} + \vec{\alpha} \times \vec{x}) (\varphi_t - U \varphi_x) \right]. \tag{4.51}$$

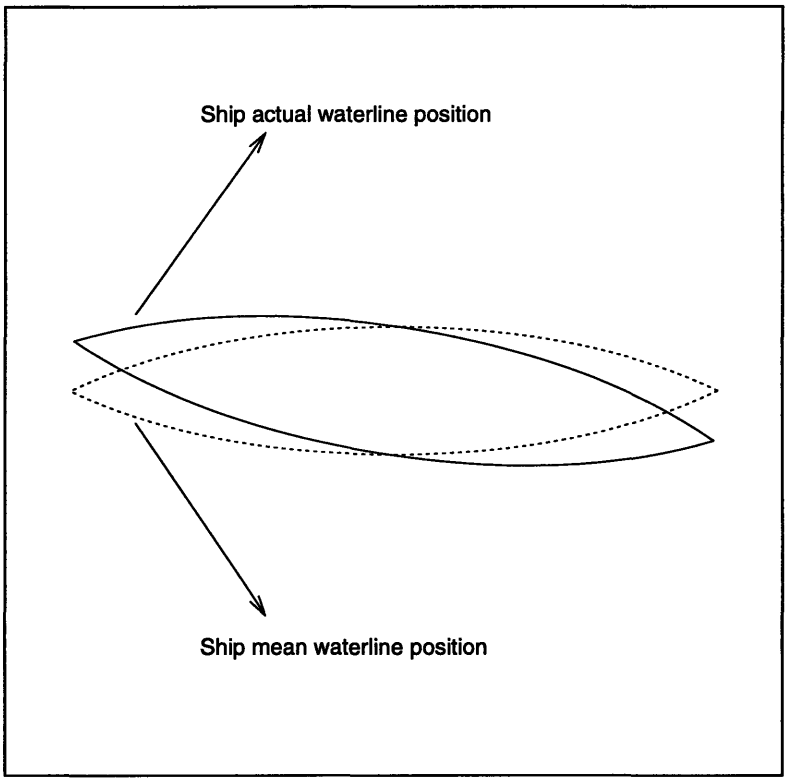

Figure 4-4: View from the waterline of a ship in its mean position and translated and rotated from its actual position. The ship motion is considered to be of $O(\varepsilon)$ and so a correction term represented as the line integral is necessary.

The last term we need to compute on (4.39) is the integral to be taken over the outer surface S_o. Substituting p from (4.1),and once more collecting the terms that will give a contribution to the second-order steady force, we will have

$$
\begin{aligned}
&-\rho \iint_{S_o} \left[\vec{n}\,(p) + \nabla\varphi \left(\frac{\partial \varphi}{\partial \vec{n}} - U_n \right) \right] dS = \\
&\quad -\rho \iint_{S_o} \vec{n} \left(-\frac{\partial \varphi}{\partial t} + U \frac{\partial \varphi}{\partial x} - gz - \frac{|\nabla\varphi|^2}{2} \right) + \nabla\varphi \left(\frac{\partial \varphi}{\partial \vec{n}} - U_n \right) dS \\
&\quad + \iint_{\Delta S_o} \vec{n}\,(\varphi_t - U\varphi_x)\, dS. \qquad (4.52)
\end{aligned}
$$

We will rewrite the right hand side of (4.52) as

$$-\rho \iint_{S_o} \vec{n} \left(-\varphi_t - \frac{|\nabla\varphi|^2}{2} - gz \right) + \nabla\varphi\, \varphi_n \, dS + \iint_{\Delta S_o} \vec{n}\, (\varphi_t - gz)\, dS$$
$$-\rho \iint_{S_o} \left(\nabla\varphi\, U_n - U \frac{\partial\varphi}{\partial x}\vec{n} \right) dS - \rho \iint_{\Delta S_o} \left(\nabla\varphi\, U_n - U \frac{\partial\varphi}{\partial x}\vec{n} \right) dS \quad (4.53)$$

Here the correction terms represented by the line integrals taken over the intersection of the outer surface S_o and the mean free surface (contour ΔS_o) exist because the outer surface S_o ends at $z = 0$, while the real surface ends at $z = \eta$, which is an error of order ε. The second order correction that will come from this integral, which contains first order quantities integrated over this first order strip, will give a contribution to the forces mathematically translated as

$$\vec{I}_{F_{S_{o1}}} = -\rho \oint_{\Gamma_o} dl \int_0^{\varepsilon\eta} dz\, \vec{n}\, (\varphi_t - gz) = -\frac{\rho}{2g} \oint_{\Gamma_o} dl\, \vec{n} \left(\varphi_t^2 - U^2 \varphi_x^2 \right), \quad (4.54)$$

and

$$\vec{I}_{F_{S_{o2}}} = -\rho \oint_{\Gamma_o} dl\, \eta \left(\nabla\varphi\, U_n - U \frac{\partial\varphi}{\partial x}\vec{n} \right). \quad (4.55)$$

Investigating the contribution coming from the third integral in (4.53) we note an advantage in separating the contribution to the vertical force and the contributions to the horizontal forces. Expanding the terms we will have

$$-\rho \iint_{S_o} \left(\nabla\varphi\, U_n - U \frac{\partial\varphi}{\partial x}\vec{n} \right) dS =$$
$$\rho U\, \hat{j} \iint_{S_o} (\varphi_y\, n_x - \varphi_x\, n_y)\, dS + \rho U\, \hat{k} \iint_{S_o} (\varphi_z\, n_x - \varphi_x\, n_z)\, dS =$$
$$\rho U\, \hat{j} \left(\iint_{S_{o-vert}} \nabla\varphi \cdot d\vec{l}\, dz + \iint_{S_{o-hor}} \nabla\varphi \cdot d\vec{l}\, dr \right)$$
$$+\rho U\, \hat{k} \iint_{S_o} (\varphi_z\, n_x - \varphi_x\, n_z)\, dS, \quad (4.56)$$

and we can see that if there is no circulation in the fluid, which is our case, the mean planar forces are determined from the first-order quantities only. So the total

contribution from the outer surface integral to the steady second-order force will be given as

$$-\rho \iint_{S_o} \left(\vec{n} \frac{|\nabla\varphi|^2}{2} - \nabla\varphi\, \varphi_n \right) dS - \frac{\rho g}{2} \oint_{\Gamma_o} dl\, \vec{n} \left(\varphi_t^2 - U^2 \varphi_x^2 \right)$$
$$+\rho U \hat{k} \iint_{S_o} \left(\varphi_z^{(2)} n_x - \varphi_x^{(2)} n_z \right) dS - \rho \oint_{\Gamma_o} dl\, \eta \left(\nabla\varphi U_n - U \frac{\partial\varphi}{\partial x} \vec{n} \right) \quad (4.57)$$

and similarly, the contribution to the moments as

$$-\rho \iint_{S_o} \left[(\vec{x} \times \vec{n}) \frac{|\nabla\varphi|^2}{2} - (\vec{x} \times \nabla\varphi)\, \varphi_n \right] dS - \frac{\rho}{2g} \oint_{\Gamma_o} dl\, (\vec{x} \times \vec{n}) \left(\varphi_t^2 - U^2 \varphi_x^2 \right)$$
$$-\rho \iint_{S_o} \left[\left(\vec{x} \times \nabla\varphi^{(2)} \right) U_n - U \frac{\partial\varphi^{(2)}}{\partial x} (\vec{x} \times \vec{n}) \right] dS$$
$$-\rho \oint_{\Gamma_o} dl\, \eta \left[(\vec{x} \times \nabla\varphi)\, U_n - U \frac{\partial\varphi}{\partial x} (\vec{x} \times \vec{n}) \right] \quad (4.58)$$

We can now collect all terms that will contribute to the total second-order steady force computed using the momentum flux formulation, from equations (4.44), (4.48), (4.50), and (4.52), to finally get:

$$\begin{aligned} \vec{F}_b^{(2)}(\omega_e) \;=\; & \vec{F}_{hst}^{(2)} - \rho \hat{k} \iint_{S_{fm}} \left[-U \varphi_x^{(2)} + \frac{|\nabla\varphi|^2}{2} - \eta \left(\varphi_{zt} - U \varphi_{xz} \right) \right] dS \\ & -\hat{k}\, \rho g \oint_{\Gamma} \left[(\xi_3 + \xi_4\, y - \xi_5\, x) \eta \right] dl + \rho U \hat{k} \iint_{S_o} \left(\varphi_z^{(2)} n_x - \varphi_x^{(2)} n_z \right) dS \\ & -\rho \iint_{S_o} \left(\vec{n} \frac{|\nabla\varphi|^2}{2} - \nabla\varphi\, \varphi_n \right) dS - \frac{\rho g}{2} \oint_{\Gamma_o} dl\, \vec{n} \left(\varphi_t^2 - U^2 \varphi_x^2 \right) \\ & -\rho \oint_{\Gamma_o} dl\, \eta \left(\nabla\varphi U_n - U \frac{\partial\varphi}{\partial x} \vec{n} \right), \end{aligned} \quad (4.59)$$

and for the moments, collecting the contributions from equations (4.45), (4.49), (4.51) and (4.58):

$$\begin{aligned}
\vec{M}_b^{(2)}(\omega_e) \;=\; & \vec{M}_{hst}^{(2)} - \rho \iint_{S_{fm}} (\vec{x}\times\vec{n}) \left[-U\,\varphi_x^{(2)} + \frac{|\nabla\varphi|^2}{2} - \eta\,(\varphi_{zt} - U\,\varphi_{xz}) \right] dS \\
& -\rho\, g \oint_{\Gamma} (\vec{x}\times\vec{n}) \left[(\xi_3 + \xi_4\, y - \xi_5\, x)\eta \right] dl \\
& -\rho \iint_{S_o} \left((\vec{x}\times\vec{n}) \frac{|\nabla\varphi|^2}{2} - \nabla\varphi\,\varphi_n \right) dS \\
& -\frac{\rho\, g}{2} \oint_{\Gamma_o} dl\, (\vec{x}\times\vec{n}) \left(\varphi_t^2 - U^2\,\varphi_x^2 \right) \\
& -\rho \iint_{S_o} \left[\left(\vec{x}\times\nabla\varphi^{(2)} \right) U_n - U \frac{\partial\varphi^{(2)}}{\partial x} (\vec{x}\times\vec{n}) \right] dS \\
& -\rho \oint_{\Gamma_o} dl\, \eta \left(\vec{x}\times\nabla\varphi\, U_n - U \frac{\partial\varphi}{\partial x} (\vec{x}\times\vec{n}) \right),
\end{aligned} \tag{4.60}$$

We can notice that this expressions are equivalent to the one Grue and Palm[10] obtained for the slow speed double-body case horizontal steady forces, and the free-surface integral is similar to the expression Zhao and Faltinsen[43] obtained, if we consider the steady basis flow to be given by the Neumann-Kelvin approximation and include the second-order steady potential contribution. Equation (4.59) also imply that for a fluid with no circulation the second-order steady potential is not necessary for the computation of the second-order steady horizontal forces, using the momentum flux computation. This will not be true for the computation of the vertical force or the moments.

4.3 Second-order Steady Neumann-Kelvin Problem

The computation of second-order steady forces for the zero forward-speed problem only requires information of first order quantities. However, as we have seen in the previous sections, and it is apparent from looking at the pressure definition in Bernoulli equation (2.2)

$$p = -\rho\left(\varphi_t + \frac{1}{2}\nabla\varphi\cdot\nabla\varphi - U\,\frac{\partial\varphi}{\partial x} + g\,z\right), \tag{4.61}$$

the second-order steady force acting on a ship with forward speed also has a contribution from the term

$$\varepsilon^2\,\rho\iint_{S_{bm}}\vec{n}\,U\,\frac{\partial\varphi^{(2)}}{\partial x}\quad dS, \tag{4.62}$$

where $\varphi^{(2)}$ is the steady second order potential. In the following subsections we will define the boundary conditions that must be satisfied by this second-order potential and the integral equation that we can build from using these boundary conditions in connection with Green's identity.

4.3.1 The Boundary Value Problem

The boundary value problem satisfied by the second-order steady potential is obtained by collecting the second-order terms coming from the boundary conditions. The first-order quantities are supposed to be known at this stage.

The second-order problem we are going to solve is defined in the frequency domain, in the sense that for each frequency we will be able to define different steady boundary conditions that will define a second-order steady potential solution. This steady boundary problem may be solved as the large time limit of a transient surge radiation problem with these boundary conditions. The computation of the second-order steady forcing from the first-order frequency domain solution only requires the use of (4.8).

Taking the second-order terms in the Laplace equation we will have

$$\nabla^2\varphi^{(2)} = 0, \qquad \text{in the entire fluid region,} \tag{4.63}$$

while the body boundary condition follows from the steady part of the second-order terms in (2.29), or

$$\frac{\partial\varphi^{(2)}}{\partial\vec{n}} = \mathcal{B}(\vec{x}), \qquad \text{on } S_{bm}, \tag{4.64}$$

where, for the freely-floating problem, $\mathcal{B}(\vec{x})$ can be computed following the same lines of Ogilvie [36], but for now we will concentrate on the fixed-body (diffraction) problem when

$$\mathcal{B}(\vec{x}) = 0. \tag{4.65}$$

The steady second-order free-surface boundary condition can be obtained from (2.21), substituting the ϕ_B definition for the Neumann-Kelvin flow and linearizing over the plane $z = 0$ or equivalently we can look at the zero velocity free-surface boundary condition as discussed for example in Ogilvie [36], and given by

$$\frac{\varphi^{(2)}_{t_0t_0}}{g} + \frac{\partial\varphi^{(2)}}{\partial z} = -\frac{1}{g}\frac{\partial}{\partial t_0}\left|\varphi^{(1)}\right|^2 + \frac{1}{g^2}\varphi^{(1)}_{t_0}\frac{\partial}{\partial z}\left(\varphi^{(1)}_{t_0t_0} + g\,\varphi^{(1)}_z\right), \qquad \text{on } z = 0, \tag{4.66}$$

and transform to the Neumann-Kelvin case substituting

$$\frac{\partial}{\partial t_0} = \frac{\partial}{\partial t} - U\frac{\partial}{\partial x}. \tag{4.67}$$

which will finally give the second-order steady-potential free-surface boundary condition as

$$\frac{U^2}{g}\varphi^{(2)}_{xx} + \frac{\partial\varphi^{(2)}}{\partial z} = \mathcal{H}(\vec{x}), \qquad \text{on } z = 0, \tag{4.68}$$

where

$$\mathcal{H}(\vec{x}) = -\frac{1}{g}\left(2\,U\,\nabla\varphi^{(1)}\cdot\nabla\varphi_x^{(1)} - \varphi_t^{(1)}\,\varphi_{zz}^{(1)} + U\,\varphi_x^{(1)}\,\varphi_{zz}^{(1)}\right)$$
$$-\frac{1}{g^2}\left(-\varphi_t^{(1)}\,\varphi_{ztt}^{(1)} + U\,\varphi_x^{(1)}\,\varphi_{ztt}^{(1)} + 2\,U\,\varphi_t^{(1)}\,\varphi_{xzt}^{(1)}\right.$$
$$\left.-2\,U^2\,\varphi_x^{(1)}\,\varphi_{xzt}^{(1)} - U^2\,\varphi_t^{(1)}\,\varphi_{xxz}^{(1)} + U^3\,\varphi_x^{(1)}\,\varphi_{xxz}^{(1)}\right). \tag{4.69}$$

We will also have that, at large distances from the body

$$\nabla\varphi^{(2)} \mapsto 0, \qquad |\vec{x}| \mapsto \infty. \tag{4.70}$$

4.3.2 Discrete Integral Equation

The boundary value problem shown in the last section is similar to the steady-state limit of the transient surge first-order problem, with the exception of the inhomogeneous right hand side in the free-surface boundary condition (4.68) and a different right hand side of the body boundary condition (4.64). The derivation of an integral equation for this problem follows the same steps of the first order, and the details are presented in Appendix A.

The potential formulation integral equation will then be given as

$$2\,\pi\,\phi(t) + \iint_{S_b} d\vec{\xi}\,\left[\phi(t)\,G_{n_\xi}(0) - \phi_{n_\xi}(t)\,G(0)\right]$$
$$-\int_{t_0}^{t} d\tau \iint_{S_b} d\vec{\xi}\,\left[\phi(\tau)\,G_{n_\xi\tau}(t-\tau) - \phi_{n_\xi}(\tau)\,G_\tau(t-\tau)\right]$$
$$-\frac{U}{g}\int_{t_0}^{t} d\tau \int_{\overline{\Gamma}} dl\,n_1\,\left[\phi(\tau)\,\left(G_{\tau\tau}(t-\tau) - U G_{\tau\xi}(t-\tau)\right)\right.$$
$$\left.-G_\tau(t-\tau)\,\left(\phi_\tau(\tau) - U\phi_\xi(\tau)\right)\right]$$
$$+\int_{t_0}^{t} d\tau \iint_{S_f(\tau)} d\vec{\xi}\,\left(\mathcal{H}(\vec{\xi})\,G_\tau(t-\tau)\right) = 0, \tag{4.71}$$

and the source formulation, with the details also presented in Appendix A, as

$$\begin{aligned}\varphi(\vec{x},t) \;=\; & \iint_{S_{bm}} d\vec{\xi}\,\left(G^{(0)}(\vec{x};\vec{\xi})\,\sigma(\vec{\xi},t)\right) + \int_{t_0}^{t} d\tau \iint_{S_{bm}} d\vec{\xi}\left(G_\tau(\vec{x};\vec{\xi},t-\tau)\sigma(\vec{\xi},\tau)\right) \\ & -\frac{U^2}{g}\int_{t_0}^{t} d\tau \int_{\Gamma} dl\,(\vec{n}_{2D}\cdot\hat{\imath})^2\,\left(G_\tau(\vec{x};\vec{\xi},t-\tau)\,\sigma(\vec{\xi},\tau)\right) \\ & +\int_{t_0}^{t} d\tau \iint_{S_f(\tau)} d\vec{\xi}\;\left(\mathcal{H}(\vec{\xi})\,G_\tau(t-\tau)\right) = 0. \end{aligned} \tag{4.72}$$

As we said before, the steady problem can be considered as the infinite time limit of the radiation surge problem. The difference is that the boundary conditions over the body surface are much simpler, as it does not involve the m-terms nor the terms proportional to the normal unit vector over the body surface. The constant in time body boundary condition given by (4.64) will only require us to compute the gradient of (4.72), and we will not need to decompose the source strength in a manner similar to what has been used with the radiation potential (3.20).

Looking at (4.72) we see that the forcing function $\mathcal{H}(\vec{\xi})$ is constant in time and not a function of the field point coordinate $\vec{x}$, but of the source point coordinate $\vec{\xi}$, and therefore constant with respect to the applied gradient. We will then have

$$\begin{aligned}\frac{\partial\varphi(\vec{x},t)}{\partial\vec{n}} \;=\; & \iint_{S_{bm}} d\vec{\xi}\,\left(G_n^{(0)}(\vec{x};\vec{\xi})\,\sigma(\vec{\xi},t)\right) + \int_{t_0}^{t} d\tau \iint_{S_{bm}} d\vec{\xi}\left(G_{n\tau}(\vec{x};\vec{\xi},t-\tau)\sigma(\vec{\xi},\tau)\right) \\ & -\frac{U^2}{g}\int_{t_0}^{t} d\tau \int_{\Gamma} dl\,(\vec{n}_{2D}\cdot\hat{\imath})^2\,\left(G_{n\tau}(\vec{x};\vec{\xi},t-\tau)\,\sigma(\vec{\xi},\tau)\right) \\ & +\int_{t_0}^{t} d\tau \iint_{S_f(\tau)} d\vec{\xi}\;\left(\mathcal{H}(\vec{\xi})\,G_{n\tau}(t-\tau)\right) = \mathcal{B}(\vec{x}) \end{aligned} \tag{4.73}$$

as the equation that needs to be solved in order to compute the large time asymptotic limit for the source strength $\sigma(\vec{\xi},\tau)$.

The first problem encountered on the computation of the solution of the steady second-order potential was the computation of the forcing function $\mathcal{H}(\vec{\xi})$. The higher order derivatives were computed using the central-difference approach in a finite difference scheme, but the forcing is not being properly computed. To look further into the problems we are having, we defined the second-order low-speed potential problem under the Neumann-Kelvin approach.

4.3.3 The Low-Speed Diffraction Second-Order Potential

Under the low-speed assumption, we will assume, as Grue & Palm [8] [9] [11] (1985, 1986, 1993), Nossen et all [34] (1991), and Zhao & Faltinsen [41] [42] [43] (1988, 1988, 1989) did in connection with the double-body flow, that terms proportional to U^2 may be considered to be of a higher order and will not affect the solution of the problem.

Calling the low-speed second-order potential as $\varphi_l^{(2)}(\vec{x})$, we will have our boundary value problem given as

$$\begin{aligned}
\nabla^2\varphi_l^{(2)} &= 0, && \text{in the entire fluid region,}\\
\tfrac{\partial\varphi_l^{(2)}}{\partial\vec{n}} &= 0, && \text{on } S_{bm},\\
\tfrac{\partial\varphi_l^{(2)}}{\partial z} &= -\tfrac{1}{g}\left(2\,U\,\nabla\varphi^{(1)}\cdot\nabla\varphi_x^{(1)} - \varphi_t^{(1)}\,\varphi_{zz}^{(1)} + U\,\varphi_x^{(1)}\,\varphi_{zz}^{(1)}\right)\\
&\quad -\tfrac{1}{g^2}\left(-\varphi_t^{(1)}\,\varphi_{ztt}^{(1)} + U\,\varphi_x^{(1)}\,\varphi_{ztt}^{(1)} + 2\,U\,\varphi_t^{(1)}\,\varphi_{xzt}^{(1)}\right) && \text{on } z=0,\\
\nabla\varphi_l^{(2)} &\mapsto 0, && |\vec{x}|\mapsto\infty,
\end{aligned} \tag{4.74}$$

where only the steady part of the right hand side is to be taken into account. The corresponding integral equation is given as

$$2\,\pi\,\varphi_l^{(2)} + \iint_{S_{bm}+S_{fm}} d\vec{\xi}\,\left(\varphi_l^{(2)}G_{n_\xi}^{(0)} - \mathcal{R}(\vec{\xi})\varphi_l^{(2)}\right) = 0, \tag{4.75}$$

where $\mathcal{R}(\vec{\xi})$ represents $\frac{\partial\varphi_l^{(2)}}{\partial\vec{n}}$ on S_{bm} and S_{fm}, as given by (4.74).

It is easy to see that far from the body, when the waves have a dependency on z like e^{kz}, and on x like e^{-ikx}, that $\mathcal{R}(\vec{\xi})$ will have no real part. In order to exemplify the numerical problems we have encountered on the computation of the forcing function we will plot the real and imaginary part of $\varphi^{(1)}$ and $\varphi_{zz}^{(1)}$, since the combination of the potential and this second derivative was the dominant term on the forcing.

For the computation of the forcing function at each point shown in the plots, over the free-surface, we used a central difference scheme with 5 points to compute the second derivatives of the potential over the plane $z=0$. The $\varphi_{zz}^{(1)}$ terms were obtained

through the use of the Laplace equation.

From the spikes that show up in the forcing function plots we have a clear indication that the computation of the potential and velocities over the free-surface is not accurate enough to allow the computation of the second-order derivatives.

As a consequence of the forcing function not being well represented, the computation of the second-order steady force coming from the second-order potential was not accurate, but nevertheless we accepted the results obtained as an indication that this contribution is small and can be disregarded in general. The idea is that the error in the representation of the forcing function shows up as the spikes, and so if it were not for these spikes the forcing function would be much smaller, leading to the computation of a second-order steady potential, velocities, and ultimately forces, smaller than the computed response. We can see in the Figures 4-15 and 4-16 that the steady forces coming from the second-order steady potential to be only a small fraction of the second-order steady force coming from the first-order potential, giving support to the idea that we may disregard this contribution.

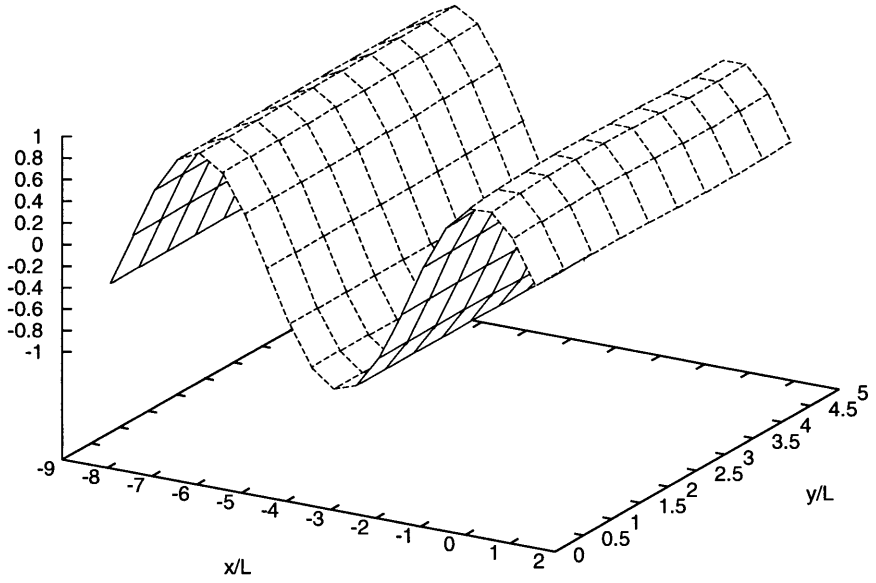

Figure 4-5: Real part of $\varphi^{(1)}$ over the free surface. $\omega_e = 1.0$, $Fr = 0.10$ and $\beta = 180$ degrees. Wigley hull is located between $-0.5 \leq x/l \leq 0.5$.

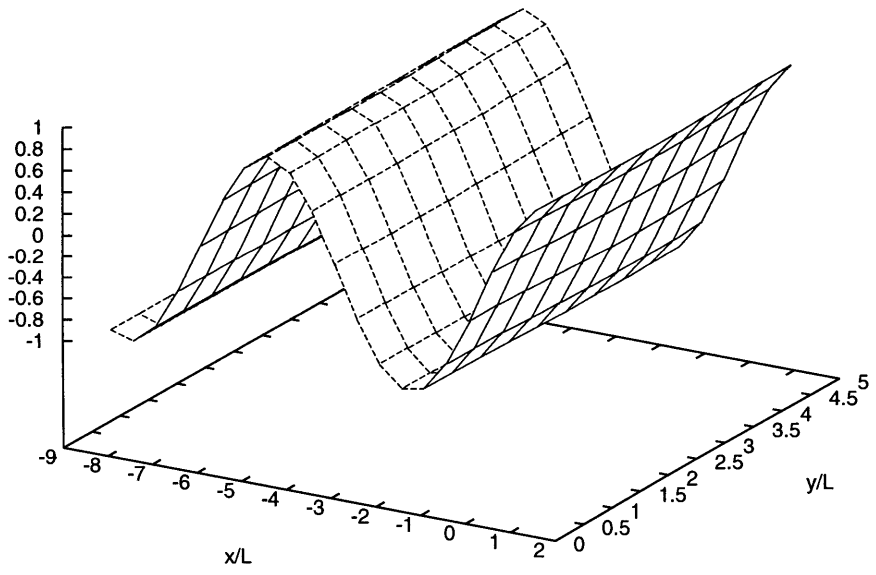

Figure 4-6: Imaginary part of $\varphi^{(1)}$ over the free surface. $\omega_e = 1.0$, $Fr = 0.10$ and $\beta = 180$ degrees. Wigley hull is located between $-0.5 \leq x/l \leq 0.5$.

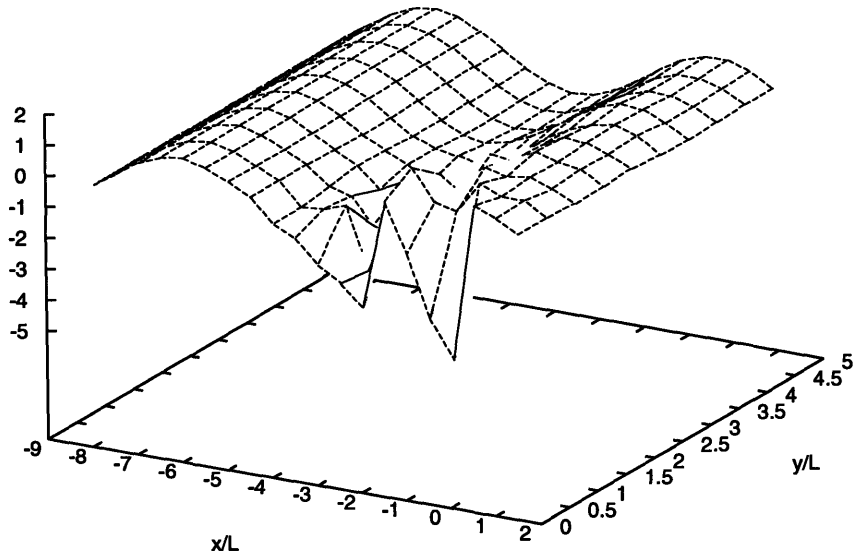

Figure 4-7: Real part of $\varphi_{zz}^{(1)}$ over the free surface. $\omega_e = 1.0$, $Fr = 0.10$ and $\beta = 180$ degrees. Wigley hull is located between $-0.5 \leq x/l \leq 0.5$.

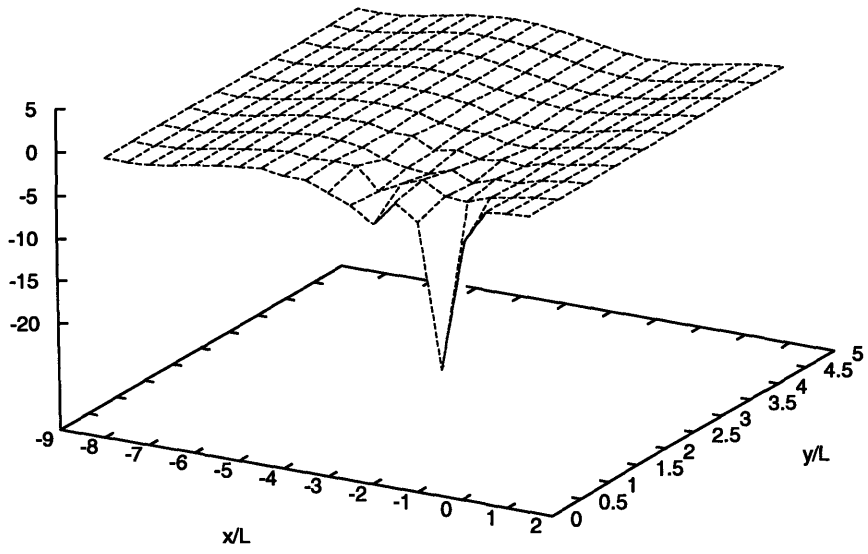

Figure 4-8: Imaginary part of $\varphi_{zz}^{(1)}$ over the free surface. $\omega_e = 1.0$, $Fr = 0.10$ and $\beta = 180$ degrees. Wigley hull is located between $-0.5 \leq x/l \leq 0.5$.

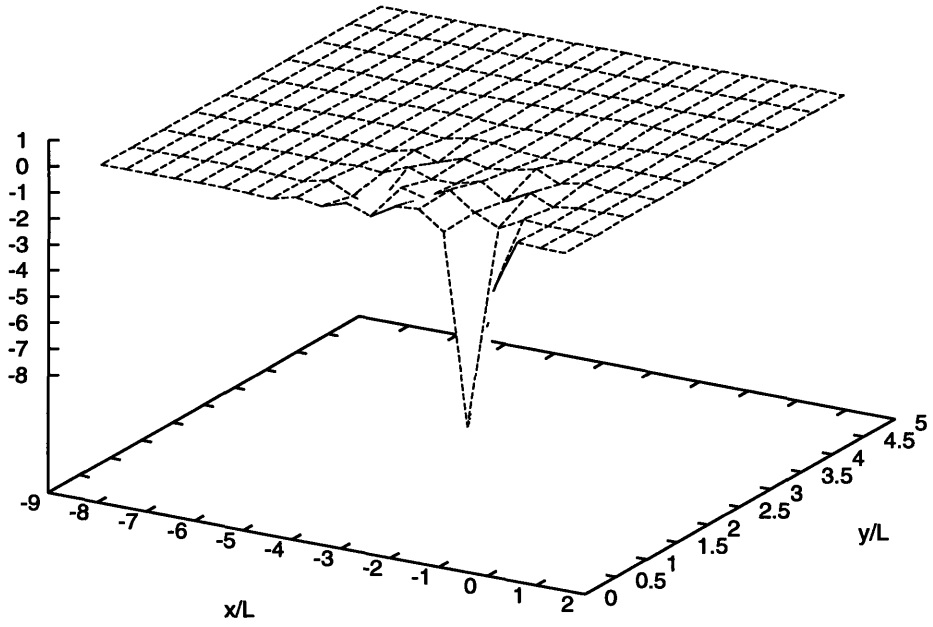

Figure 4-9: The total forcing function over the free surface. $\omega_e = 1.0$, $Fr = 0.10$ and $\beta = 180$ degrees. Wigley hull is located between $-0.5 \leq x/l \leq 0.5$.

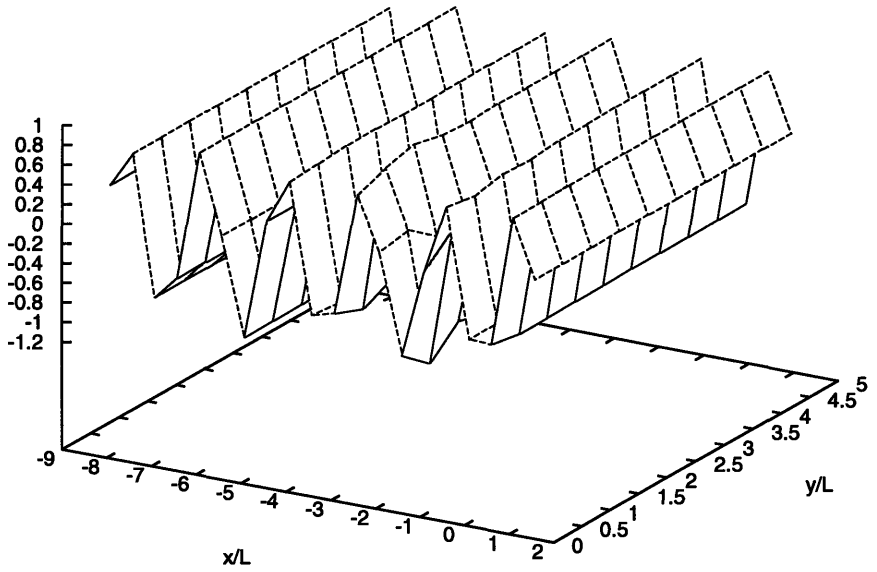

Figure 4-10: Real part of $\varphi^{(1)}$ over the free surface. $\omega_e = 3.0$, $Fr = 0.10$ and $\beta = 180$ degrees. Wigley hull is located between $-0.5 \leq x/l \leq 0.5$.

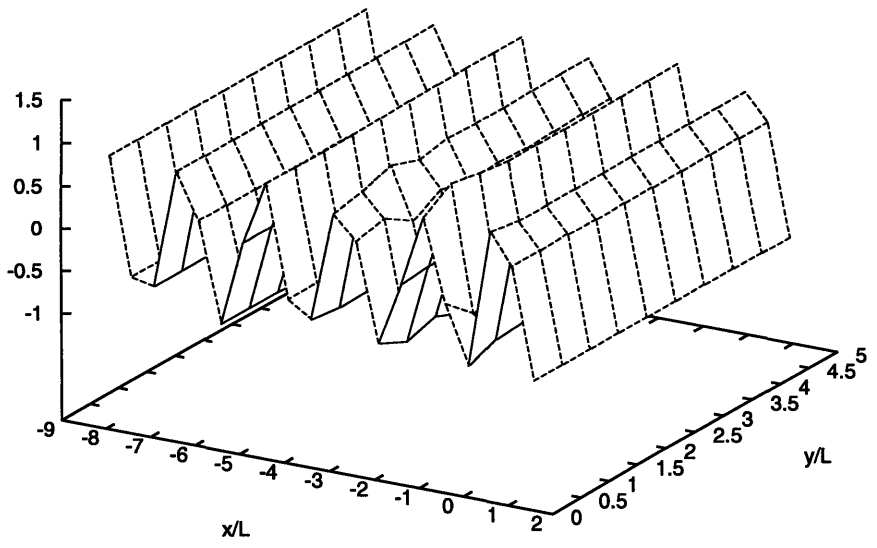

Figure 4-11: Imaginary part of $\varphi^{(1)}$ over the free surface. $\omega_e = 3.0$, $Fr = 0.10$ and $\beta = 180$ degrees. Wigley hull is located between $-0.5 \leq x/l \leq 0.5$.

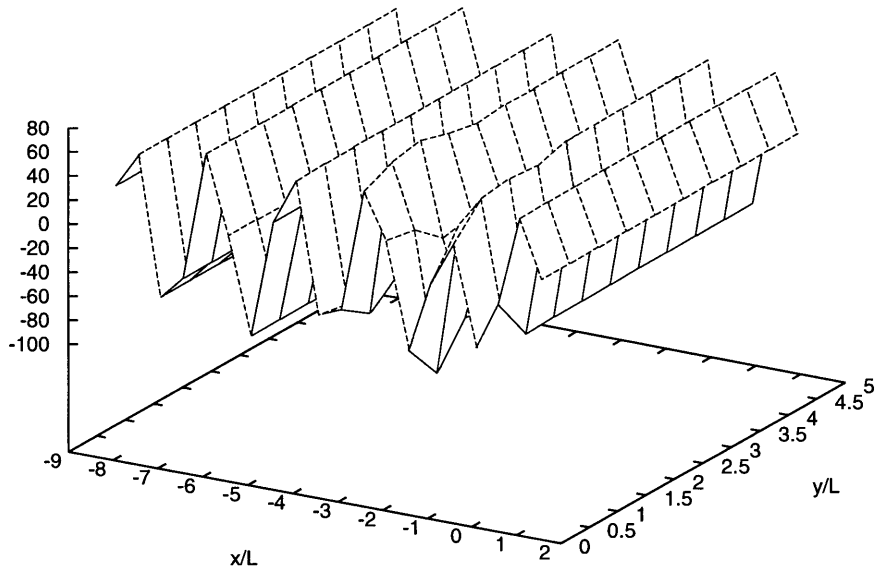

Figure 4-12: Real part of $\varphi_{zz}^{(1)}$ over the free surface. $\omega_e = 3.0$, $Fr = 0.10$ and $\beta = 180$ degrees. Wigley hull is located between $-0.5 \leq x/l \leq 0.5$.

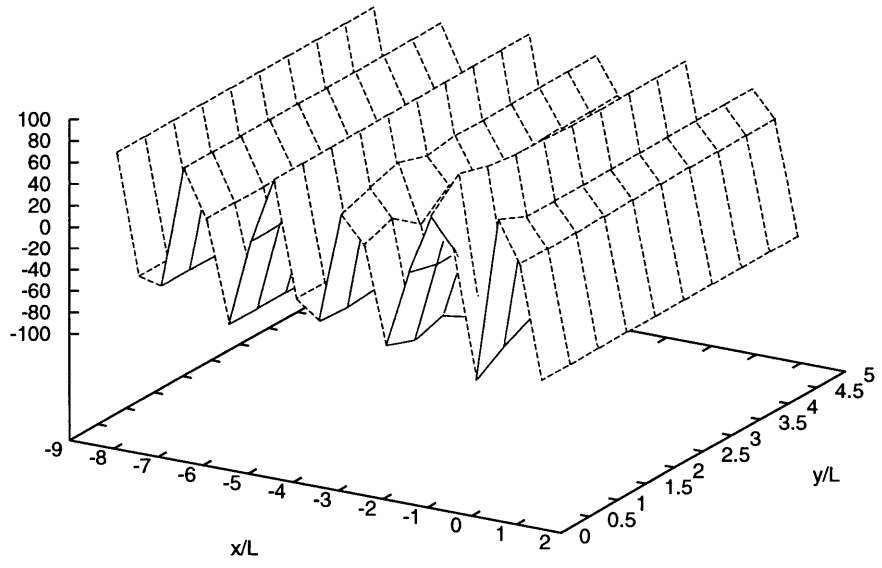

Figure 4-13: Imaginary part of $\varphi_{zz}^{(1)}$ over the free surface. $\omega_e = 3.0$, $Fr = 0.10$ and $\beta = 180$ degrees. Wigley hull is located between $-0.5 \leq x/l \leq 0.5$.

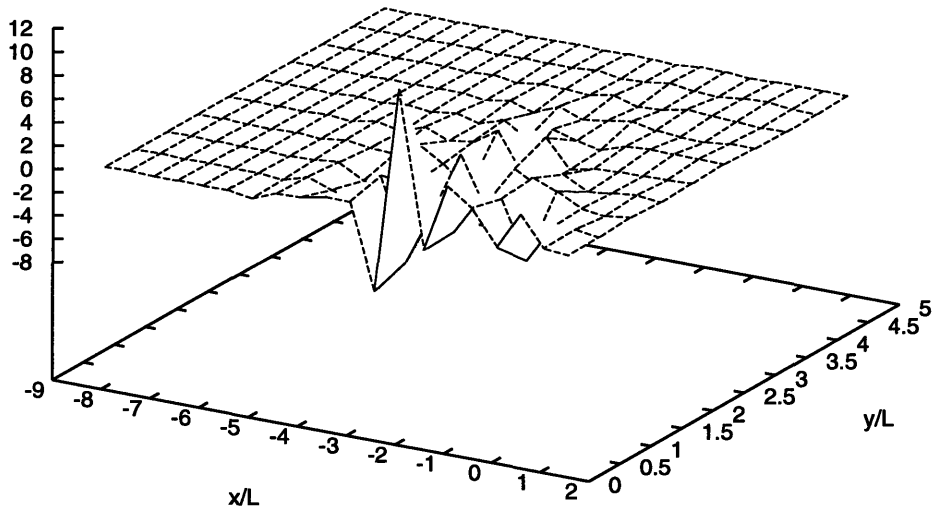

Figure 4-14: The total forcing function over the free surface. $\omega_e = 3.0$, $Fr = 0.10$ and $\beta = 180$ degrees. Wigley hull is located between $-0.5 \leq x/l \leq 0.5$.

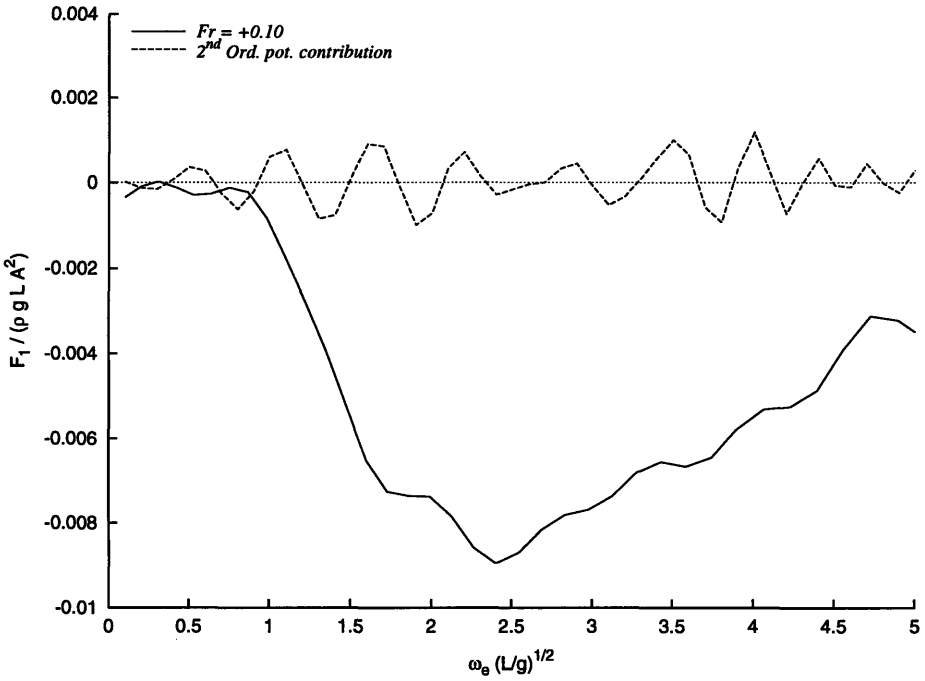

Figure 4-15: Comparison between the contribution from the second-order steady potential and the total second-order steady surge force coming from the first-order potential. $Fr = 0.10$ and $\beta = 180$ degrees.

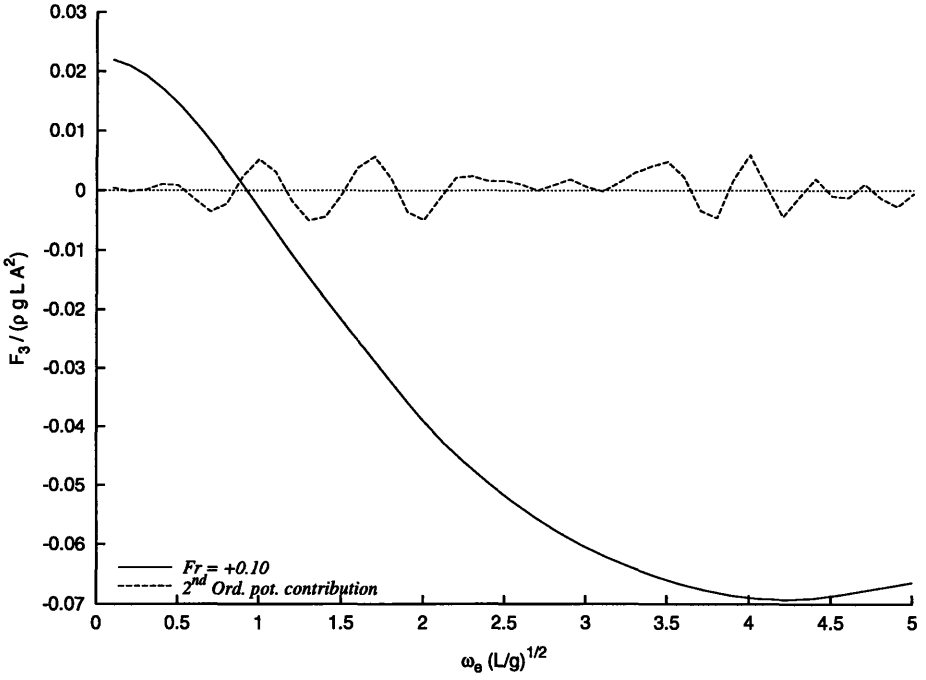

Figure 4-16: Comparison between the contribution from the second-order steady potential and the total second-order steady heave force coming from the first-order potential. $Fr = 0.10$ and $\beta = 180$ degrees.

Chapter 5

Results

This chapter contains the second-order steady force results for different floating body geometries. We want to show the advantages of using the approach just described here as well as check the limits of its applicability.

We will first present results for the Wigley hull, which is a slender body that has been extensively tested and had results computed using many different programs.

Going to examples when we will try to stretch the slender body assumption, we will start with the circular floating hemisphere.

Finally we will try comparisons with a shallow cylinder, which besides not being slender, has sharp corners close to the free surface which may represent a numerical challenge since we know that the velocity will go to infinity as $R^{-1/3}$ as we approach a 270 degrees corner in the bidimensional case.

For each case studied we will first compare results with WAMIT, an extensively tested 3-D panel method computer program described in [3] which computes first and second-order forces including the steady ones for the zero-velocity problem.

For the Wigley hull we will also compare results with SWAN, a forward speed Rankine panel method described in [26] and that also has extensive use in the computations of loads and responses of ocean-going ships and floating structures.

5.1 The Wigley Hull

We are going to use here the modified Wigley hull, as in Bingham [2], with a ratio of the length (L) to the breadth (B) equal to 10 and of the length to the draft (T) equal to 16.

This hull is mathematically described as

$$\begin{aligned} \zeta_2 &= (1-\zeta_3)^2(1-\zeta_1^2)(1+0.2\zeta_1^2)+\zeta_3(1-\zeta_3^8)(1-\zeta_1^2)^4 \\ & -1 \le \zeta_1 \le 1, \qquad -1 \le \zeta_3 \le 0 \end{aligned} \tag{5.1}$$

with

$$\{x, y, z\} = \{(\zeta_1 L)/2, (\zeta_2 B)/2, \zeta_3 T\} \tag{5.2}$$

The discretization of the hull was made using 128, 512 and 1080 panels. As the program takes advantage of the hull symmetry about the plane $y = 0$, only half of the body needs to be discretized. The meshes can be visualized for the whole body in Figures 5-1, 5-2, and 5-3.

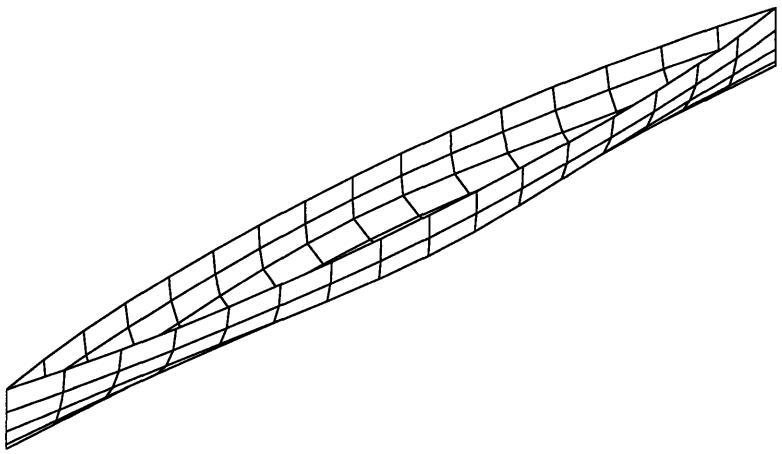

Figure 5-1: Wigley hull mesh with 128 panels. Actual numerical model uses the symmetry with respect to the xz–plane.

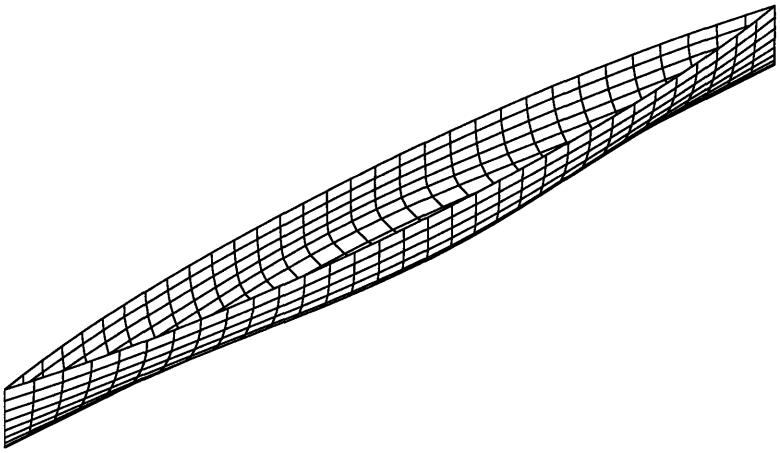

Figure 5-2: Wigley hull mesh with 512 panels. Actual numerical model uses the symmetry with respect to the xz–plane.

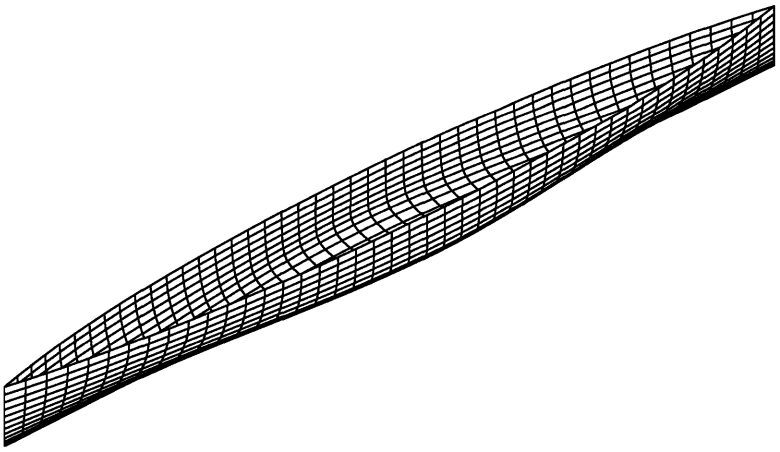

Figure 5-3: Wigley hull mesh with 1080 panels. Actual numerical model uses the symmetry with respect to the xz–plane.

5.1.1 The diffraction problem

Computing the second-order steady force for the diffraction problem alone, is equivalent to computing this force without allowing the ship to oscillate due to the presence of the incoming waves, but only to move with forward velocity.

The computations were done using the pressure integration method and compared against results obtained by WAMIT. In all simulations we have used a total time history equal to $22.5\sqrt{g/L}$ with a time step equal to $0.05\sqrt{g/L}$. The results for the diffraction second-order steady forces are shown below, for a heading of 180 degrees and 135 degrees. In Figures 5-4 to 5-6 we can see that the agreement between our results (called TIMIT results from now on) and WAMIT results were excellent.

We should note that for the heading equal to 135 degrees case, with results in Figures 5-7 to 5-12, the convergence between TIMIT and WAMIT results were not as fast, although it is clear that they do converge. The problem now is numerically more challenging, since the slenderness of the Wigley hull will, with front and rear edges, will create sharp corners for flows due to incident waves with headings different than 180 or 0 degrees. The velocities computed on panels too close to those edges present discrepancies compared to WAMIT velocities, but as we increase the number of panels the relative weight of these panels on the total force decreases and we can see the results converging. We should conclude that as we go to higher frequencies we must increase the number of panels over the hull. We should also say that then we will have panel centroids closer to the free-surface which may require smaller time steps. In the following examples the chosen time step of $0.05\sqrt{g/L}$ was good enough for all three meshes.

Some of the results show inconsistencies like positive steady force in surge when the wave is heading in the negative direction, for high frequencies, and this fact should be seen as an indication that the results for this mesh is not converged at those higher frequencies. We can see that increasing the number of panels, and consequently obtaining more converged results, will eliminate this behavior.

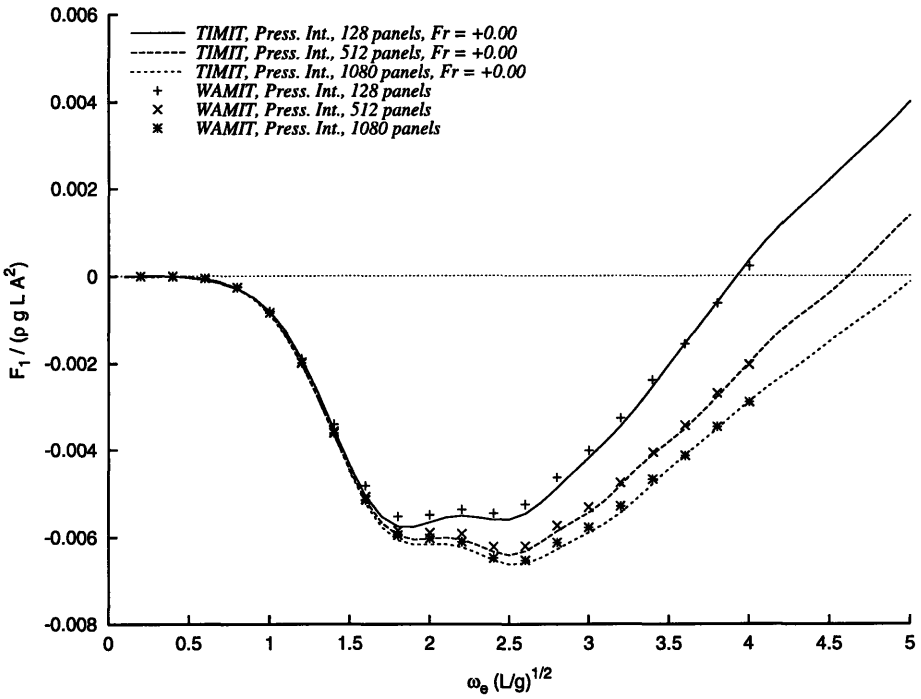

Figure 5-4: Wigley hull. Surge diffraction second-order steady force. Comparison with WAMIT. Heading = 180.

In Figures 5-13 to 5-18 The influence of the ship speed on the diffraction second-order steady force are shown in the following plots, for a heading equal to 180 degrees, with the ship moving ahead or going backwards. Another way of looking at this problem is to consider the ship fixed and suppose the presence of currents in the same direction as the waves (head seas) and in the opposite direction (following seas).

In the following seas case we have stopped the computation of the second-order steady forces as the group velocity got close to the ship velocity. There is a physical problem when the ship moves with the same speed as the waves group velocity and the Fourier transform of the hydrodynamic quantities would also require a long time record, which would be infeasible. The sharp increase of the steady forces as we approach these frequencies should be regarded as a consequence of this problem.

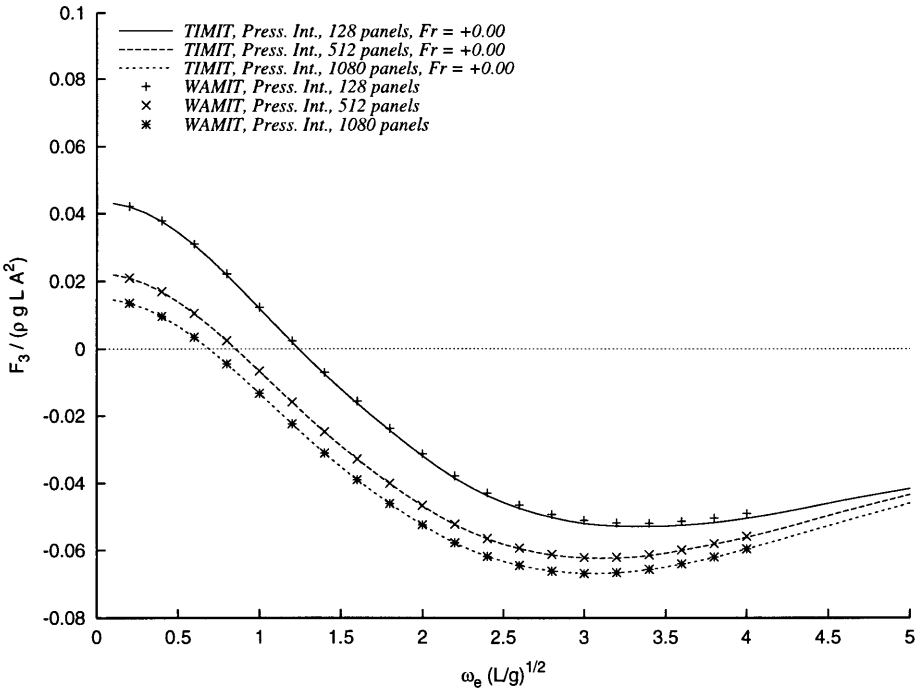

Figure 5-5: Wigley hull. Heave diffraction second-order steady force. Comparison with WAMIT. Heading = 180.

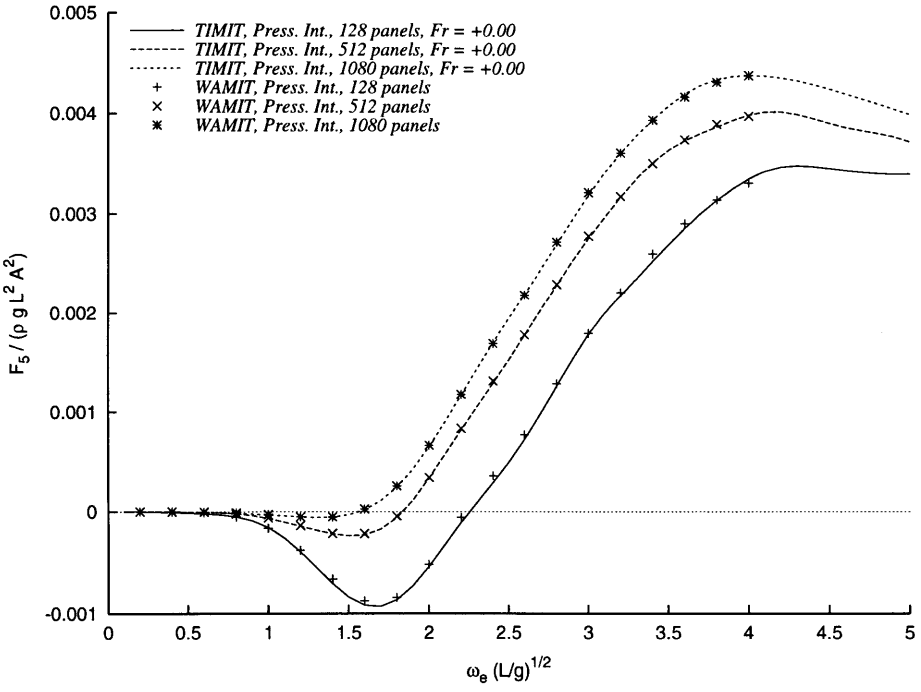

Figure 5-6: Wigley hull. Pitch diffraction second-order steady force. Comparison with WAMIT. Heading = 180.

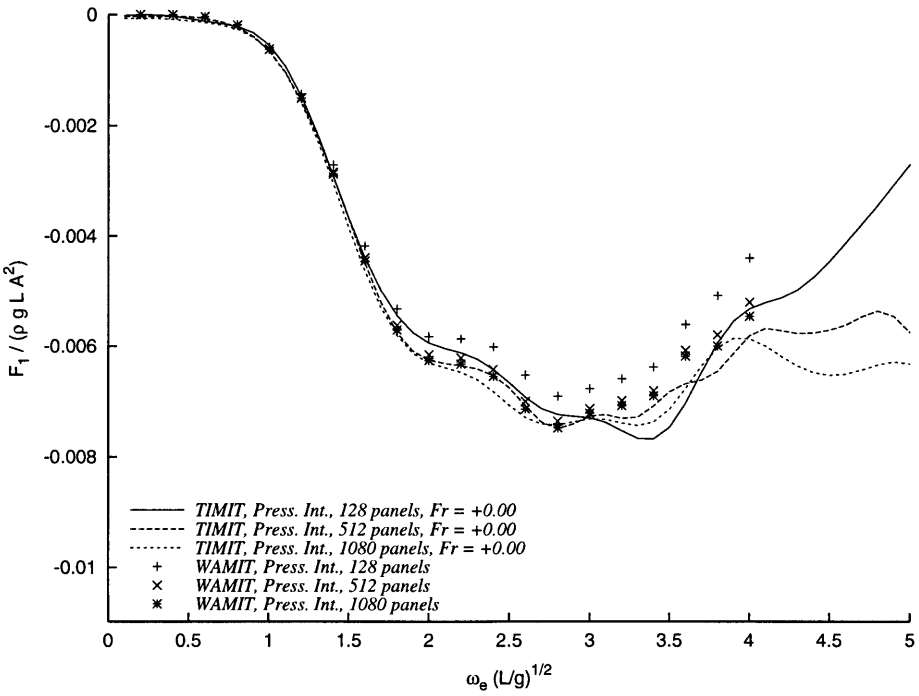

Figure 5-7: Wigley hull. Surge diffraction second-order steady force. Comparison with WAMIT. Heading = 135.

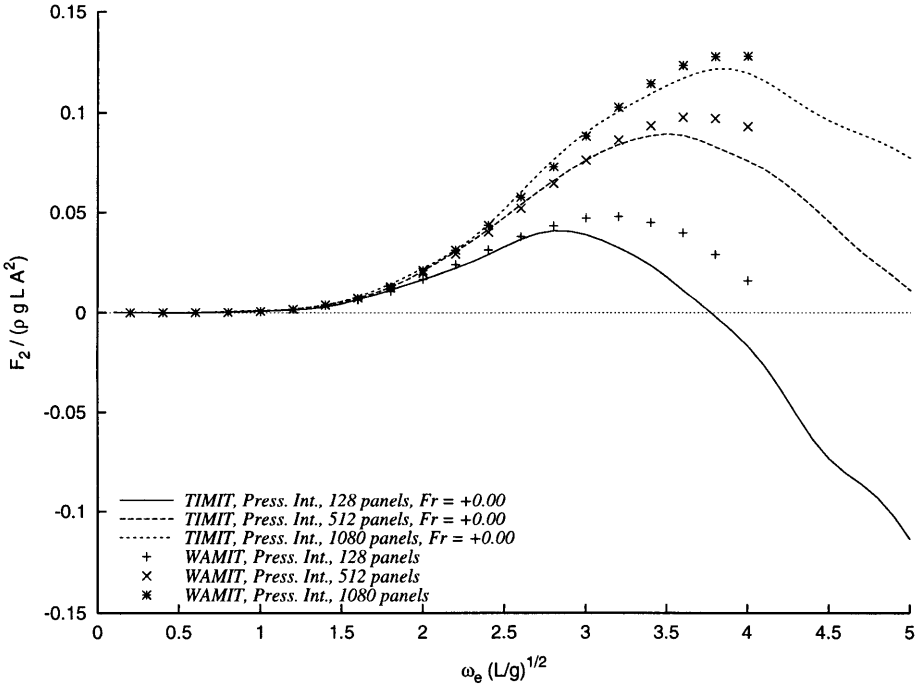

Figure 5-8: Wigley hull. Sway diffraction second-order steady force. Comparison with WAMIT. Heading = 135.

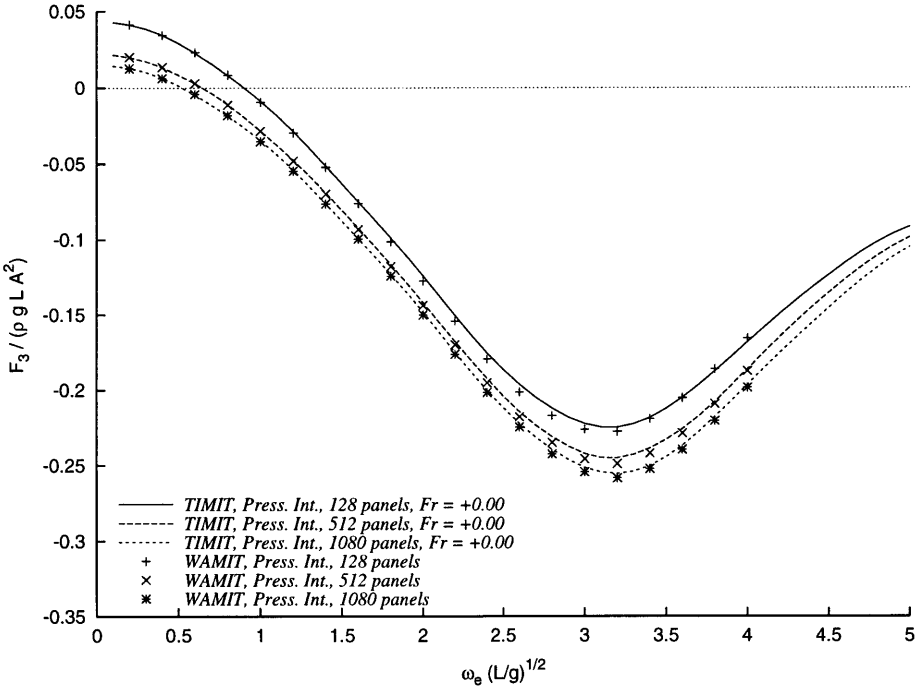

Figure 5-9: Wigley hull. Heave diffraction second-order steady force. Comparison with WAMIT. Heading = 135.

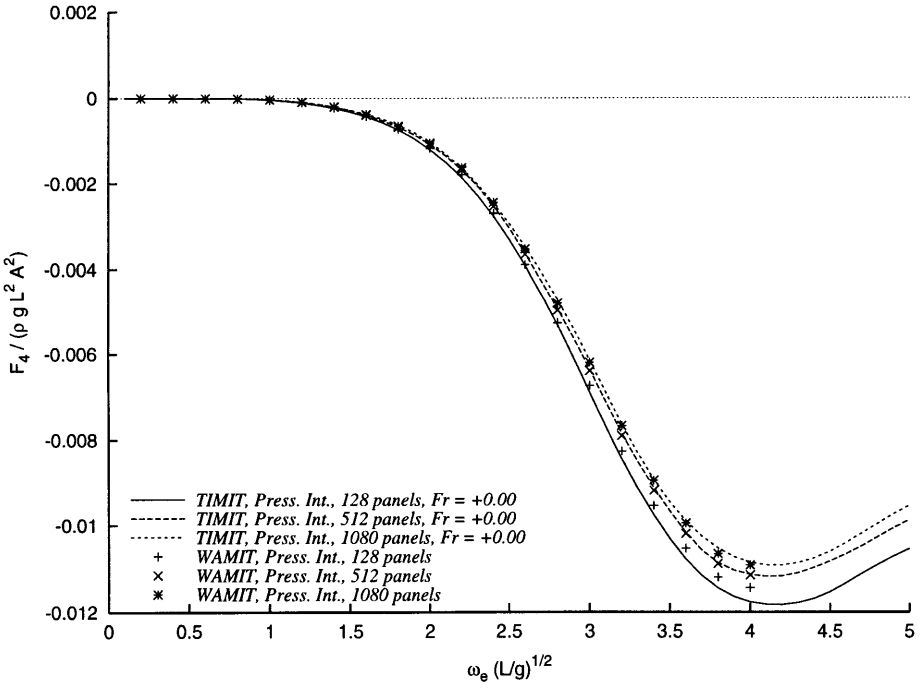

Figure 5-10: Wigley hull. Roll diffraction second-order steady force. Comparison with WAMIT. Heading = 135.

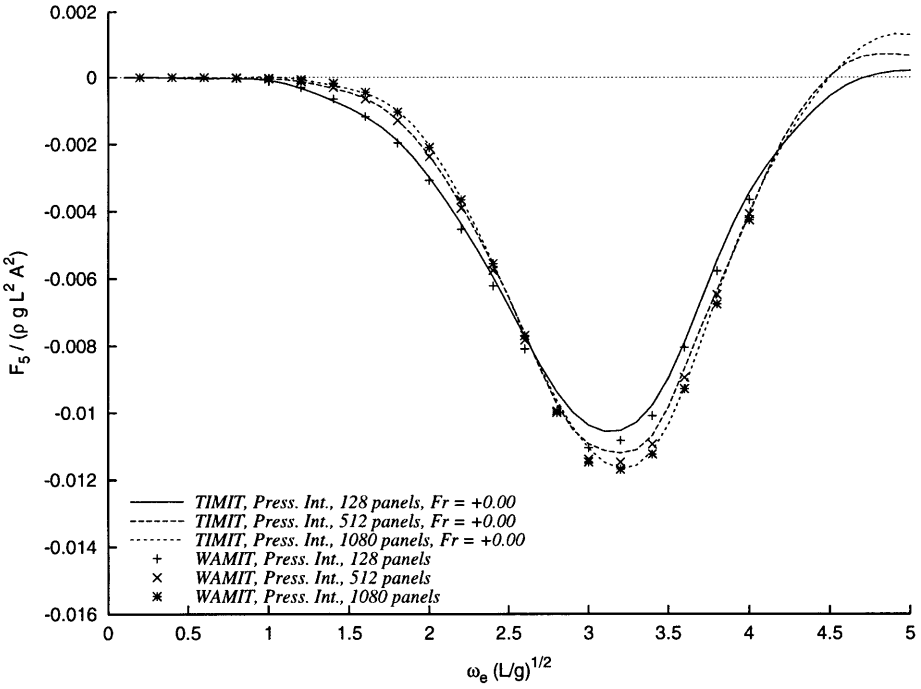

Figure 5-11: Wigley hull. Pitch diffraction second-order steady force. Comparison with WAMIT. Heading = 135.

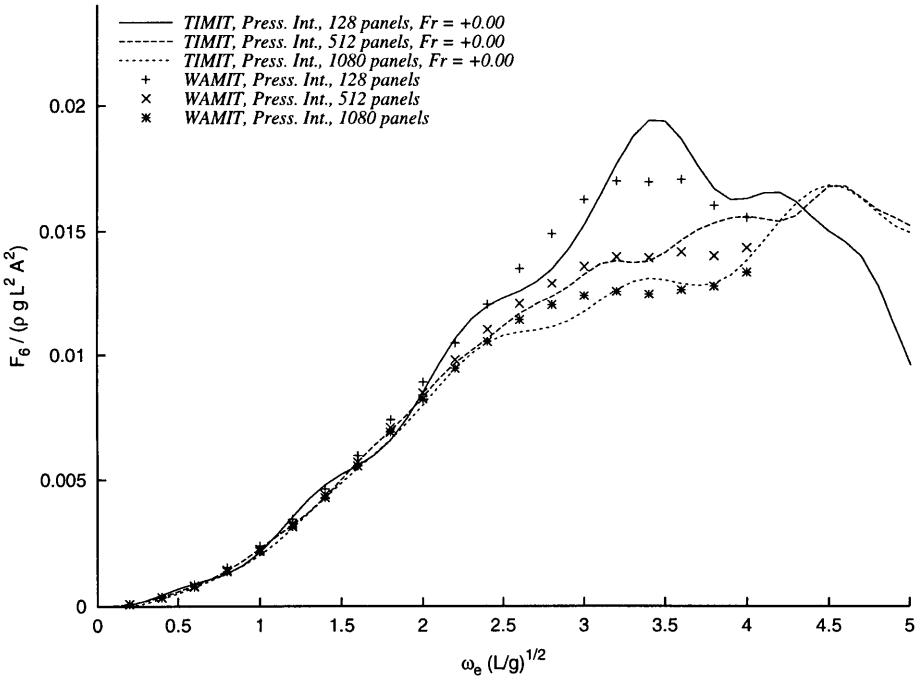

Figure 5-12: Wigley hull. Yaw diffraction second-order steady force. Comparison with WAMIT. Heading = 135.

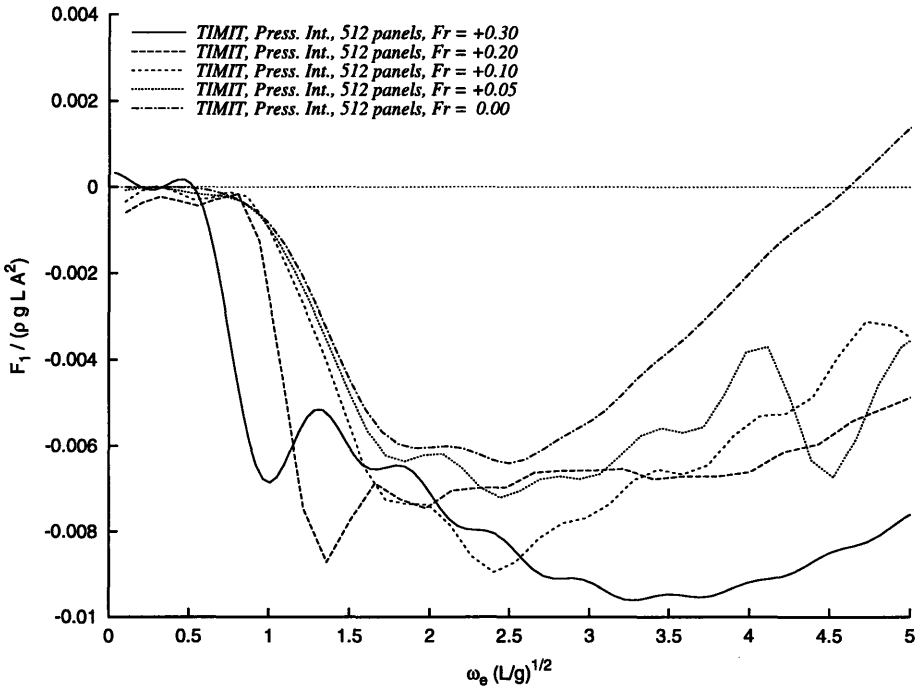

Figure 5-13: Wigley hull. Surge diffraction second-order steady force. Different Froude numbers, Ship moving ahead. Heading = 180.

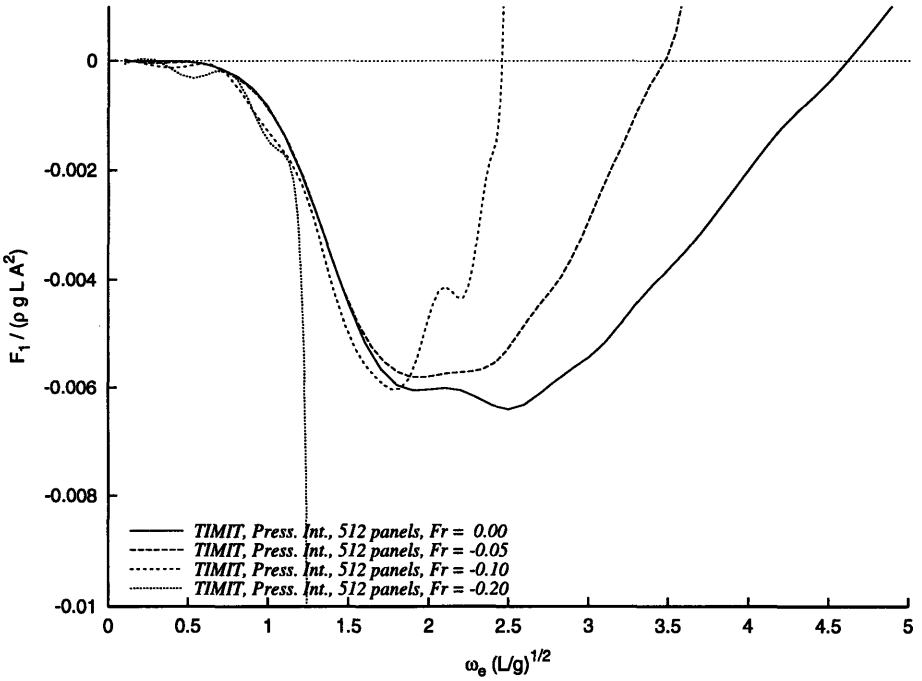

Figure 5-14: Wigley hull. Surge diffraction second-order steady force. Different Froude numbers, Ship moving backwards. Heading = 180.

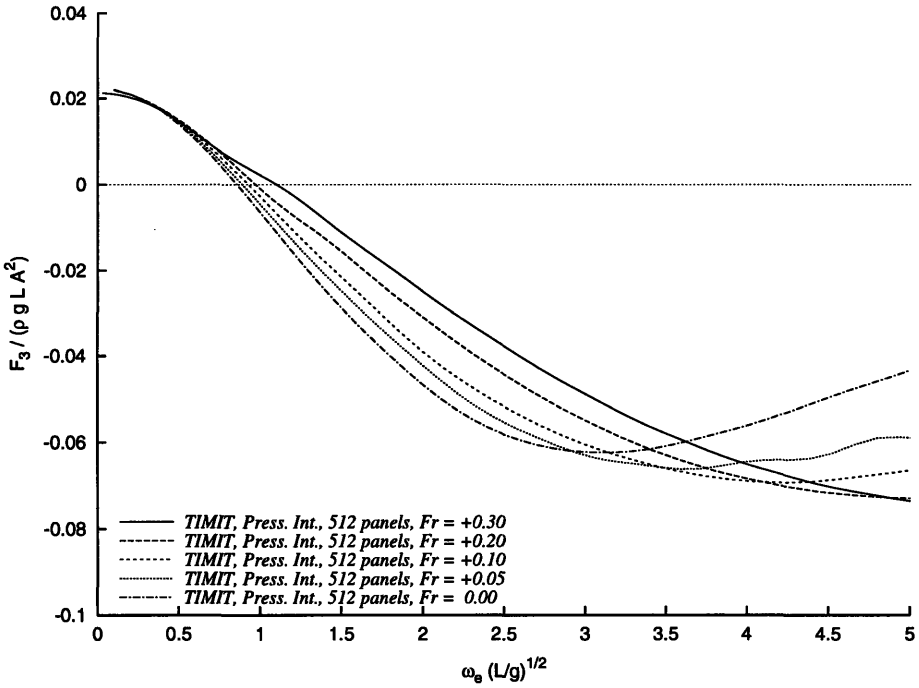

Figure 5-15: Wigley hull. Heave diffraction second-order steady force. Different Froude numbers. Ship moving ahead. Heading = 180.

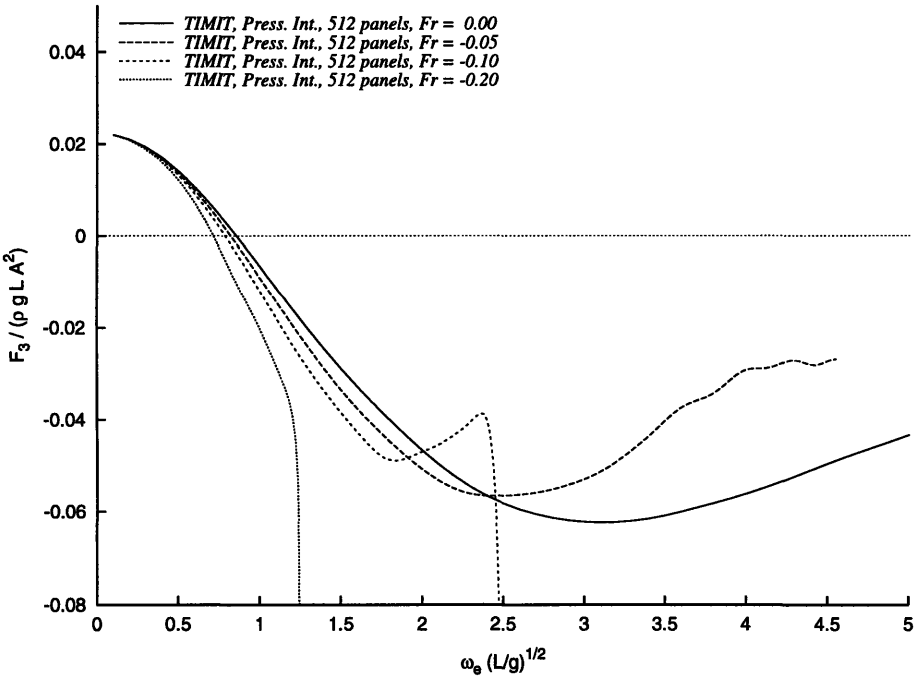

Figure 5-16: Wigley hull. Heave diffraction second-order steady force. Different Froude numbers. Ship moving backwards. Heading = 180.

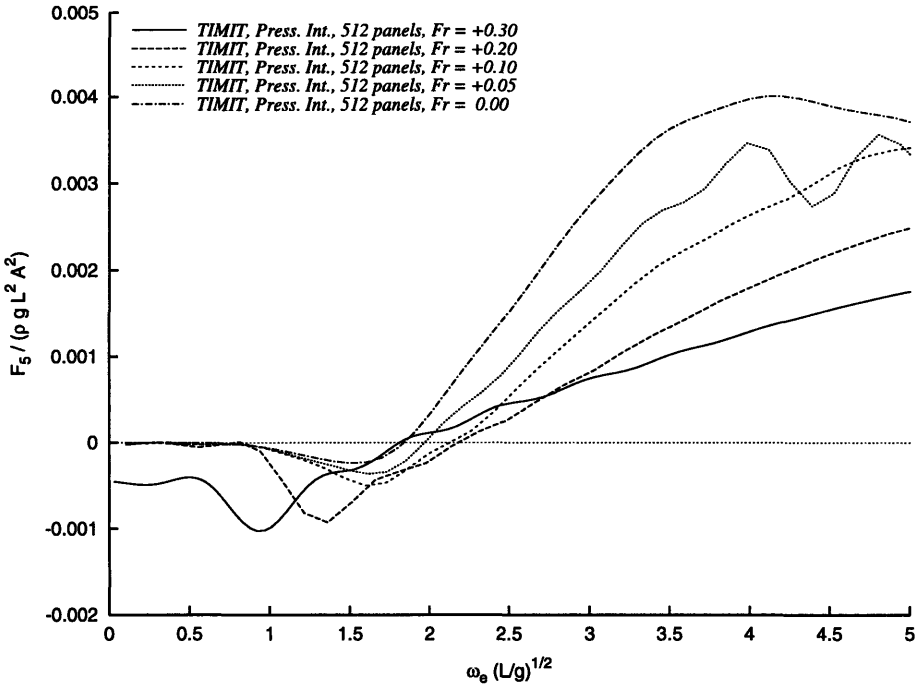

Figure 5-17: Wigley hull. Pitch diffraction second-order steady force. Different Froude numbers. Ship moving ahead. Heading = 180.

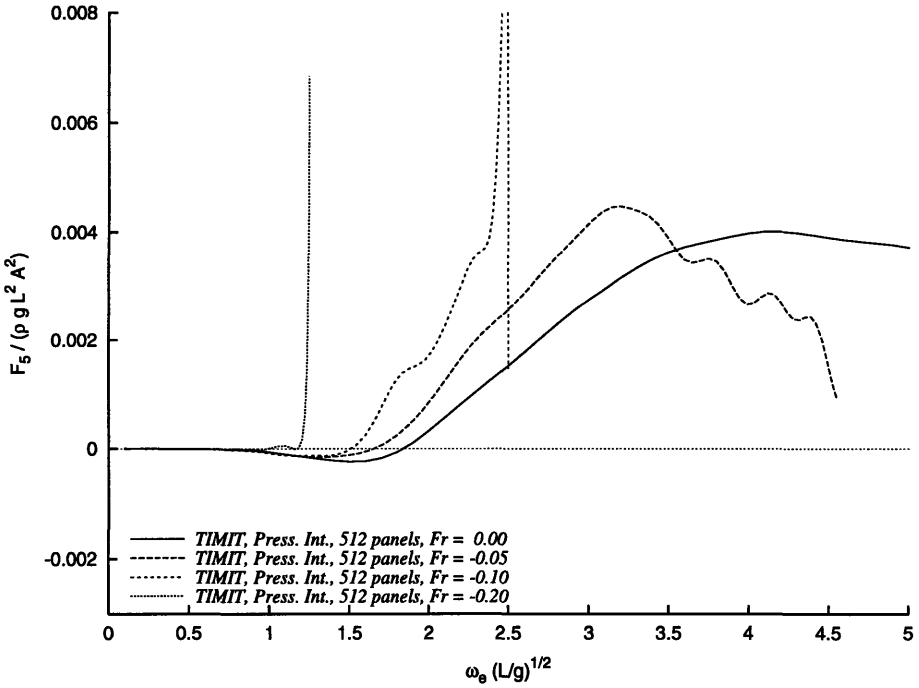

Figure 5-18: Wigley hull. Pitch diffraction second-order steady force. Different Froude numbers. Ship moving backwards. Heading = 180.

5.1.2 The freely-floating body problem

In this problem, besides moving with constant speed and being in the presence of incident waves, the ship is free to oscillate due to this incoming waves and therefore will also radiate waves.

We show in Figures 5-19 to 5-27 a comparison of the first-order body motions in waves against WAMIT, since these motions are an important factor for the computation of the second-order steady forces. We can see that the Fourier transforming technique gives poor hydrodynamic results close to an absolute frequency of zero. This happens because our time history will never be sufficient long to have enough information at very small frequencies. Ship motions having hydrostatic restoration (heave, roll and pitch) will show good results because the hydrostatic forces will dominate the problem in the low frequency range. In this range, degrees of freedom where the motions do not cause hydrostatic restoring forces (surge, sway and yaw) will show unreliable motion computations. We can also comment on the peak that shows up in the sway response in Figure 5-23, since this is unusual. This is related to the strong roll resonance that occurs due to the very small potential damping in roll, which is non-physical since actually there would be damping from other sources, as viscous effects. The roll and sway motions are coupled, and as a result we have this peak in the sway motions.

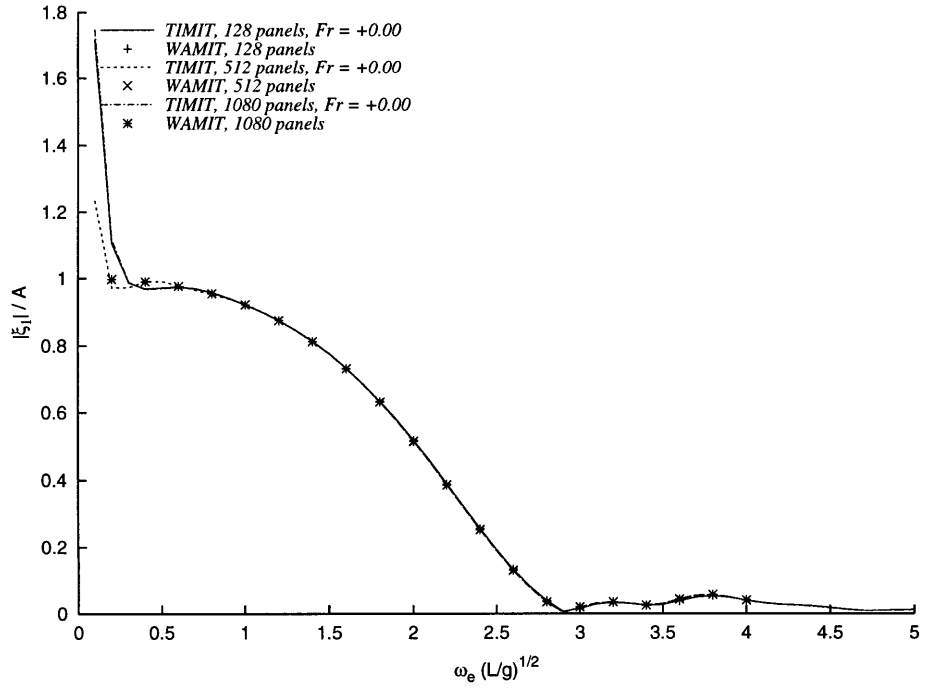

Figure 5-19: Wigley hull. Surge absolute motion. Comparison with WAMIT. Heading = 180.

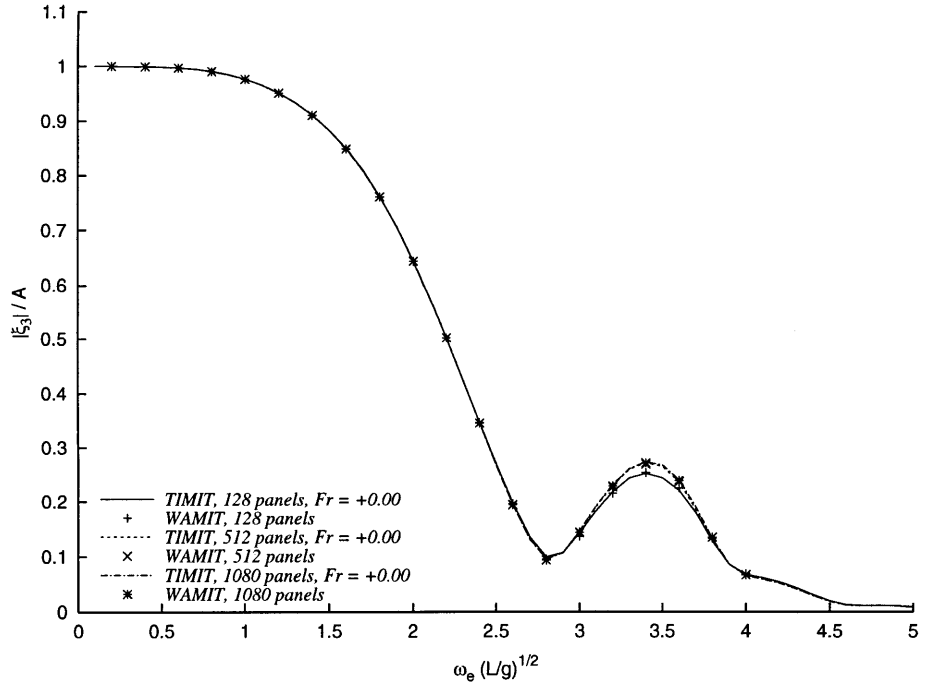

Figure 5-20: Wigley hull. Heave absolute motion. Comparison with WAMIT. Heading = 180.

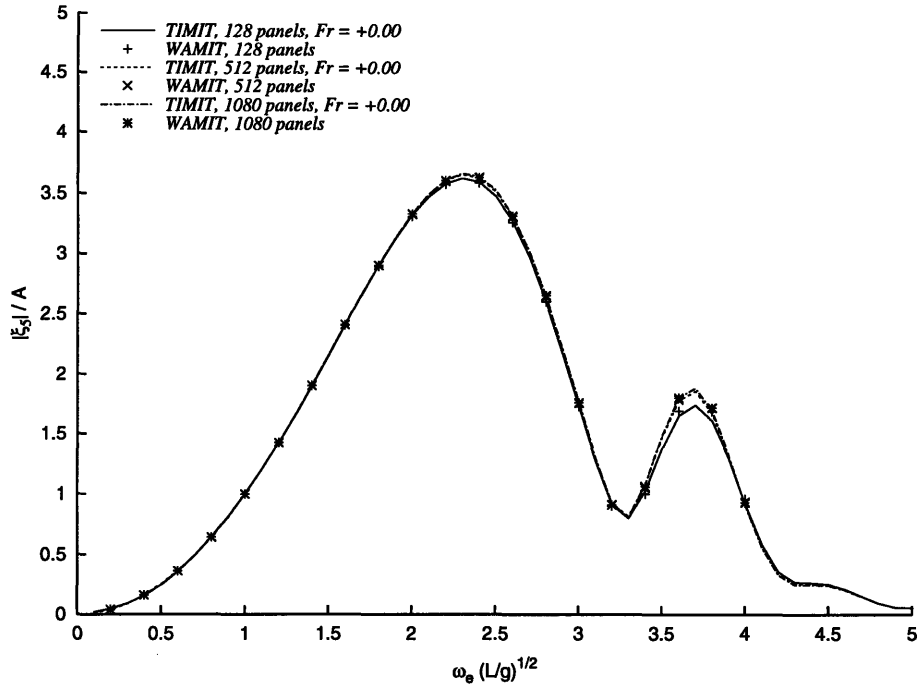

Figure 5-21: Wigley hull. Pitch absolute motion. Comparison with WAMIT. Heading = 180.

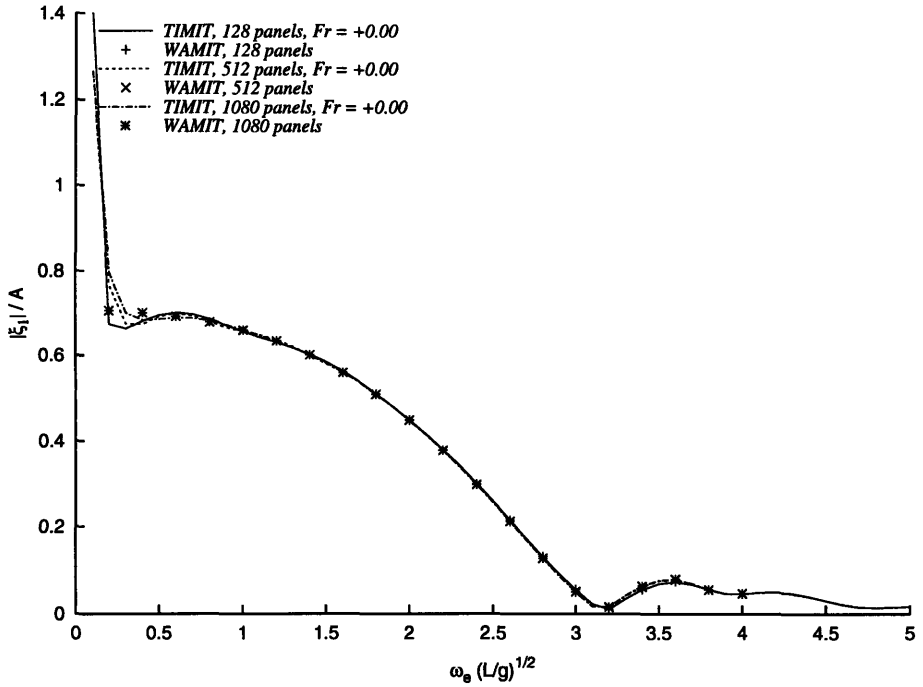

Figure 5-22: Wigley hull. Surge absolute motion. Comparison with WAMIT. Heading = 135.

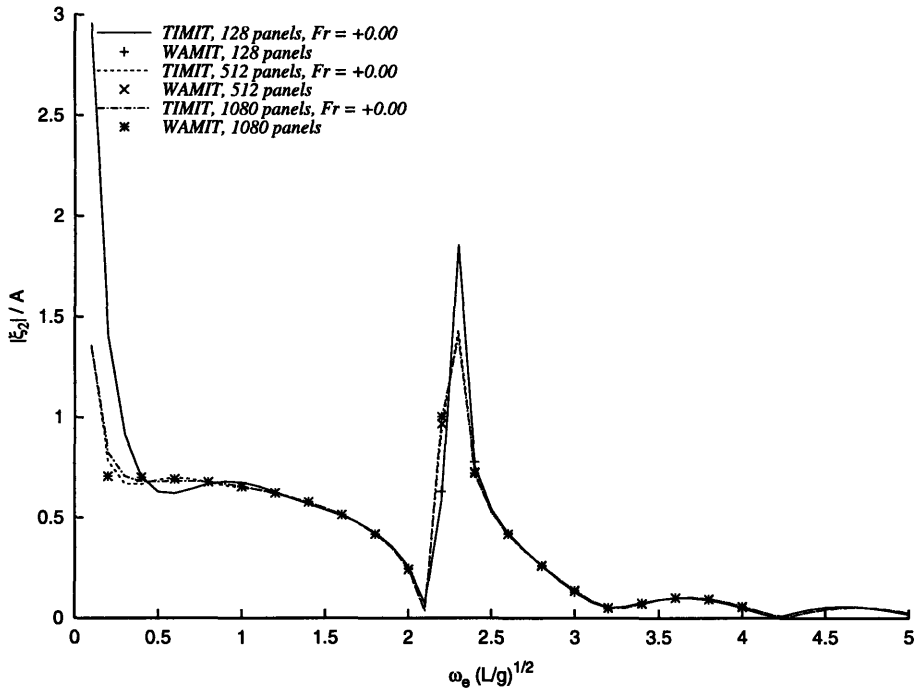

Figure 5-23: Wigley hull. Sway absolute motion. Comparison with WAMIT. Heading = 135.

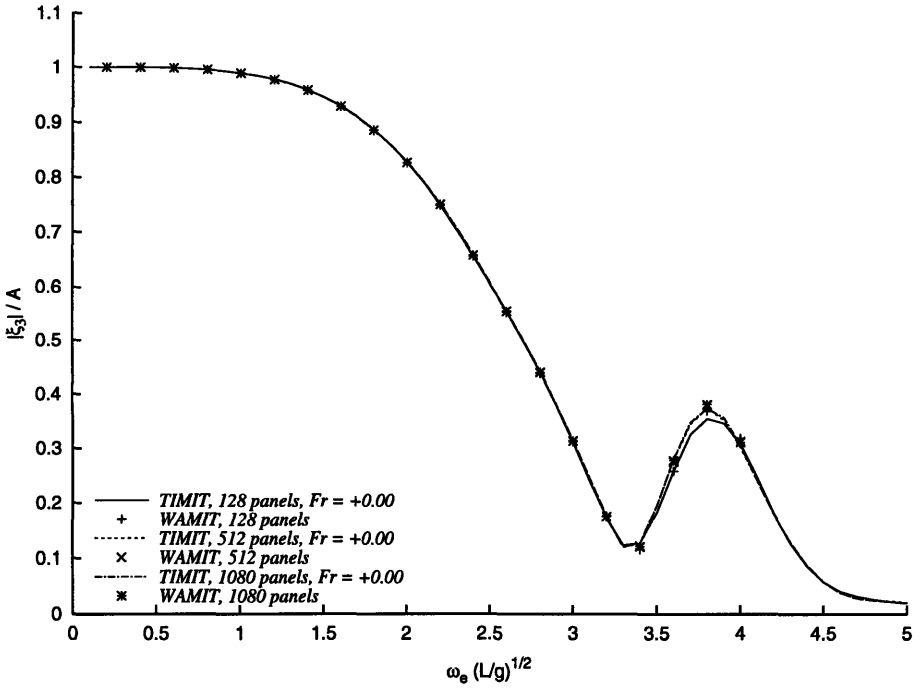

Figure 5-24: Wigley hull. Heave absolute motion. Comparison with WAMIT. Heading = 135.

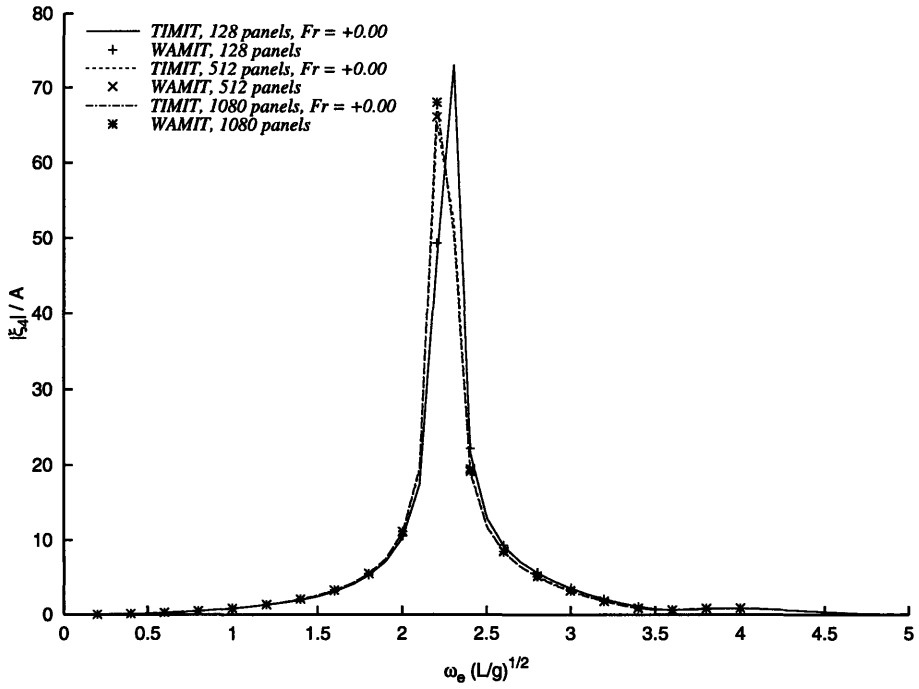

Figure 5-25: Wigley hull. Roll absolute motion. Comparison with WAMIT. Heading = 135.

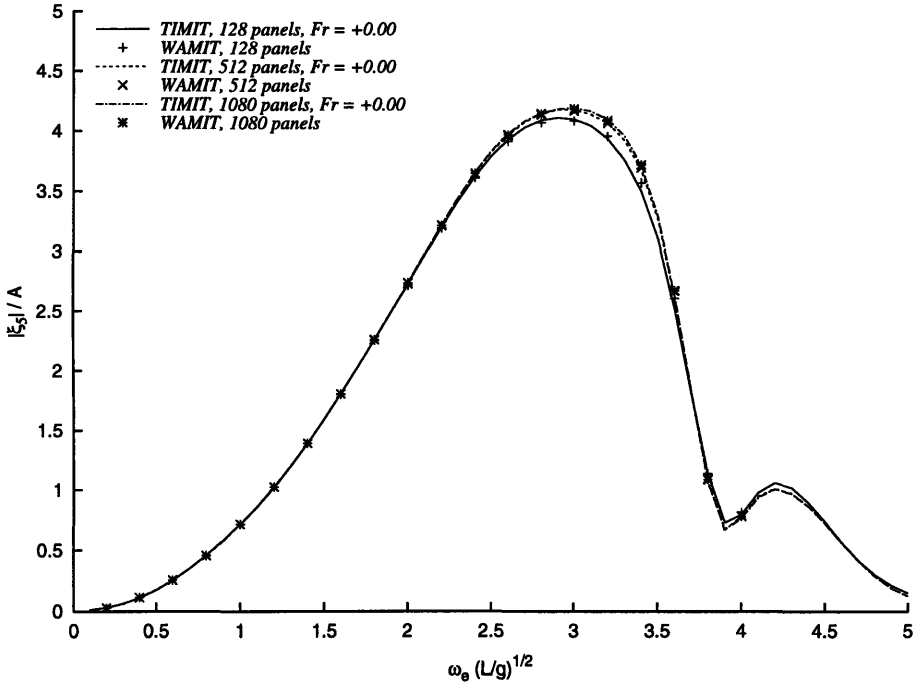

Figure 5-26: Wigley hull. Pitch absolute motion. Comparison with WAMIT. Heading = 135.

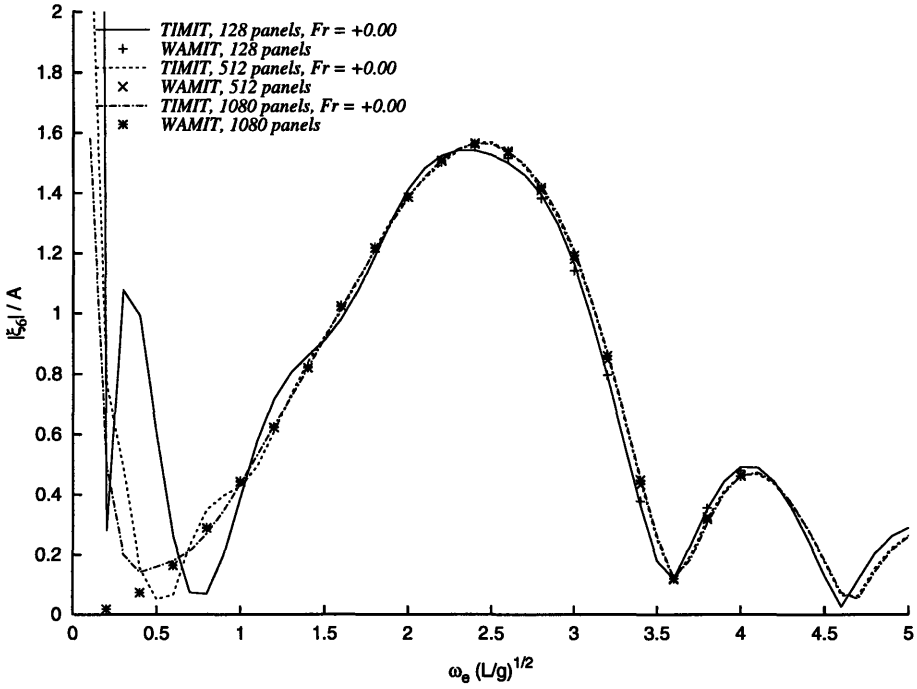

Figure 5-27: Wigley hull. Yaw absolute motion. Comparison with WAMIT. Heading = 135.

The results for the diffraction and radiation second-order steady forces, checking the convergence of the method in comparison with WAMIT are shown in Figures 5-28 to 5-36 below, for a heading of 180 degrees and 135 degrees. We can see that the convergence of the results as a function of an increase in the number of panels was again very satisfactory.

Figures 5-37 to 5-44 show the influence of the ship speed on the diffraction and radiation second-order steady-force, with Figures 5-39 and 5-40 showing the comparison of our code against the program SWAN, for head and following seas (actually the ship moving backwards), and we can see that the results also compared quite well. It is clear that the following seas forces are quite small when compared to the head seas situation, and we are actually only showing that the forces under this condition are small. Very small oscillatory behavior of these small steady force as a function of the frequency when we go to large absolute frequencies, like those in Figure 5-38, should be regarded as difficult of the present mesh to accurately represent the physics involved and not as a fundamental problem with the formulation. We may also note that the surge second-order steady force that we are comparing against SWAN results is also know as added resistance in waves, because it represents the additional resistance the ship has to overcome to keep its forward speed constant in spite of the presence of waves. And although they represent the same value, they have opposite signs, since a positive resistance represents a negative force.

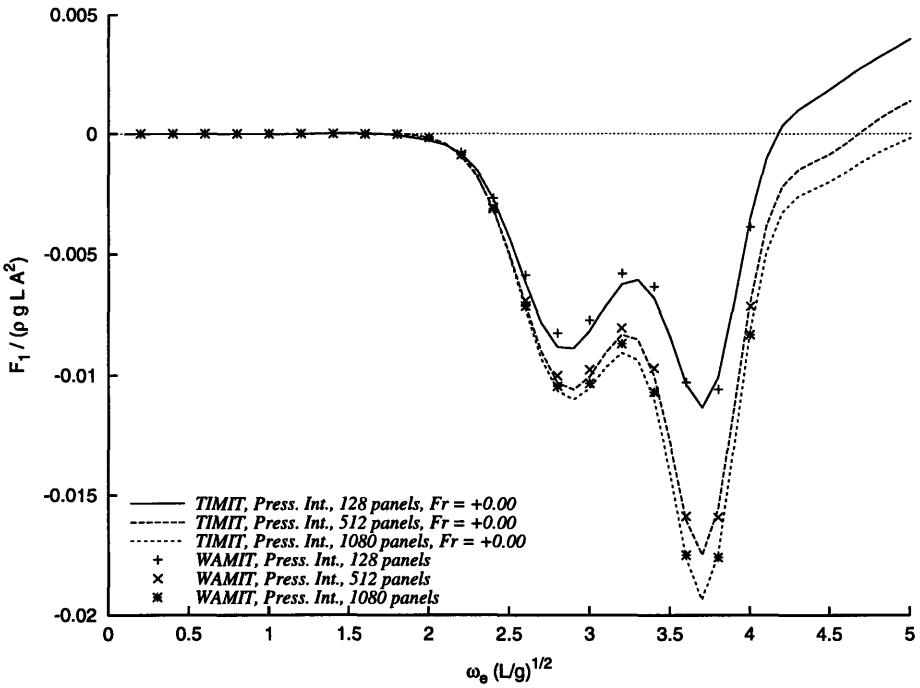

Figure 5-28: Wigley hull, free to move in waves. Surge second-order steady force. Comparison with WAMIT. Heading = 180.

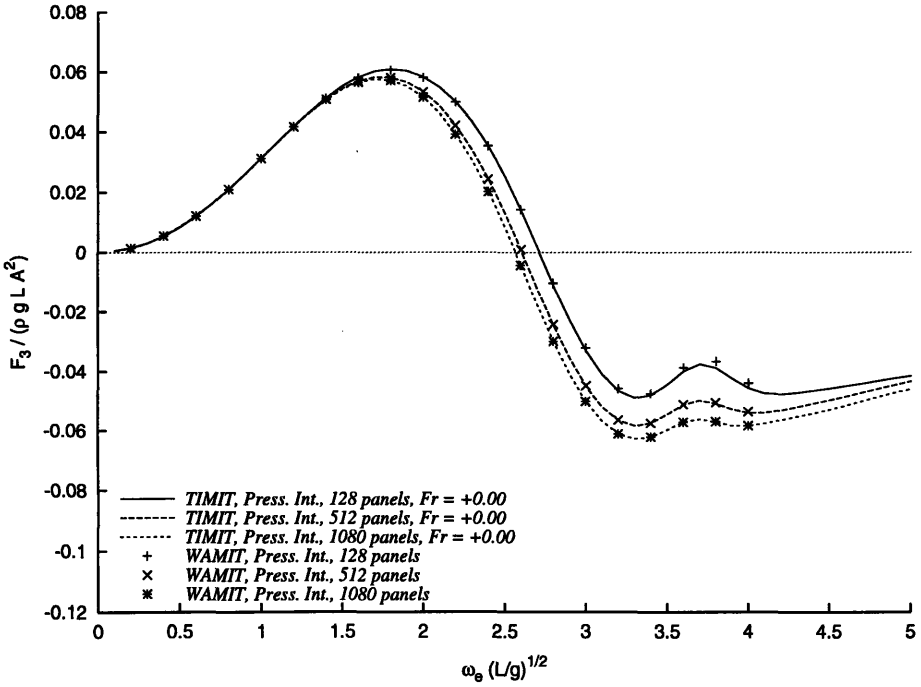

Figure 5-29: Wigley hull, free to move in waves. Heave second-order steady force. Comparison with WAMIT. Heading = 180.

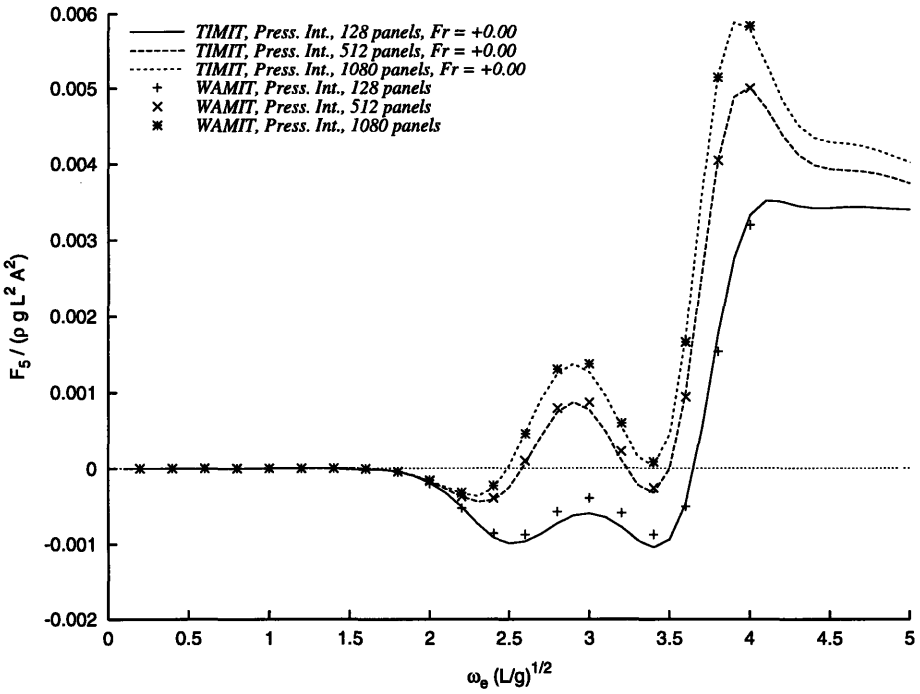

Figure 5-30: Wigley hull, free to move in waves. Pitch second-order steady force. Comparison with WAMIT. Heading = 180.

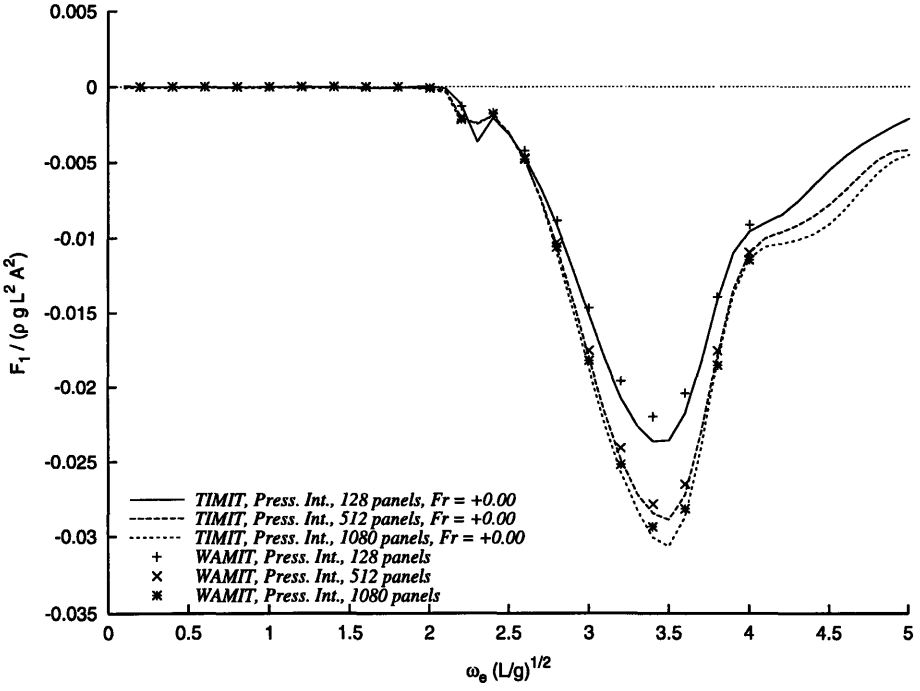

Figure 5-31: Wigley hull, free to move in waves. Surge second-order steady force. Comparison with WAMIT. Heading = 135.

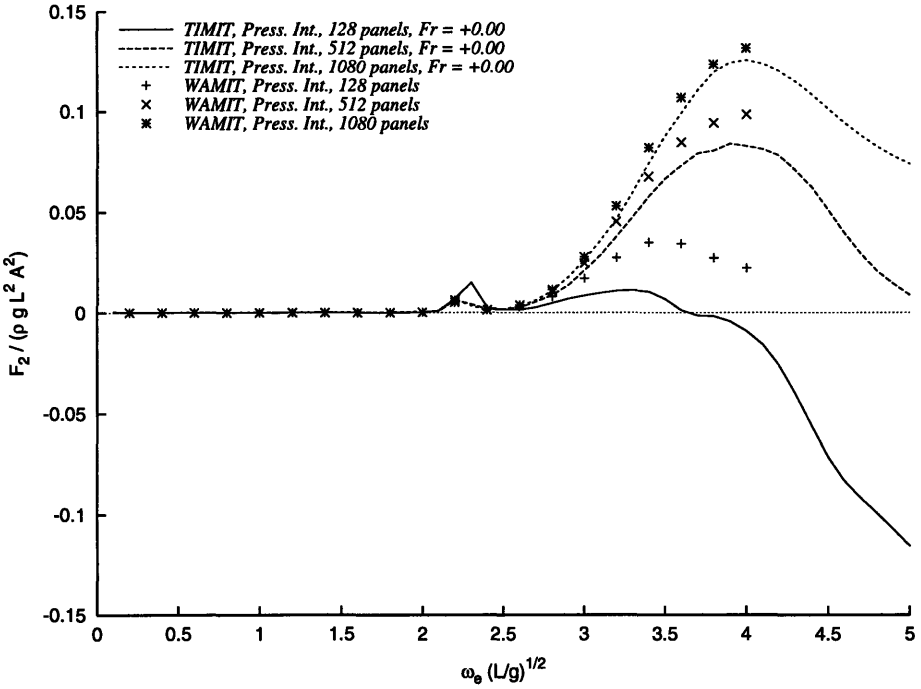

Figure 5-32: Wigley hull, free to move in waves. Sway second-order steady force. Comparison with WAMIT. Heading = 135.

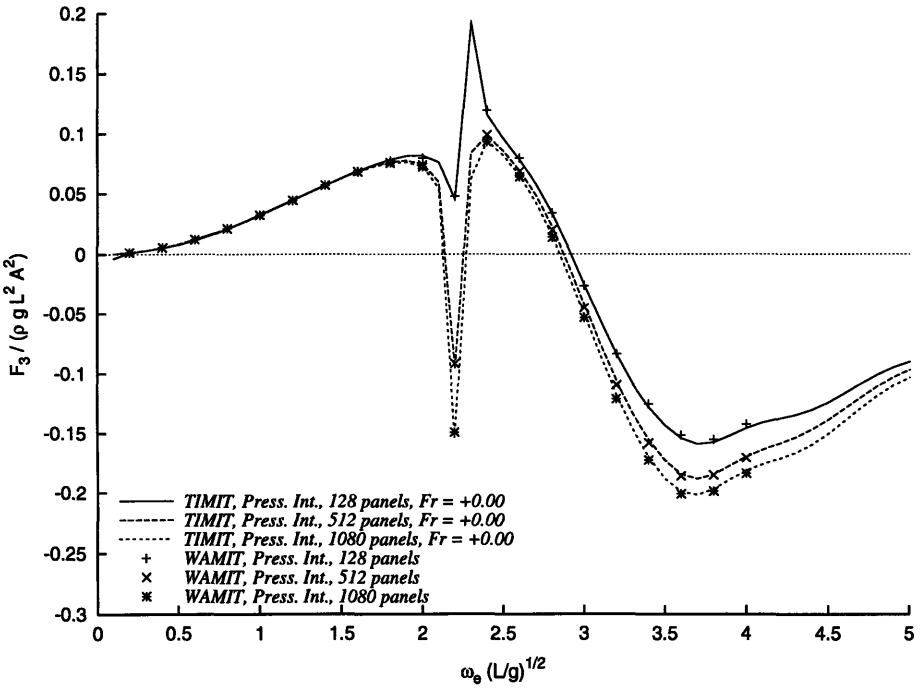

Figure 5-33: Wigley hull, free to move in waves. Heave second-order steady force. Comparison with WAMIT. Heading = 135.

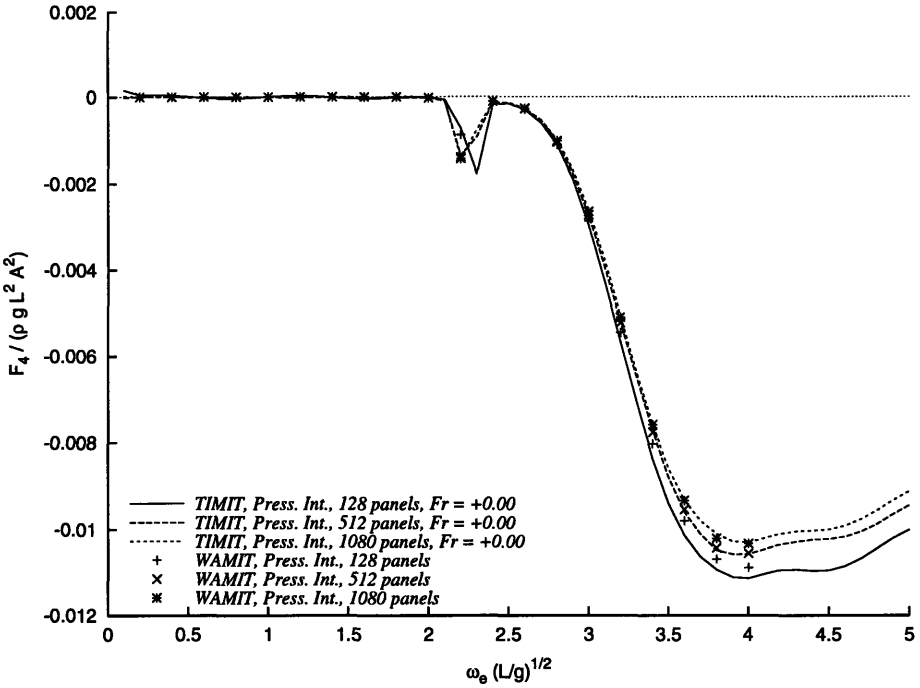

Figure 5-34: Wigley hull, free to move in waves. Roll second-order steady force. Comparison with WAMIT. Heading = 135.

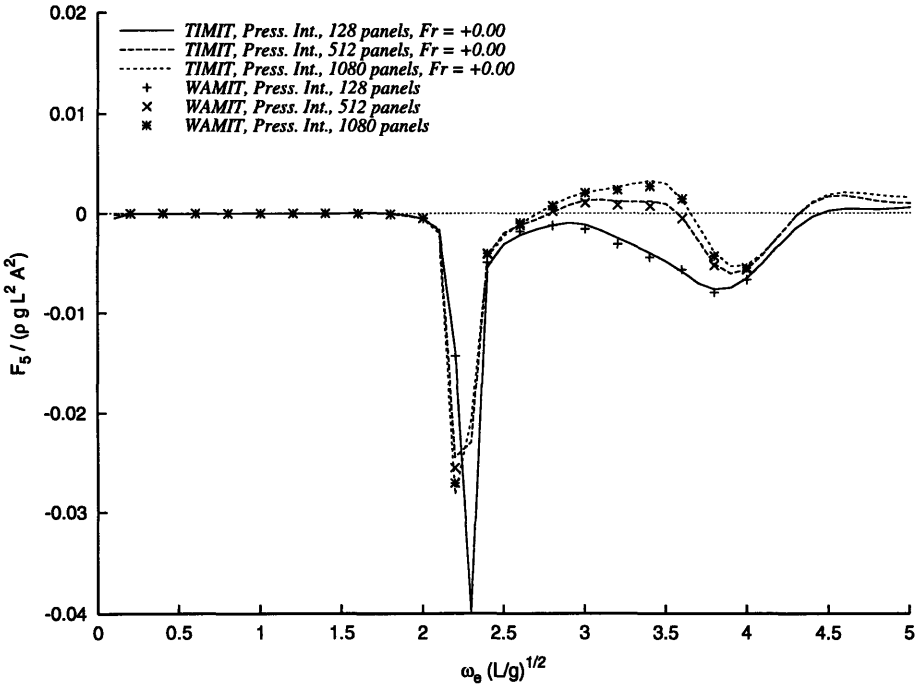

Figure 5-35: Wigley hull, free to move in waves. Pitch second-order steady force. Comparison with WAMIT. Heading = 135.

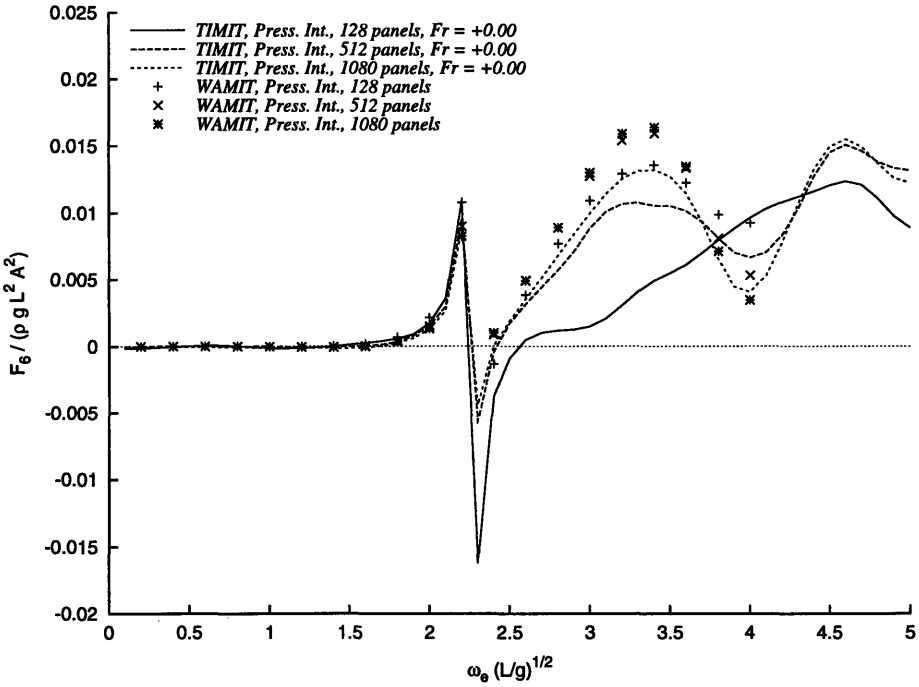

Figure 5-36: Wigley hull, free to move in waves. Yaw second-order steady force. Comparison with WAMIT. Heading = 135.

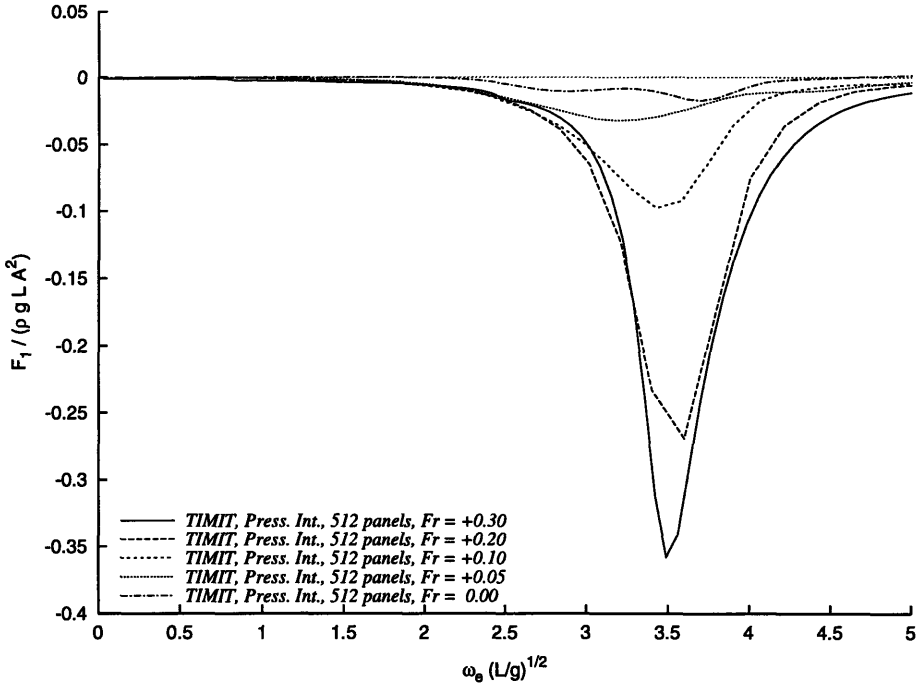

Figure 5-37: Wigley hull, free to move in waves. Surge second-order steady force. Different Froude numbers, ship moving ahead. Heading = 180.

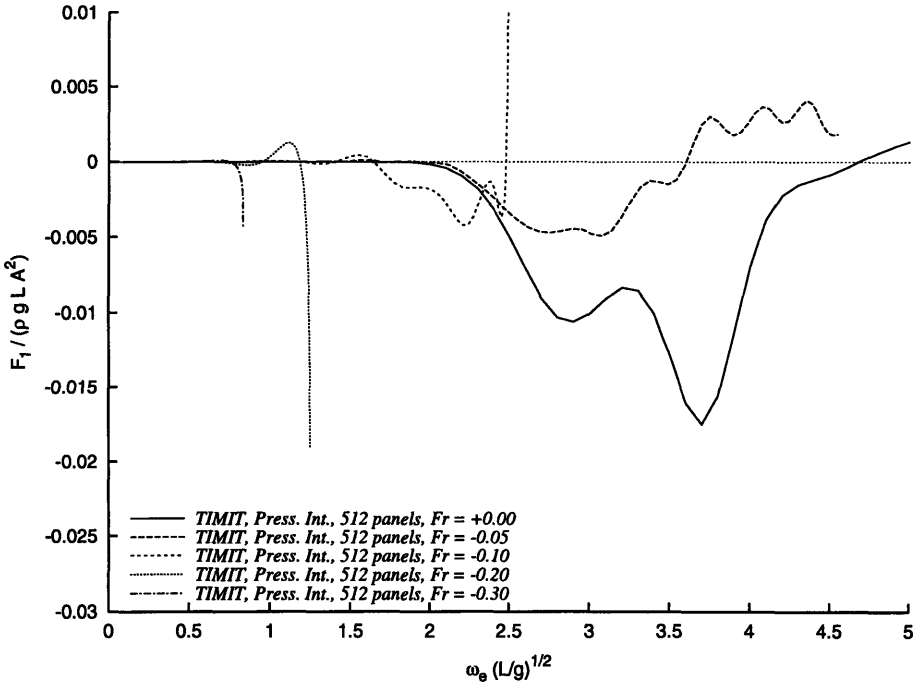

Figure 5-38: Wigley hull, free to move in waves. Surge second-order steady force. Different Froude numbers, ship moving backwards. Heading = 180.

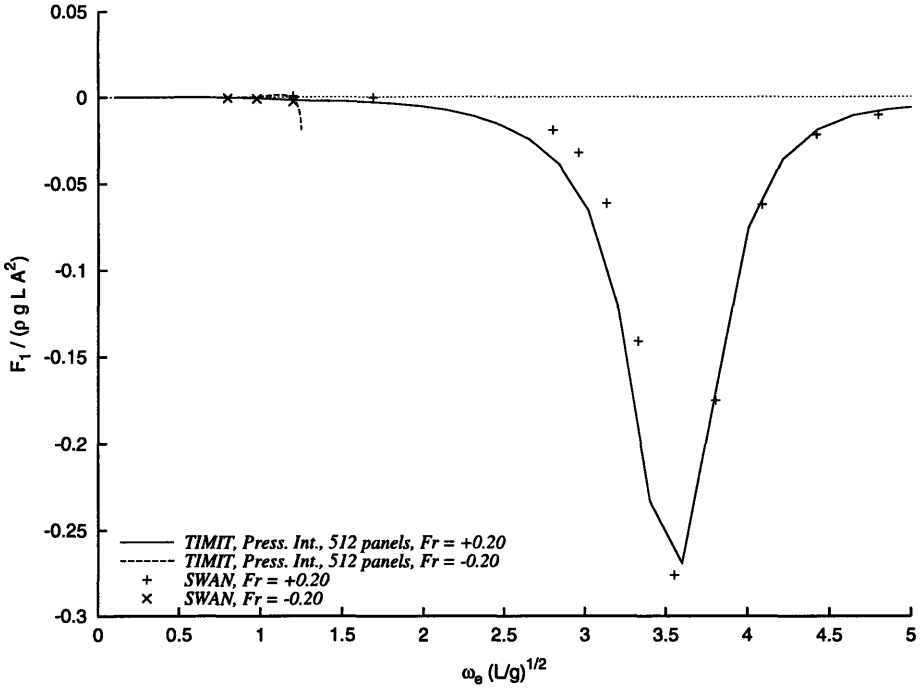

Figure 5-39: Wigley hull, free to move in waves at Fr= ± 0.20. Surge second-order steady force. Comparison with SWAN code. Heading = 180.

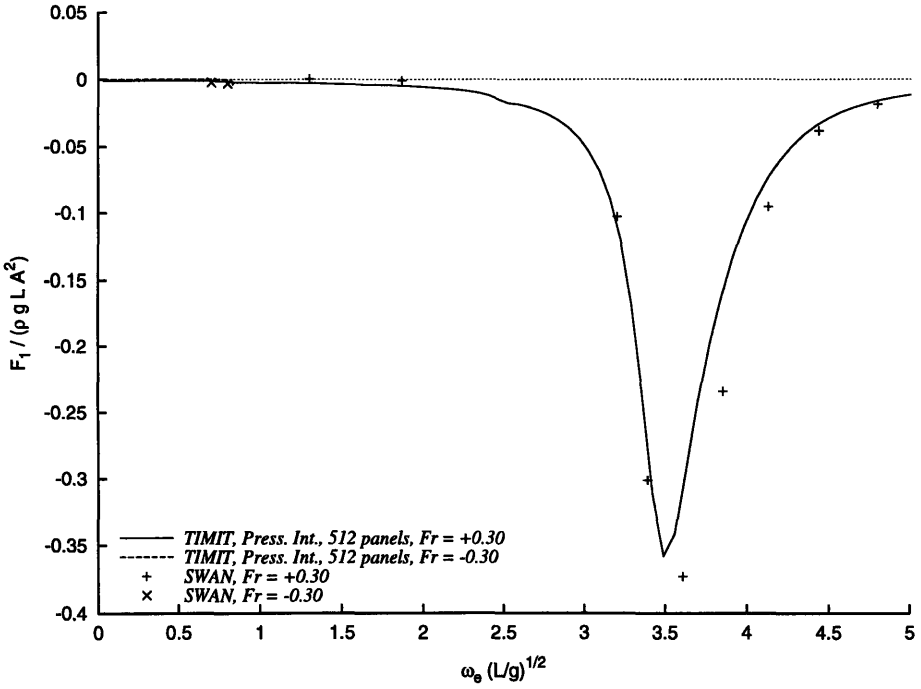

Figure 5-40: Wigley hull, free to move in waves at Fr= ± 0.30. Surge second-order steady force. Comparison with SWAN code. Heading = 180.

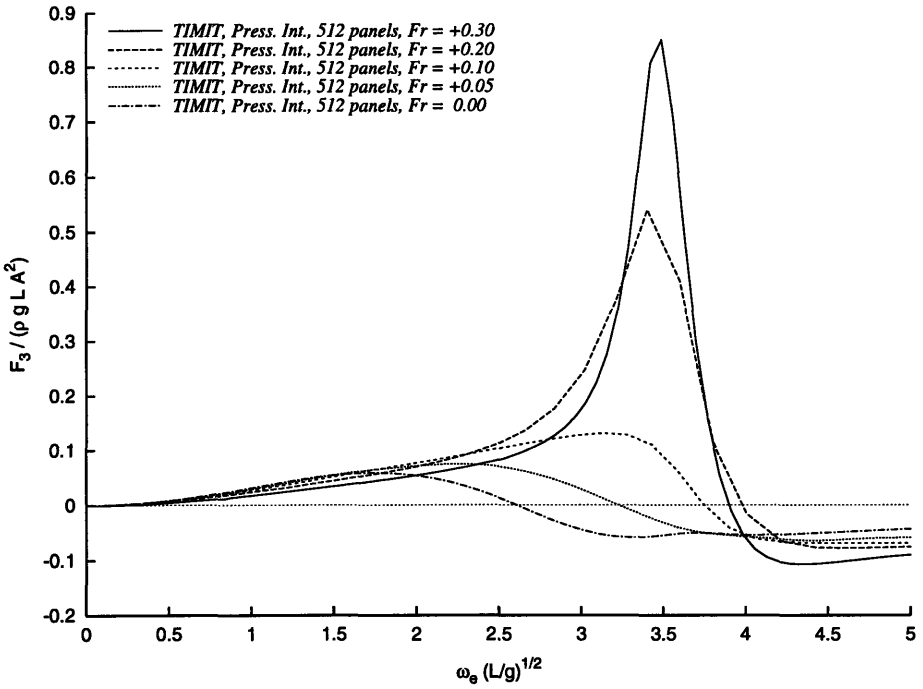

Figure 5-41: Wigley hull, free to move in waves. Heave second-order steady force. Different Froude numbers. Ship moving ahead. Heading = 180.

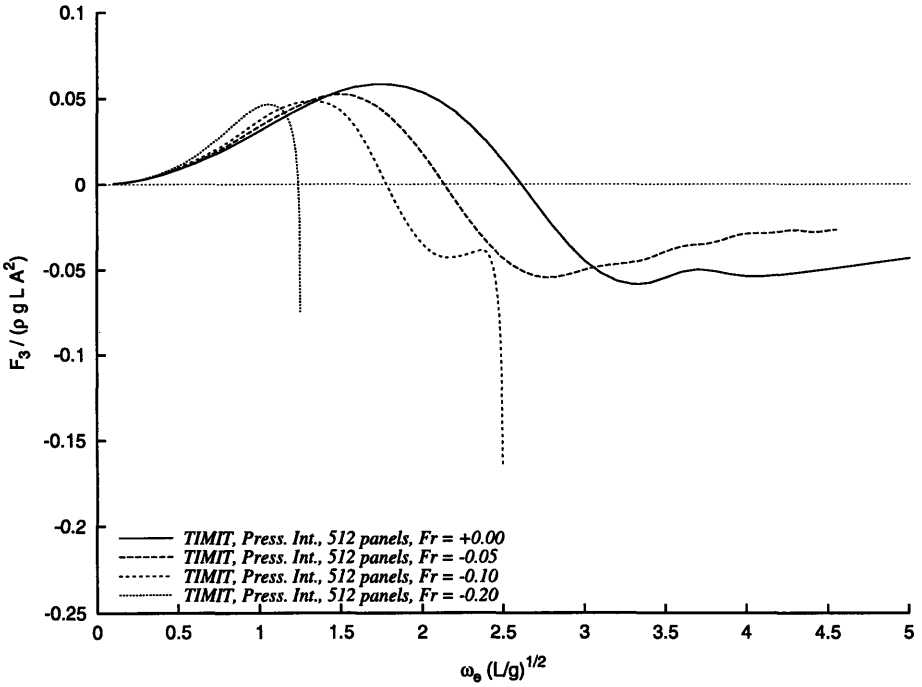

Figure 5-42: Wigley hull, free to move in waves. Heave second-order steady force. Different Froude numbers. Ship moving backwards. Heading = 180.

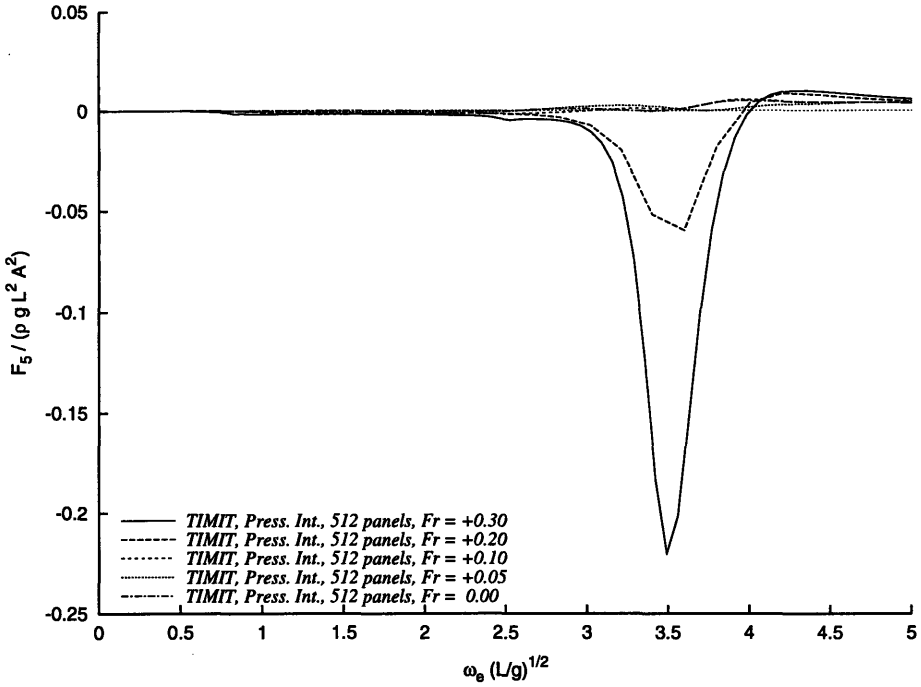

Figure 5-43: Wigley hull, free to move in waves. Pitch second-order steady force. Different Froude numbers. Ship moving ahead. Heading = 180.

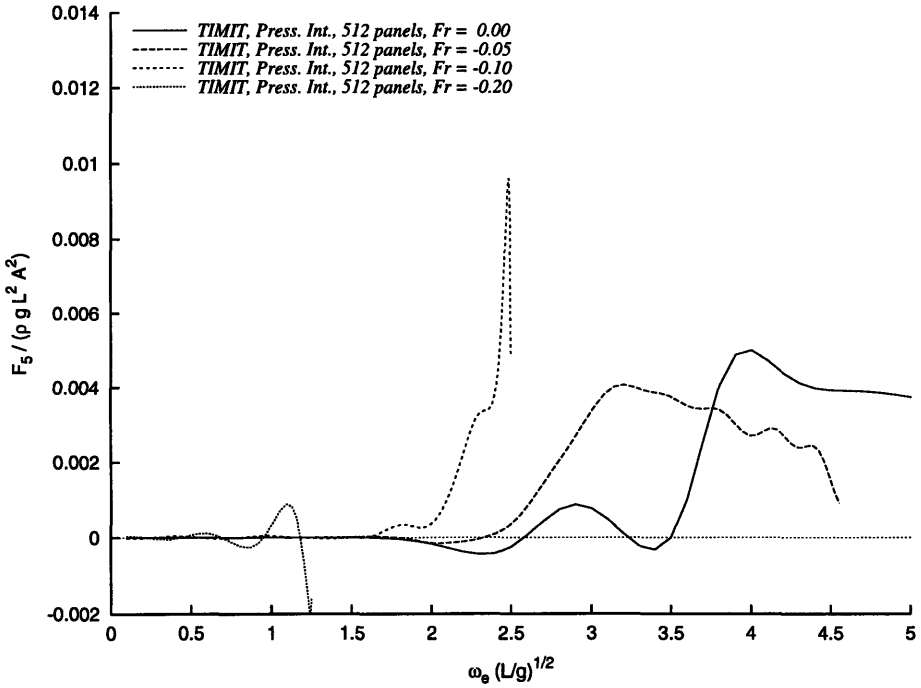

Figure 5-44: Wigley hull, free to move in waves. Pitch second-order steady force. Different Froude numbers. Ship moving backwards. Heading = 180.

5.2 The Floating Hemisphere

The floating hemisphere under consideration has radius equal to one, and the panelization of the hull was made using 368 and 992 elements. As the program takes advantage of the hull symmetry, only half of the body was discretized.

The meshes can be seen in Figures 5-45 and 5-46 below. First we will show

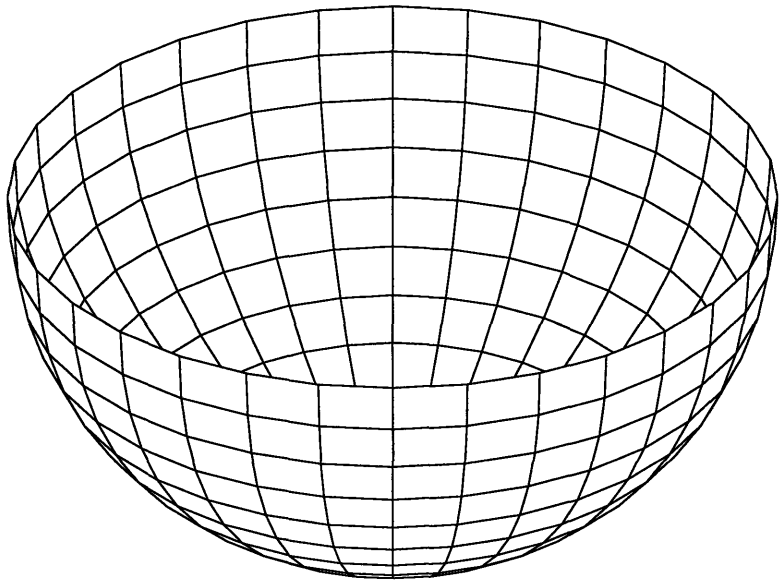

Figure 5-45: Floating hemisphere represented by a mesh with 368 panels. Actual numerical model uses the symmetry with respect to the xz–plane.

that the computations made for zero Froude number are consistent with the results calculated by the WAMIT code. These results can be seen in Figure 5-47. We can see a good agreement between TIMIT and WAMIT for the second-order steady forces using both the pressure integration method and momentum flux computation approach, when the hemisphere has 368 panels. For all cases we have used a total time history equal to $36\sqrt{g/R}$ with a time step equal to $0.08\sqrt{g/R}$. For the outer mesh, where the control points used for the momentum flux computations are located, we have used 416 points and a radius equal to $1.4/R$ and a draft equal to $1.2/R$.

The case with 992 panels, which was only computed using the pressure integration method, since the momentum flux computation would take a very long CPU time due

to the local quantities needed to be computed on the outer mesh, is not converged, and this is probably due to the time step being too large. Since we can see from the WAMIT results and this TIMIT simulation that 992 panels would not be enough for having good results on this comparison, we used the results from the momentum flux computation, which are converged as we can see from the WAMIT results with 368 and 992 panels.

We will now see how good are the computed second-order steady forces for small Froude numbers when the Neumann-Kelvin hypothesis of the body being slender will not be fulfilled, for the hemisphere case. We compared our results against computations done by Nossen, Grue and Palm [34] using a slow (quadratic terms of the basis flow potential were disregarded) double-body approach, and with the current having speed equivalent to a Froude number equal to 0.04 in Figure 5-48. We also compared our results for the second-order steady force on a fixed hemisphere against results published by Zhao and Faltinsen [42], which uses the same approach as Nossen *et al*, with the difference that Zhao and Faltinsen solve an internal problem using the Rankine Green function and match with a multipole expansion at some distance away from the body, while Nossen *et al* use a slow-speed approximation for the free-surface Green function. A comparison with our results is shown in Figure 5-49 below. We should note that the Froude number now changed to 0.032. We can see a reasonably good agreement with Nossen *et al*, and a not so good agreement with the Zhao and Faltinsen's result, even for the zero speed case.

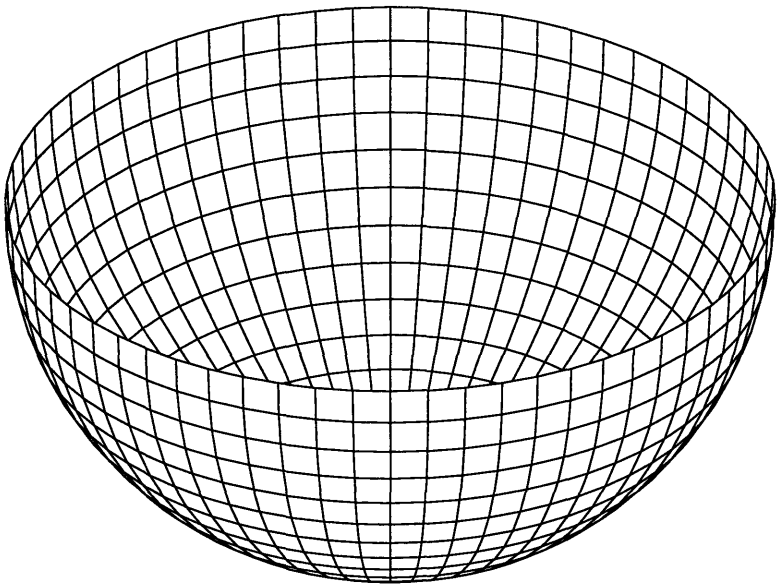

Figure 5-46: Floating hemisphere represented by a mesh with 992 panels. Actual numerical model uses the symmetry with respect to the xz–plane.

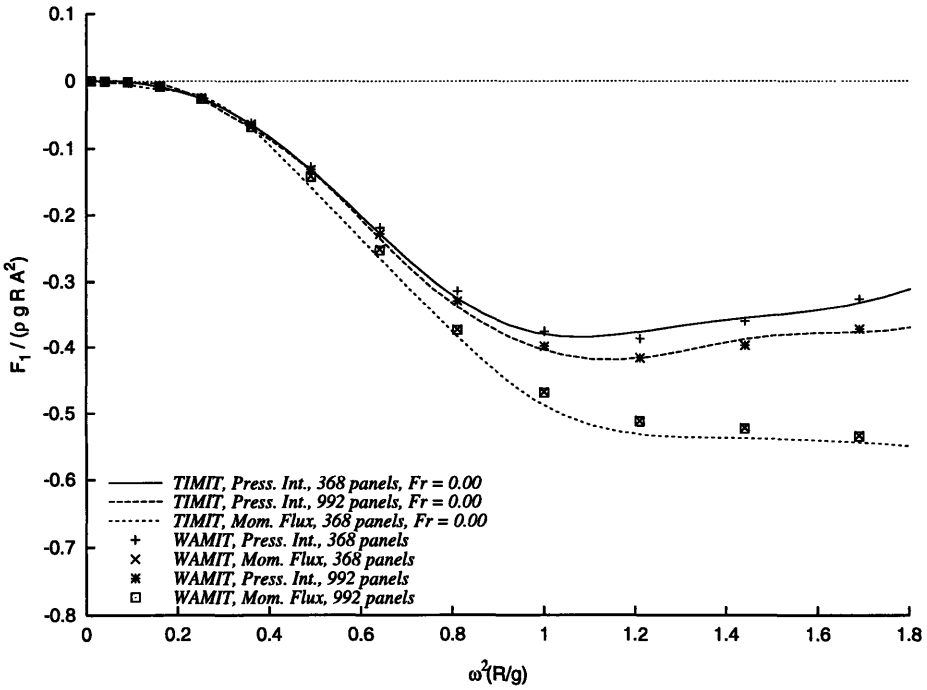

Figure 5-47: Floating hemisphere with $R = 1$, Surge diffraction second-order steady force. Comparison with WAMIT. Heading = 180.

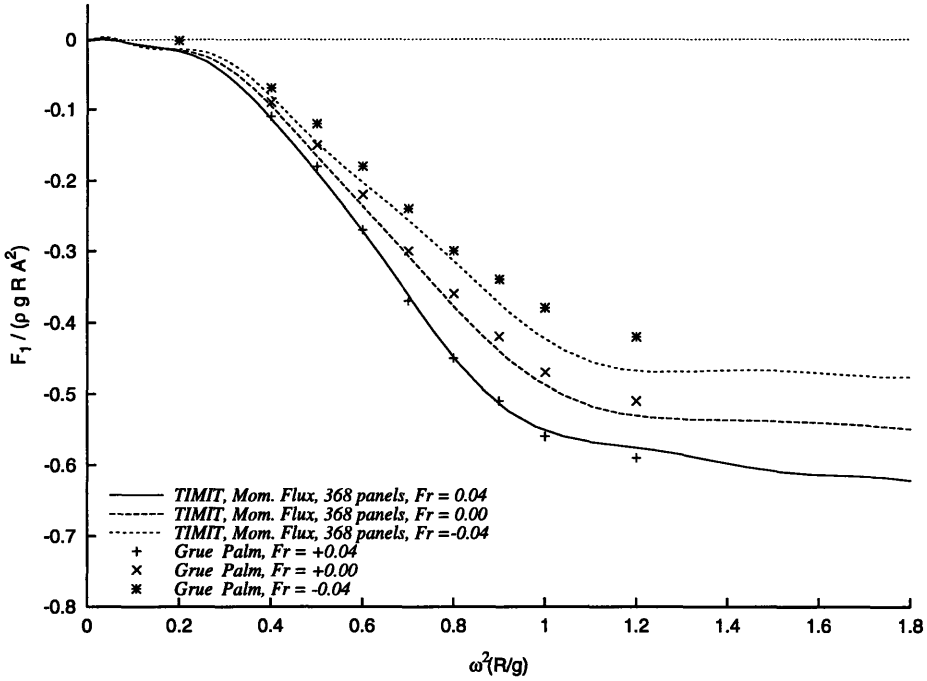

Figure 5-48: Floating hemisphere with $R = 1$, Surge diffraction second-order steady force. Comparison with results from Grue and Palm. Heading = 180.

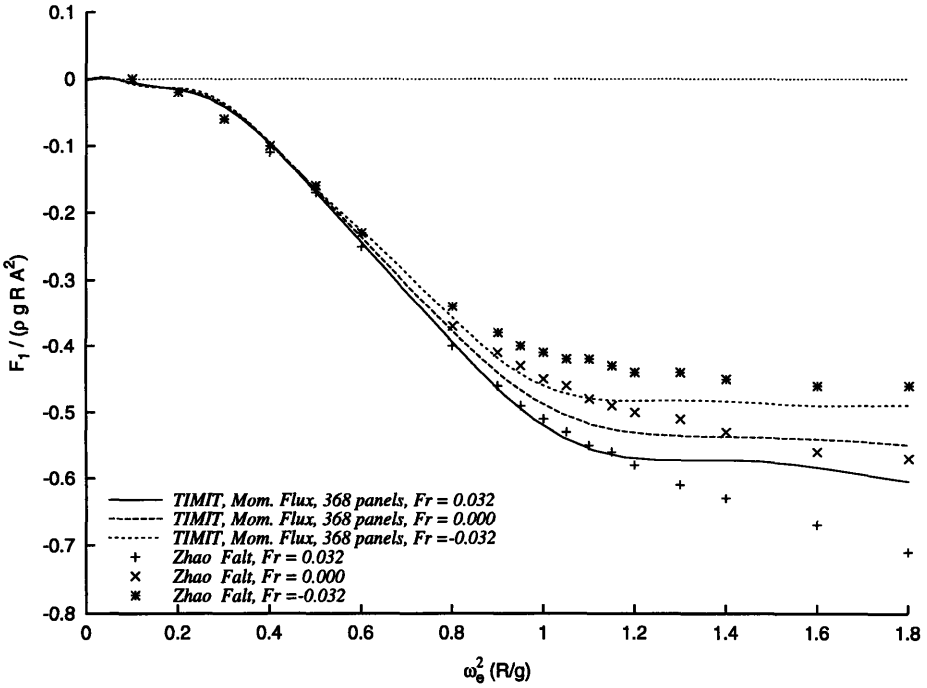

Figure 5-49: Floating hemisphere with $R = 1$, Surge diffraction second-order steady force. Comparison with results from Zhao and Faltinsen. Heading = 180.

5.3 The Circular Cylinder

The shallow circular cylinder has a radius R equal to 1 and draft T equal to 0.25. The discretization of the hull was made using 288 panels and 1080 panels. Due to its symmetry, only half of the body needs to be discretized. The meshes are shown in the Figures 5-50 and 5-51 below. For the outer mesh, associated with the computation using the momentum flux approach, we have used 416 points and an outer radius equal to $1.4/R$ and a draft equal to $1.2/R$.

We can see in Figure 5-52 computations for the zero Froude number case against the WAMIT code. In all simulations we have used a total time history equal to $24\sqrt{g/R}$ with a time step equal to $0.05\sqrt{g/R}$. The results agree well with the WAMIT code and we can see that the pressure method using 1080 panels give a second-order steady force which is close to the one got using the momentum flux computation.

We then compared our second-order steady forces against those from Zhao and Faltinsen [43] for zero current speed and for a current equivalent to a Froude number equal to 0.0478. The results, as we can see in Figure 5-53 agree reasonably well. One explanation for the good agreement in this case is that in some sense the shallow cylinder agree with respect to the Neumann-Kelvin hypothesis in the sense that the flow can to a great extent divert to underneath the cylinder without having to go sideways.

In Figure 5-54 we compare results from pressure integration and momentum flux computations, both using TIMIT, and we can see a reasonably good convergence, indicating that the contribution coming from the second-order steady potential is small, as we concluded from the analysis in Chapter 4.

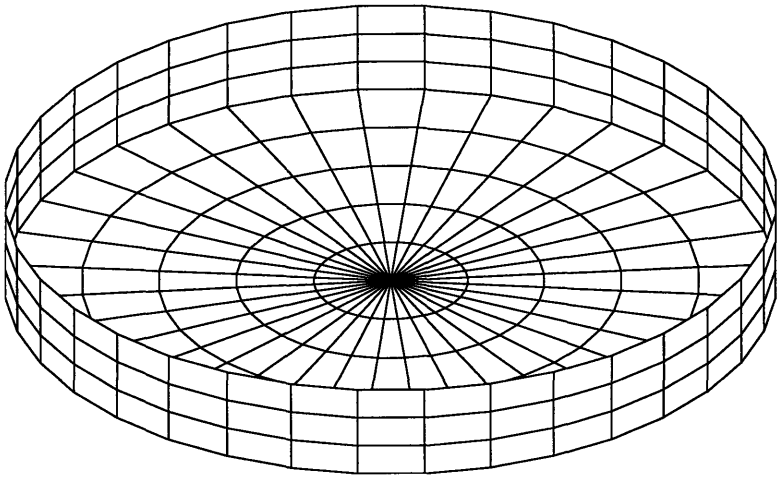

Figure 5-50: Floating circular cylinder with $T/R = 1/4$, represented by a mesh with 288 panels. Actual numerical model uses the symmetry with respect to the xz–plane.

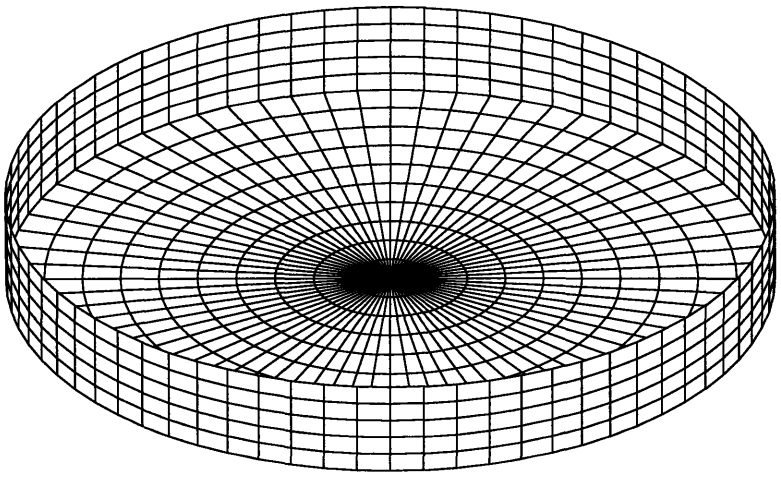

Figure 5-51: Floating circular cylinder with $T/R = 1/4$, represented by a mesh with 1080 panels. Actual numerical model uses the symmetry with respect to the xz–plane.

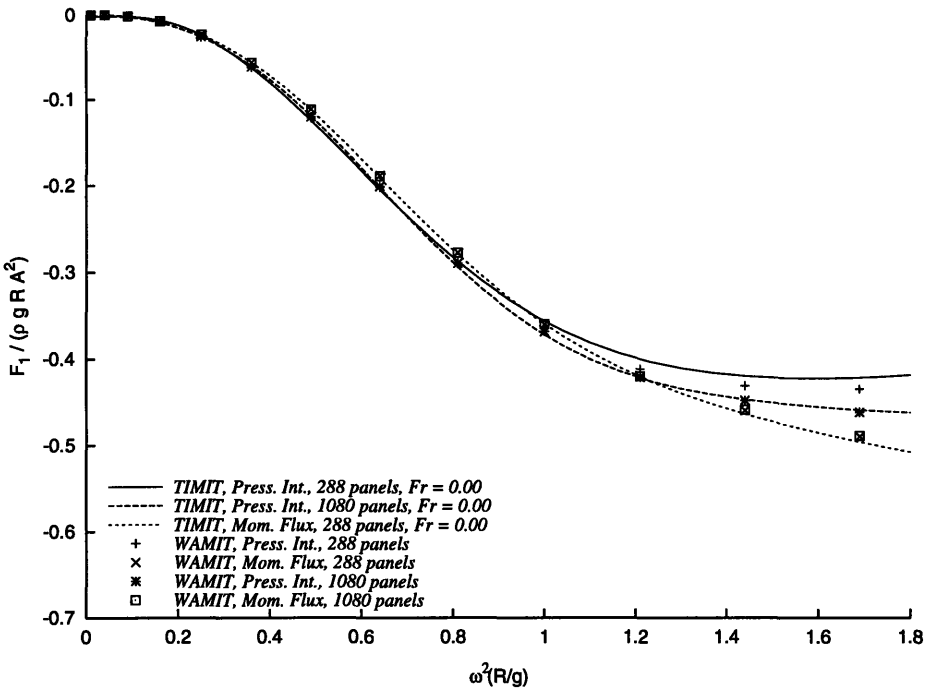

Figure 5-52: Floating circular cylinder with $T/R = 1/4$, Surge diffraction second-order steady force. Comparison with WAMIT. Heading = 180.

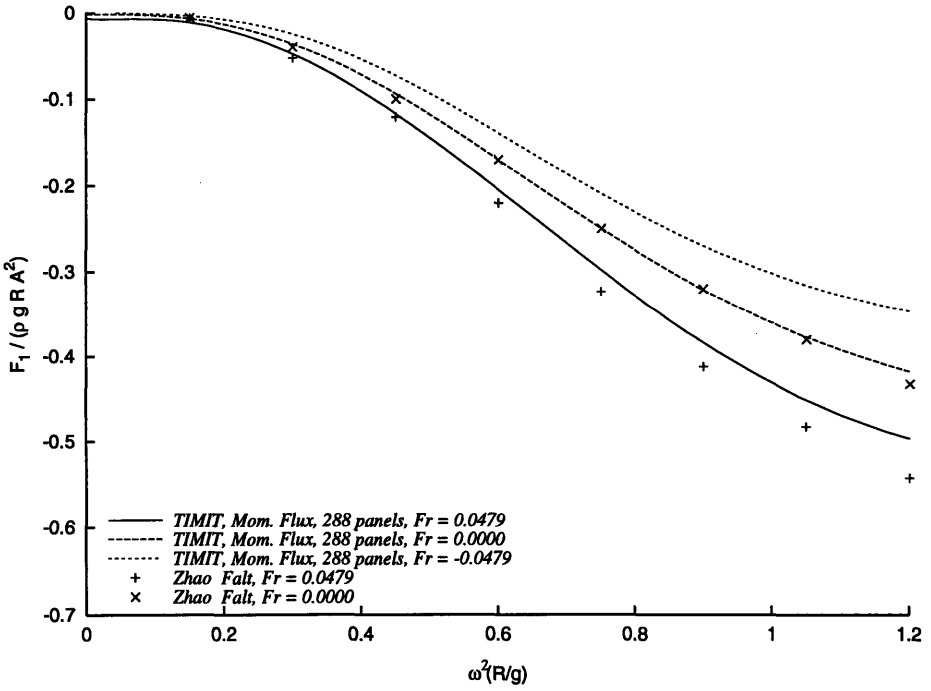

Figure 5-53: Floating circular cylinder with $T/R = 1/4$, Surge diffraction second-order steady force. Comparison with results from Zhao and Faltinsen. Heading = 180.

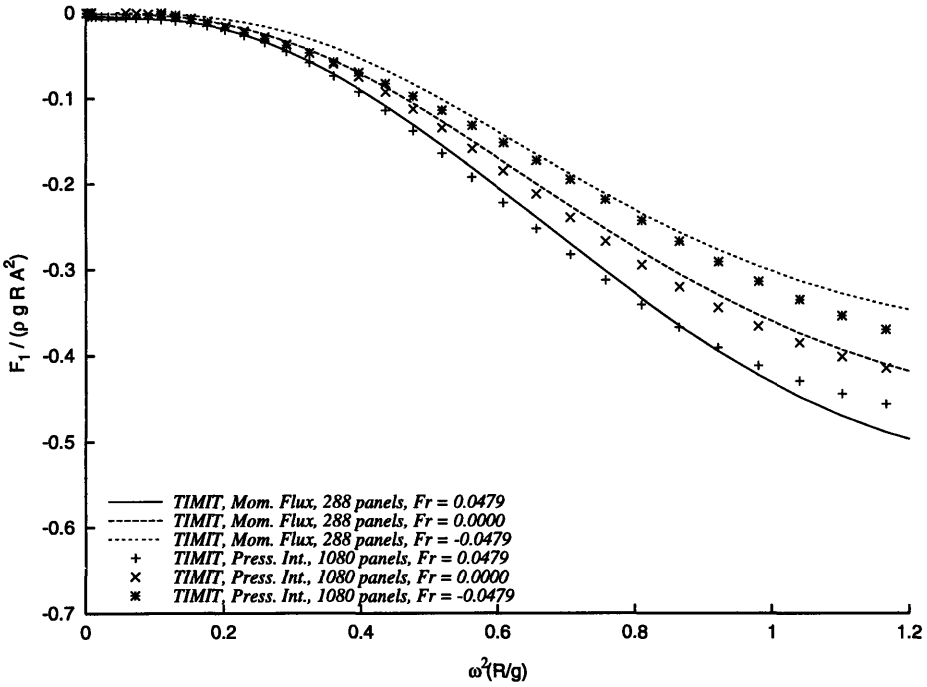

Figure 5-54: Floating circular cylinder with $T/R = 1/4$, Surge diffraction second-order steady force. Comparison between the pressure integration method and the momentum flux computation. Heading = 180.

Chapter 6

Discussion

A numerical solution has been developed for computing the second-order steady forces acting on a ship with forward speed in the presence of incident waves. The assumptions include potential flow, small wave amplitudes and body motions, and use of the Neumann-Kelvin hypothesis that the unsteady problem is linearized with respect to the uniform incoming flow.

A description of the boundary-value problem is made, and other choices of linearization are presented. The first-order problem is formulated as an initial boundary-value problem, an then reformulated as the solution of an integral equation, using the free-surface Green function.

In addition to the more common head-seas condition, the following-seas case is considered, with the decomposition of the incident wave in three separate regions which are defined according to the signs of the phase and group velocity of the waves, with respect to the steadily moving reference system.

The frequency-domain representation of the global and local quantities were derived, and implemented together with the computation of the potential and velocities inside the fluid region, using the source formulation. The latter information is needed in the momentum flux computations.

The equations for the computation of the second-order steady forces and moments are then presented. These are implemented in the code TIMIT in two complementary approaches, (1) integrating pressures over the body and (2) computing the momentum

flux over a compact surface surrounding the floating body.

It is necessary in principle to compute also the solution of the second-order steady Neumann-Kelvin boundary-value problem. The problem is formulated in the frequency domain, and it is shown that the boundary conditions are functions of the frequency of the incident and radiated waves. An integral equation formulation is proposed for the solution of this problem, as the large-time asymptotic of the equivalent time-domain problem with constant boundary condition for each frequency. Due to the numerical problems in the computation of higher order derivatives of the potential, the convergence of the above problem is very poor for the discretization of the free-surface we have used. An alternate problem, valid for small forward speed, was defined in order to estimate the order of magnitude of the second-order steady force coming from the second-order steady potential. For the Wigley hull, despite the unsatisfactory approximation of the forcing function on the free surface, it is suggested that this contribution is small in comparison with the contribution from the other terms and can be disregarded. Comparisons made between the pressure integration results with momentum flux computations also indicates that this conclusion is true.

The main contributions of this work are the numerical proof that Fourier transforming local quantities from the time to the frequency domain is a valid approach, as well as the subsequent computation of the second-order steady forces using these local quantities and the Neumann-Kelvin approach.

Prior to this work Fourier transforming from the time domain had only been used for integrated quantities. It was unclear if good results could be computed in the frequency domain for local quantities, such as fluid velocities, particularly at points close to a sharp edge or the free surface. Indeed our results for the oblique case showed that there is some difficulty to correctly represent the potential and velocities at the panels located close to the edge. This effect is stronger as we increase the frequency and diminished as we decrease the panels size. Increasing the number of panels that defines the mesh, we will see that this fluctuations are restricted to panels close to the edges of the Wigley hull. Another consequence of increasing the number of panels is that the relative weight of the panels where those fluctuations occur will decrease,

since we will have a higher proportion of panels that will be situated not so close to the edges.

It became also clear that when refining the meshes we should keep the aspect ratio of the panels close to 1, mainly if the panel is located close to the mean free surface. Large aspect-ratio panels, which are a common place in the frequency domain through the use of the cosine-spacing approach, are not attractive near the free surface in the time domain. We need to filter out high-frequency waves that will not have their wavelengths well resolved, and one easy approach is to keep the panels approximately square close to the free surface.

The integrated second-order steady forces always converge with an increase of the number of panels, time length of simulation and a decrease of the time step. But these refinements are intertwined, and an increase of the number of panels will bring more high-frequency wave components which will require smaller time steps.

The solution of the first-order problem can be very computer expensive. One run time increases with the square of the number of panels and time. We can also add the number of the field points to the number of panels to have a notion of its cost. A run with 64 panels on half body and 200 time steps took 20 minutes cpu time on a DEC-Alpha station 5/333. This went to around 4 hours for the circular cylinder with 144 panels on the half body, 209 control points for the momentum flux computation and 300 time steps. The hemisphere with 194 panels on the body, 209 control points in the fluid domain and 400 time steps, which took 11 hours. The 499 panels case of the hemisphere, without any control points and the same 400 time steps took 17.6 hours. If we used finer meshes such as are used in frequency-domain programs like WAMIT, and knowing that with the space refinement we may need more time refinement we may be talking about months of cpu time. But computers do get faster, the program is not fully optimized as it stands now, and we could see that the results obtained although not using the fine discretization we would hope are quite good on an engineering basis.

We only ran the momentum approach formulation on the least refined meshes. Convergence for the momentum approach is known to be faster than for the pressure

integration, and this was once more confirmed. The pressure integration results were always in close agreement with the computer program WAMIT, for the zero speed case. This was always the first check of the convergence of the solution. WAMIT computes the solution with data from the geometry and frequency. By achieving convergence with this program, we can be sure that the time step being used is small enough and the transient time response was carried long enough so as to get convergent solutions, for the range of frequencies used.

The results obtained for the Wigley hull, the hemisphere, and the cylinder supported the approach used in this work.

With the Wigley hull comparisons we could see that the pressure integration method presented a convergence rate comparable with the WAMIT program, and with the mesh with 512 panels we were able to obtain results that compared quite well with the SWAN code for the surge second-order steady force.

The comparisons made for the hemisphere case brought a situation when the pressure integration method presented a low convergence rate. We could not go on refining the mesh to achieve converged results under the pressure integration approach because the cpu time required would be impractical. As we have highlighted before, if we were using the WAMIT code we could have speeded this convergence rate through the use of the cosine spacing distribution of elements, while this is not possible using our time domain approach. The momentum flux computation approach was employed and gave results which were converged based on the comparison with WAMIT, and which agreed reasonably well with the results computed from Nossen, Grue and Palm [34]. A comparison was also made against results obtained by Zhao and Faltinsen [42], and the results were only similar, not agreeing too well. It should be observed though that the results were not very good even for the zero current velocity case, which suggests that the results from Zhao and Faltinsen are not accurate.

The shallow cylinder case presented reasonably good convergence rates for the pressure integration method and excellent convergence rates for the momentum flux computation approach. For this case the agreement was very good in comparison with results published by Zhao and Faltinsen [43]. Through a comparison between

the results obtained from the pressure integration approach and the momentum flux approach we can see that the second-order steady force contribution from the second-order steady potential should is relatively small, as suggested by the earlier investigations done in Chapter 4.

Another conclusion that can be taken from this exposition is that the resulting program is not trivial to use. In comparison with frequency domain codes, it is clear that there are more parameters to adjust. Besides the number of points used in the mesh definition, the time history length of the unsteady problem, and the time step used, are also very important and should be checked for convergence. Checks with results from a frequency domain code to ensure properly convergence for the zero speed case should be made. A good insight into the theory behind the problem is advised. It is the author's opinion, though, that this should always be the case.

The Green function employed on the solution of the first order problem is very useful in the sense that it enables us not to need to discretize the free surface, avoiding problems like the satisfaction of the dispersion relation, the time integration, and having to devise a scheme that is stable and accurate. On the other hand, trying to implement other choices of basis flow turns out to be much more complicated, since panelization of even a small part of the free surface close to the floating body will imply the evaluation of the transient Green function between two points on the free surface and this is numerically difficult, since the Green function itself will consist of an oscillatory kernel that will not decay as the wave number increases, because both the source and field points will have zero vertical coordinate. One solution for implementing other basis flows would be the use of a mixed solution, employing the Rankine Green function inside a region close to the body and matching this interior solution with an outer solution based on the transient Green function. This is similar to the solution obtained by Zhao and Faltinsen [41] [42] [43], but in this case instead of the transient Green function they used a multipole expansion inside the body.

A path that is being followed by some and that looks very promising is the use of higher order panel methods, particularly in connection with the use of splines as basis functions. Computations made by Maniar [22] showed excellent results in the

frequency domain and early results from Danmeier [5] in connection with the time domain approach are very promising. One problem though is that the centroids are replaced by control points nearer the free-surface and may require a separate filter, to ensure the correct representation of all the waves coming into the problem. This higher-order approach would enable us to more properly represent higher order derivatives of the potential, improving the computation of the boundary conditions for the second-order steady problem and giving more accurate results for this problem. Thus it can be expected that the use of higher-order panel methods in conjunction with the techniques developed in this thesis will lead to more accurate results and faster convergence rates, with a consequent decrease of the cpu time.

Appendix A

Second-Order Problem Integral Equation

We may obtain the integral equation for the second-order problem by getting the integral equation for the unsteady ship velocity case, described in the global coordinate system and after that restrict the resulting expression for the steady forward velocity in the moving reference system, or by defining the problem in the moving coordinate system, establishing the boundary value problem and, through the use of Green's identities, arrive at the final form of the integral equation. In this appendix we will follow the first path, obtaining the integral equations for the steady and unsteady problems.

A.1 The unsteady-forward-speed ship problem

The boundary value problem for the unsteady-forward-speed ship problem can be established as

$$\nabla^2 \phi(\vec{x},t) = 0 \qquad \text{in the whole fluid domain} \tag{A.1}$$

$$\tfrac{1}{g}\phi_{tt}(\vec{x},t) + \phi_z(\vec{x},t) = \mathcal{H}(\vec{x},t) \qquad \text{on } S_f(t) \tag{A.2}$$

$$\vec{n}.\nabla\phi(\vec{x},t) = \mathcal{B}(\vec{x},t) \qquad \text{on } S_b(t), \text{for} t > t_0 \tag{A.3}$$

$$\nabla\phi(\vec{x},t) \to 0 \qquad \text{on } S_\infty \text{ for finite time} \tag{A.4}$$

$$\phi(x,y,0,t_0) = 0 \tag{A.5}$$

$$\phi_t(x,y,0,t_0) = 0. \tag{A.6}$$

The Green's function $G(\vec{x},\vec{\xi};t-\tau)$ we are going to use for this problem is given by (3.1). Applying Green's second identity on $\phi_t(\vec{x};t)$, $G(\vec{x},\vec{\xi};t-\tau)$ and omitting from now on the spatial parameters x and ξ, assuming them implicitly, we will have

$$2\pi\,\phi_\tau(\tau) + \iint_{S_b(\tau)+S_f(\tau)+S_\infty} d\vec{\xi}\Big[\phi_\tau(\tau)\,G_{n_\xi}(t-\tau) - \phi_{n_\xi\tau}(\tau)\,G(t-\tau)\Big] = 0. \tag{A.7}$$

Integrating in time from $\tau = t_0$ to $\tau = t$, and also integrating by parts, we will have

$$\begin{aligned} 2\pi \int_{t_0}^{t} \phi_\tau(\tau)d\tau &+ \iint_{S_b(t)+S_f(t)} d\vec{\xi}\,\Big[\phi(t)\,G_{n_\xi}(0) - \phi_{n_\xi}(t)\,G(0)\Big] \\ &- \iint_{S_b(t_0)+S_f(t_0)} d\vec{\xi}\,\Big[\phi(t_0)\,G_{n_\xi}(t-t_0) - \phi_{n_\xi}(t_0)\,G(t-t_0)\Big] \\ - \int_{t_0}^{t} d\tau \iint_{S_b(\tau)+S_f(\tau)} d\vec{\xi}\,&\Big[\phi(\tau)\,G_{n_\xi\tau}(t-\tau) - \phi_{n_\xi}(\tau)\,G_\tau(t-\tau)\Big] = 0. \end{aligned} \tag{A.8}$$

Writing Green's second identity for $\tau = t_0$,

$$2\,\pi\,\phi(t_0) + \iint_{S_b(t_0)+S_f(t_0)} d\vec{\xi}\ \left[\phi(t_0)\,G_{n_\xi}(t-t_0) - \phi_{n_\xi}(t_0)\,G(t-t_0)\right] = 0 \qquad \text{(A.9)}$$

we see that we can take this terms out of (A.8) in order to get

$$\begin{aligned} 2\,\pi\,\phi(t) + \iint_{S_b(t)} d\vec{\xi}\ \left[\phi(t)\,G_{n_\xi}(0) - \phi_{n_\xi}(t)\,G(0)\right] + \iint_{S_f(t)} d\vec{\xi}\ \left[\phi(t)\,G_{n_\xi}(0)\right] \\ - \int_{t_0}^{t} d\tau \iint_{S_b(\tau)+S_f(\tau)} d\vec{\xi}\ \left[\phi(\tau)\,G_{n_\xi\tau}(t-\tau) - \phi_{n_\xi}(\tau)\,G_\tau(t-\tau)\right] = 0. \qquad \text{(A.10)} \end{aligned}$$

Concentrating on the last term of equation A.10, we will have

$$\mathcal{I}_{S_f 1} = -\int_{t_0}^{t} d\tau \iint_{S_f(\tau)} d\vec{\xi}\ \left[\phi(\tau)\,G_{n_\xi\tau}(t-\tau) - \phi_{n_\xi}(\tau)\,G_\tau(t-\tau)\right] = 0, \qquad \text{(A.11)}$$

applying the free-surface boundary conditions satisfied by the potential and by the green function, we will have

$$\begin{aligned} \mathcal{I}_{S_f 1} \;=\; & \frac{1}{g}\int_{t_0}^{t} d\tau \iint_{S_f(\tau)} d\vec{\xi}\ \frac{\partial}{\partial t}\left(\phi(\tau)\,G_{\tau\tau}(t-\tau) - \phi_\tau(\tau)\,G_\tau(t-\tau)\right) \\ & + \int_{t_0}^{t} d\tau \iint_{S_f(\tau)} d\vec{\xi}\ \left(\mathcal{H}(\tau)\,G_\tau(t-\tau)\right). \qquad \text{(A.12)} \end{aligned}$$

Now we will apply a two-dimensional form of the transport theorem given by

$$\frac{d}{dt}\iint_{S_f(\tau)} d\vec{\xi}\ f(\vec{\xi},t) = \iint_{S_f(\tau)} d\vec{\xi}\ \frac{\partial f(\vec{\xi},t)}{\partial t} + \int_{\Gamma(t)+\Gamma_\infty} d\vec{\xi}\ f(\vec{\xi},t)\vec{U(t)}.\vec{n}_{2D} \qquad \text{(A.13)}$$

to the first integral of expression (A.12),

$$\begin{aligned} \mathcal{I}_{S_f 2} \;=\; & \frac{1}{g}\frac{d}{dt}\int_{t_0}^{t} d\tau \iint_{S_f(\tau)} d\vec{\xi}\ \left(\phi(\tau)\,G_{\tau\tau}(t-\tau) - \phi_\tau(\tau)\,G_\tau(t-\tau)\right) \\ & -\frac{1}{g}\int_{t_0}^{t} d\tau \int_{\Gamma(\tau)} d\vec{\xi}\ \left(\phi(\tau)\,G_{\tau\tau}(t-\tau) - \phi_\tau(\tau)\,G_\tau(t-\tau)\right)\vec{U(\tau)}.\vec{n}_{2D} \end{aligned} \qquad \text{(A.14)}$$

or

$$\begin{aligned}\mathcal{I}_{S_f 2} &= \frac{1}{g}\iint_{S_f(\tau)} d\vec{\xi}\ \left(\phi(t)\, G_{\tau\tau}(0) - \phi_\tau(t)\, G_\tau(0)\right) \\ &\quad -\frac{1}{g}\iint_{S_f(\tau)} d\vec{\xi}\ \left(\phi(t_0)\, G_{\tau\tau}(t-t_0) - \phi_\tau(t_0)\, G_\tau(t-t_0)\right) \\ &\quad -\frac{1}{g}\int_{t_0}^{t} d\tau \int_{\Gamma(\tau)} d\vec{\xi}\ \left(\phi(\tau)\, G_{\tau\tau}(t-\tau) - \phi_\tau(\tau)\, G_\tau(t-\tau)\right) U(\vec{\tau}).\vec{n}_{2D}.\end{aligned} \tag{A.15}$$

Knowing that $G_\tau(0) = \phi(t_0) = \phi_\tau(t_0) = 0$, and using the boundary condition on the free-surface for $G_{\tau\tau}(0)$,

$$\begin{aligned}\mathcal{I}_{S_f 2} &= -\iint_{S_f(\tau)} d\vec{\xi}\ \left(\phi(t)\, G_{n_\xi}(0)\right) \\ &\quad -\frac{1}{g}\int_{t_0}^{t} d\tau \int_{\Gamma(\tau)} d\vec{\xi}\ \left(\phi(\tau)\, G_{\tau\tau}(t-\tau) - \phi_\tau(\tau)\, G_\tau(t-\tau)\right) U(\vec{\tau}).\vec{n}_{2D}.\end{aligned} \tag{A.16}$$

Substituting (A.16) in (A.12), and the resulting equation in (A.10) we will finally arrive at

$$\begin{aligned}&2\,\pi\,\phi(t) + \iint_{S_b(t)} d\vec{\xi}\ \left[\phi(t)\, G_{n_\xi}(0) - \phi_{n_\xi}(t)\, G(0)\right] \\ &\quad -\int_{t_0}^{t} d\tau \iint_{S_b(\tau)} d\vec{\xi}\ \left[\phi(\tau)\, G_{n_\xi\tau}(t-\tau) - \phi_{n_\xi}(\tau)\, G_\tau(t-\tau)\right] \\ &-\frac{1}{g}\int_{t_0}^{t} d\tau \int_{\Gamma(\tau)} d\vec{\xi}\ \left(\phi(\tau)\, G_{\tau\tau}(t-\tau) - \phi_\tau(\tau)\, G_\tau(t-\tau)\right) U(\vec{\tau}).\vec{n}_{2D} \\ &\quad +\int_{t_0}^{t} d\tau \iint_{S_f(\tau)} d\vec{\xi}\ \left(\mathcal{H}(\tau)\, G_\tau(t-\tau)\right) = 0,\end{aligned} \tag{A.17}$$

which represents the second-order integral equation for the forward unsteady-speed problem.

A.2 The steady-forward-velocity problem

In translating equation (A.17) from the previous arbitrary velocity case to the more particular steady velocity case, it is worthwhile to define the problem with respect to a moving coordinate system fixed with respect to the ship mean position. By doing that we will have to make the following substitutions in equation (A.17):

$$\begin{aligned}
\vec{U}(t) &= U\,\vec{i} \\
\vec{U}(t).\vec{n}_{2D} &= U n_1 \\
S_b(t) &= \overline{S}_b \\
\Gamma(t) &= \overline{\Gamma} \\
\mathcal{H}(\vec{x},t) &= \mathcal{H}(\vec{x}) \\
\frac{\partial}{\partial t} &= \frac{\partial}{\partial t} - U\frac{\partial}{\partial x},
\end{aligned} \tag{A.18}$$

so we will have

$$\begin{aligned}
&2\pi\,\phi(t) + \iint_{\overline{S}_b} d\vec{\xi}\,\left[\phi(t)\,G_{n_\xi}(0) - \phi_{n_\xi}(t)\,G(0)\right] \\
&\qquad - \int_{t_0}^{t} d\tau \iint_{\overline{S}_b} d\vec{\xi}\,\left[\phi(\tau)\,G_{n_\xi\tau}(t-\tau) - \phi_{n_\xi}(\tau)\,G_\tau(t-\tau)\right] \\
&+ U\int_{t_0}^{t} d\tau \iint_{\overline{S}_b} d\vec{\xi}\,\left[\phi(\tau)\,G_{n_\xi\xi}(t-\tau) - \phi_{n_\xi}(\tau)\,G_\xi(t-\tau)\right] \\
&-\frac{U}{g}\int_{t_0}^{t} d\tau \int_{\overline{\Gamma}} dl\,n_1\,\left[\phi(\tau)\,\left(G_{\tau\tau}(t-\tau) - 2UG_{\tau\xi}(t-\tau) + U^2G_{\xi\xi}(t-\tau)\right)\right. \\
&\left. - \left(\phi_\tau(\tau) - U\phi_\xi(\tau)\right)\,\left(G_\tau(t-\tau) - UG_\xi(t-\tau)\right)\right] \\
&\qquad + \int_{t_0}^{t} d\tau \iint_{S_f(\tau)} d\vec{\xi}\,\left(\mathcal{H}(\tau)\,G_\tau(t-\tau) - U\mathcal{H}(\tau)\,G_\xi(t-\tau)\right) = 0,
\end{aligned} \tag{A.19}$$

calling the line integral term as $I_{\overline{\Gamma}}$, we may rewrite it as

$$\begin{aligned}
I_{\overline{\Gamma}} &= -\frac{U}{g}\int_{t_0}^{t} d\tau \int_{\overline{\Gamma}} dl\,n_1\,\left[\phi(\tau)\,\left(G_{\tau\tau}(t-\tau) - UG_{\xi\tau}(t-\tau)\right)\right. \\
&\qquad \left. - G_\tau(t-\tau)\,\left(\phi_\tau(\tau) - U\phi_\xi(\tau)\right)\right] \\
&\quad -\frac{U^2}{g}\int_{t_0}^{t} d\tau \int_{\overline{\Gamma}} dl\,n_1\,\left[G_\xi(t-\tau)\,\left(\phi_\tau(\tau) - U\phi_\xi(\tau)\right)\right. \\
&\qquad \left. - \phi(\tau)\,\left(G_{\xi\tau}(t-\tau) - UG_{\xi\xi}(t-\tau)\right)\right].
\end{aligned} \tag{A.20}$$

Concentrating on the second integral of $I_{\overline{\Gamma}}$, which we are going to call $I_{\overline{\Gamma}2}$, we will use Stokes' theorem applied over the free-surface plane in order to transform this line integral into an integral over the free-surface. So we may write

$$\begin{aligned}
I_{\overline{\Gamma}2} &= -\frac{U^2}{g}\int_{t_0}^{t} d\tau \int_{\overline{\Gamma}} dl\, n_1\, [G_\xi(t-\tau)\,(\phi_\tau(\tau) - U\phi_\xi(\tau)) \\
&\qquad - \phi(\tau)\,(G_{\xi\tau}(t-\tau) - UG_{\xi\xi}(t-\tau))] \\
&= U\int_{t_0}^{t} d\tau \iint_{\overline{S}_f} d\vec{\xi}\left(\frac{-U}{g}\right)\frac{\partial}{\partial\xi}[G_\xi(t-\tau)\,(\phi_\tau(\tau) - U\phi_\xi(\tau)) \\
&\qquad - \phi(\tau)\,(G_{\xi\tau}(t-\tau) - UG_{\xi\xi}(t-\tau))] \\
&= U\int_{t_0}^{t} d\tau \iint_{\overline{S}_f} d\vec{\xi}\left(\frac{-U}{g}\right)[G_\xi(t-\tau)\,(\phi_{\xi\tau}(\tau) - U\phi_{\xi\xi}(\tau)) \\
&\qquad -\phi(\tau)\,(G_{\xi\xi\tau}(t-\tau) - UG_{\xi\xi\xi}(t-\tau)) \\
&\quad +G_{\xi\xi}(t-\tau)\,(\phi_\tau(\tau) - U\phi_\xi(\tau)) \\
&\qquad - \phi_\xi(\tau)\,(G_{\xi\tau}(t-\tau) - UG_{\xi\xi}(t-\tau))]. \qquad \text{(A.21)}
\end{aligned}$$

Using the free-surface boundary conditions for $\phi(\tau)$ and $G(t-\tau)$ in the moving coordinate system, and deriving the latter with respect to ξ, we may write

$$\frac{U^2}{g}\phi_{\xi\xi}(\tau) - \frac{U}{g}\phi_{\xi\tau}(\tau) = -\frac{1}{g}\phi_{\tau\tau}(\tau) + \frac{U}{g}\phi_{\xi\tau}(\tau) - \phi_{n_\xi}(\tau) + \mathcal{H}(\vec{x}), \qquad \text{(A.22)}$$

and

$$-\frac{U^2}{g}G_{\xi\xi\xi}(t-\tau) + \frac{U}{g}G_{\xi\xi\tau}(t-\tau) = \frac{1}{g}G_{\xi\tau\tau}(t-\tau) - \frac{U}{g}G_{\xi\xi\tau}(t-\tau) + G_{\xi n_\xi}(t-\tau). \qquad \text{(A.23)}$$

Substituting (A.22) and (A.23) in (A.21), we will get

$$
\begin{aligned}
I_{\overline{\Gamma}2} &= U\int_{t_0}^{t} d\tau \iint_{\overline{S}_f} d\vec{\xi}\left[G_{\xi}(t-\tau)\left(-\phi_{n_\xi}(\tau)+\frac{U}{g}\phi_{\xi\tau}(\tau)-\frac{1}{g}\phi_{\tau\tau}(\tau)\right)\right.\\
&\quad +\phi(\tau)\left(G_{\xi n_\xi}(t-\tau)-\frac{U}{g}G_{\xi\xi\tau}(t-\tau)+\frac{1}{g}G_{\xi\tau\tau}(t-\tau)\right)\\
&\quad \left.-\frac{U}{g}G_{\xi\xi}(t-\tau)\phi_{\tau}(\tau)+\frac{U}{g}G_{\xi\tau}(t-\tau)\phi_{\xi}(\tau)\right]\\
&\quad +U\int_{t_0}^{t} d\tau \iint_{\overline{S}_f} d\vec{\xi}\left(\mathcal{H}(\vec{x})G_{\xi n_\xi}(t-\tau)\right) \qquad \text{(A.24)}
\end{aligned}
$$

or

$$
\begin{aligned}
I_{\overline{\Gamma}2} &= U\int_{t_0}^{t} d\tau \iint_{\overline{S}_f} d\vec{\xi}\left(G_{\xi n_\xi}(t-\tau)\,\phi(\tau)-G_{\xi}(t-\tau)\,\phi_{n_\xi}(\tau)\right)\\
&\quad +U\int_{t_0}^{t} d\tau \iint_{\overline{S}_f} d\vec{\xi}\left[\frac{U}{g}(G_{\xi}(t-\tau)\phi_{\xi\tau}(\tau)+G_{\xi\tau}(t-\tau)\phi_{\xi}(\tau)\right.\\
&\quad \left.-G_{\xi\xi\tau}(t-\tau)\phi(\tau)-G_{\xi\xi}(t-\tau)\phi_{\tau}(\tau))\frac{1}{g}(G_{\xi\tau\tau}(t-\tau)\phi(\tau)-G_{\xi}(t-\tau)\phi_{\tau\tau}(\tau))\right]\\
&\quad +U\int_{t_0}^{t} d\tau \iint_{\overline{S}_f} d\vec{\xi}\left(\mathcal{H}(\vec{x})G_{\xi n_\xi}(t-\tau)\right). \qquad \text{(A.25)}
\end{aligned}
$$

Integrating the second integral in (A.25) by parts we will arrive at

$$
\begin{aligned}
I_{\overline{\Gamma}2} &= U\int_{t_0}^{t} d\tau \iint_{\overline{S}_f} d\vec{\xi}\left(G_{\xi n_\xi}(t-\tau)\,\phi(\tau)-G_{\xi}(t-\tau)\,\phi_{n_\xi}(\tau)\right)\\
&\quad +U\int_{t_0}^{t} d\tau \iint_{\overline{S}_f} d\vec{\xi}\left(\mathcal{H}(\vec{x})G_{\xi n_\xi}(t-\tau)\right)\\
&\quad +U\iint_{\overline{S}_f} d\vec{\xi}\,\frac{U}{g}(G_{\xi}(t-\tau)\phi_{\xi}(\tau)-G_{\xi\xi}(t-\tau)\phi(\tau)\\
&\quad -G_{\xi}(t-\tau)\phi_{\tau}(\tau)-G_{\xi\tau}(t-\tau)\phi(\tau))\Big|_{t_0}^{t}. \qquad \text{(A.26)}
\end{aligned}
$$

Applying the initial boundary conditions on the free-surface of null $\phi(t_0)$, $\phi_\tau(t_0)$, $G(0)$, and $G_\tau(0)$, and noting that this also implies that $G_\xi(0)$ and $G_{\xi\xi}(0)$ will be zero at this initial moment, we will be able to disregard the contribution from the last integral.

Substituting (A.26) in (A.19) and the result in (A.19), noting that applying Green's identity to $\phi(t_0)$ and $G_\xi(t-\tau)$ we will arrive at

$$\iint_{\overline{S}_b+\overline{S}_f} d\vec{\xi}\ \Big(G_{\xi n_\xi}(t-\tau)\,\phi(\tau) - G_\xi(t-\tau)\,\phi_{n_\xi}(\tau)\Big) = 0, \tag{A.27}$$

and doing the cancelations we will finally get

$$\begin{aligned}
&2\,\pi\,\phi(t) + \iint_{\overline{S}_b} d\vec{\xi}\ \Big[\phi(t)\,G_{n_\xi}(0) - \phi_{n_\xi}(t)\,G(0)\Big] \\
&\qquad - \int_{t_0}^{t} d\tau \iint_{\overline{S}_b} d\vec{\xi}\ \ \Big[\phi(\tau)\,G_{n_\xi\tau}(t-\tau) - \phi_{n_\xi}(\tau)\,G_\tau(t-\tau)\Big] \\
&-\frac{U}{g}\int_{t_0}^{t} d\tau \int_{\overline{\Gamma}} dl\, n_1\ [\phi(\tau)\ (G_{\tau\tau}(t-\tau) - UG_{\tau\xi}(t-\tau)) \\
&\quad -G_\tau(t-\tau)\,(\phi_\tau(\tau) - U\phi_\xi(\tau))] \\
&\qquad + \int_{t_0}^{t} d\tau \iint_{\overline{S}_f} d\vec{\xi}\ \ (\mathcal{H}(\tau)\,G_\tau(t-\tau)) = 0,
\end{aligned} \tag{A.28}$$

which represents our second-order integral equation, with a steady forcing function on the free-surface given by $\mathcal{H}(\tau)$.

Another way to write this integral equation is integrating by parts the $\phi(\tau)\,G_{\tau\tau}(t-\tau)$ term in the line integral to get

$$\begin{aligned}
&2\,\pi\,\phi(t) + \iint_{\overline{S}_b} d\vec{\xi}\ \Big[\phi(t)\,G_{n_\xi}(0) - \phi_{n_\xi}(t)\,G(0)\Big] \\
&\qquad - \int_{t_0}^{t} d\tau \iint_{\overline{S}_b} d\vec{\xi}\ \ \Big[\phi(\tau)\,G_{n_\xi\tau}(t-\tau) - \phi_{n_\xi}(\tau)\,G_\tau(t-\tau)\Big] \\
&+\frac{U}{g}\int_{t_0}^{t} d\tau \int_{\overline{\Gamma}} dl\, n_1\ [2\,\phi_\tau(\tau)\,G_\tau(t-\tau) + U\,(\phi(\tau)G_{\tau\xi}(t-\tau) - \phi_\xi(\tau)G_\tau(t-\tau))] \\
&\qquad + \int_{t_0}^{t} d\tau \iint_{\overline{S}_f} d\vec{\xi}\ \ (\mathcal{H}(\tau)\,G_\tau(t-\tau)) = 0,
\end{aligned} \tag{A.29}$$

A.3 The source formulation approach

An alternate way to write down the integral equation is through the use of the so-called source formulation. In the form of the integral equation used in the last section, also known as the potential formulation, we will have a distribution of sources (the Green function $G(\vec{\xi},t)$) and dipoles ($G_{n_\xi}(\vec{\xi},t)$) over the boundary surfaces. The source formulation makes use only of a distribution of sources over the problem surfaces, and this formulation can be derived from the potential formulation through the definition of an auxiliary internal problem in the case we are studying (body in a semi-infinite flow), as has been noted in Chapter 3.

As Bingham [2] showed for the first-order integral equation, we may define a potential $\phi'(\vec{x},t)$ which solves the same boundary value problem as $\phi(\vec{x},t)$, with the normal vector pointing outwards from the ship hull, and in our case assuming $\mathcal{H}(\vec{x})$ to be zero over the internal free-surface. The internal-problem integral equation will then be given as

$$\begin{aligned}
&2\,\pi\,\phi'(t) - \iint_{\overline{S}_b} d\vec{\xi}\,\left[\phi'(t)\,G_{n_\xi}(0) - \phi'_{n_\xi}(t)\,G(0)\right] \\
&\qquad + \int_{t_0}^{t} d\tau \iint_{\overline{S}_b} d\vec{\xi}\,\left[\phi'(\tau)\,G_{n_\xi\tau}(t-\tau) - \phi'_{n_\xi}(\tau)\,G_\tau(t-\tau)\right] \\
&+\frac{U}{g}\int_{t_0}^{t} d\tau \int_{\overline{\Gamma}} dl\,n_1\,\left[2\,\phi'_\tau(\tau)\,G_\tau(t-\tau) + U\left(\phi'(\tau)G_{\tau\xi}(t-\tau) - \phi'_\xi(\tau)G_\tau(t-\tau)\right)\right] \\
&= 0, \qquad \text{(A.30)}
\end{aligned}$$

Defining the "source strength" to be $\sigma(\vec{x},t) = \frac{1}{4\pi}(\phi_n - \phi'_n)$, and adding (A.29) to (A.30), we will have the source integral equation given as

$$\begin{aligned}
\phi(t) = &+ \iint_{\overline{S}_b} d\vec{\xi}\,\left[\sigma(t)\,G(0)\right] + \int_{t_0}^{t} d\tau \iint_{\overline{S}_b} d\vec{\xi}\,\left[\sigma\,G_\tau(t-\tau)\right] \\
&+\frac{U^2}{4\,\pi\,g}\int_{t_0}^{t} d\tau \int_{\overline{\Gamma}} dl\,n_1\,G_\tau(t-\tau)\,(\phi_\tau - \phi_\tau)\,. \qquad \text{(A.31)}
\end{aligned}$$

Writing the spatial derivative in a coordinate system with unit vectors tangent and normal to the hull at the waterline, we can see that only the normal component will

contribute, since $\phi = \phi'$ at all times over the hull surface, and we will have

$$\phi(t) = + \iint_{\overline{S}_b} d\vec{\xi} \; [\sigma(t)\, G(0)] + \int_{t_0}^{t} d\tau \iint_{\overline{S}_b} d\vec{\xi} \; \; [\sigma\, G_\tau(t-\tau)]$$
$$+ \frac{U^2}{4\,\pi\, g} \int_{t_0}^{t} d\tau \int_{\overline{\Gamma}} dl\, n_1^2 \; \sigma G_\tau(t-\tau). \qquad \text{(A.32)}$$

Bibliography

[1] Y. Agnon and C. C. Mei. Slow-drift motion of a two-dimensional block in beam seas. *Journal of Fluid Mechanics*, 151:279–294, 1985.

[2] H. B. Bingham. *Simulating ship motions in the time domain.* PhD thesis, Massachusetts Institute of Technology, Ocean Engineering Department, 1994.

[3] J. N. Newman C. H. Lee. *The WAMIT Manual.* MIT, Ocean Engineering Department, 1988-97.

[4] M. S. Chang. Computations of three-dimensional ship motions with forward speed. *2nd International Conference on Numerical Ship Hydrodynamics*, 1977.

[5] D. Danmeier. Body-exact simulations of multiple bodies. *TIMIT and WAMIT J.I.P. Group Meeting*, 1997.

[6] M. S. Dawson. A practical computer method for solving ship-wave problems. *2nd International Conference on Numerical Ship Hydrodynamics*, 1977.

[7] M. D. Ferreira and C. H. Lee. Computation of second-order mean wave forces and moments in multibody interaction. *Behaviour of Offshore Structures' 94*, 3, 1994.

[8] J. Grue and E. Palm. Wave radiation and wave diffraction from a submerged body in a uniform current. *Journal of Fluid Mechanics*, 151:257–278, 1985.

[9] J. Grue and E. Palm. The influence of a uniform current on slowly varying forces and displacements. *Applied Ocean Research*, 8:232–239, 1986.

[10] J. Grue and E. Palm. Mean forces on floating bodies in waves and current. *Fifth Int. Workshop on Water Waves and Floating Bodies*, 1990.

[11] J. Grue and E. Palm. The mean drift force and yaw moment on marine structures in waves and current. *Journal of Fluid Mechanics*, 250:121–242, 1993.

[12] J. N. Newman H. B. Bingham, F. T. Korsmeyer and G. E. Osborne. The simulation of ship motions. *6th Intl. Conf. on Numerical Ship Hydro.*, 1993.

[13] M. D. Haskind. Oscillation of a ship on the calm sea. *Bulletin of the Academy of Sciences of the USSR ,(translated by SNAME in 1953)*, 1:23–34, 1946.

[14] W. Thompson (Lord Kelvin). On ship waves. *Proc. Inst. Mech. Eng.*, 1887.

[15] B. King. *Time-domain analysis of ship-motions.* PhD thesis, University of Michigan, Department of naval architecture and marine engineering, 1986.

[16] Bradley King. *Time-domain analysis of wave exciting forces on ships and bodies.* PhD thesis, University of Michigan, Department of naval architecture and marine engineering, 1987.

[17] F. T. Korsmeyer. *The first- and second-order transient free-surface wave radiation problem.* PhD thesis, Massachusetts Institute of Technology, Ocean Engineering Department, 1988.

[18] F. T. Korsmeyer, C. H. Lee, J. N. Newman, and P. D. Sclavounos. The analysis of wave effects on tension leg platforms. *7th International OMAE Conference*, 1988.

[19] F. T. Korsmeyer and H. B. Binghamand J. N. Newman. The forward speed diffraction problem. *Journal of Ship Research*, 1995.

[20] C. H. Lee, J. N. Newman, M.-H. Kim, and D. K. P. Yue. The computation of second-order wave loads. *9th International OMAE Conference*, 1991.

[21] M J Lighthill. *Waves in Fluids.* Cambridge University Press, 1978.

[22] H. D. Maniar. *A three dimensional higher order panel method based on B-splines.* PhD thesis, Massachusetts Institute of Technology, Ocean Engineering Department, 1995.

[23] H. Maruo. The drift of a body floating in waves. *Journal of Ship Research*, 1960.

[24] H. Maruo. On the free surface flow around full hull forms at low froude number. *Bull. Fac. Engin.*, 16, 1980.

[25] J. H. Michell. The wave resistance of a ship. *Phil. Mag.*, 45:106–123, 1898.

[26] D. E. Nakos. *Ship wave patterns and motions by a three dimensional rankine panel method.* PhD thesis, Massachusetts Institute of Technology, Ocean Engineering Department, 1990.

[27] J. N. Newman. The drift force and moment on ships in waves. *Journal of Ship Research*, 1967.

[28] J. N. Newman. Linearized wave resistance theory. *International Seminar on Wave Resistance*, 1976.

[29] J. N. Newman. *Marine Hydrodynamics.* MIT Press, 1977.

[30] J. N. Newman. The theory of ship motions. *Advances in Applied Mechanics*, 1978.

[31] J. N. Newman. The evaluation of free-surface green functions. *Fourth International Conference on Numerical Ship Hydrodynamics*, 1985.

[32] J. N. Newman. The approximation of free-surface green functions. *Wave Asymptotics*, pages 107–135, 1992.

[33] J. N. Newman. Wave-drift damping of floating bodies. *Journal of Fluid Mechanics*, 249:241–259, 1993.

[34] J. Nossen, J. Grue, and E. Palm. Wave forces on three-dimensional floating bodies with small forward speed. *Journal of Fluid Mechanics*, 227:135–160, 1991.

[35] T. F. Ogilvie. Wave resistance: the low speed limit. *University of Michigan*, 1968.

[36] T. F. Ogilvie. Second-order hydrodynamic effects on ocean platforms. *International Workshop on Ship and Platform Motions, University of California in Berkeley*, 1983.

[37] T. F. Ogilvie and E. O. Tuck. A rational strip theory for ship motions - part 1. *University of Michigan*, 1969.

[38] J. A. Pinkster. Low frequency second order wave forces on vessels moored at sea. *Netherlands Ship Model Basin Pub n. 650*, 1980.

[39] J. V. Wehausen and E. V. Laitone. Surface waves. In S. Fluegge, editor, *Handbuch der Physik*, volume 9, pages 446–778. Springer-Verlag, Berlin, New York, 1960.

[40] G. X. Wu and R. Eatock-Taylor. The hydrdynamic force on an oscillating ship with low forward speed. *Journal of Fluid Mechanics*, 211:333–353, 1990.

[41] R. Zhao and Odd M. Faltinsen. Interaction between waves and current on a two-dimensional body in the free-surface. *Applied Ocean Research*, 1988.

[42] R. Zhao and Odd M. Faltinsen. Wave-current interaction effects on large-volume structures. *Behaviour of Offshore Structures'88*, 1988.

[43] R. Zhao and Odd M. Faltinsen. Interaction between current, waves and marine structures. *5th International Conference on Numerical Ship Hydrodynamics*, 1989.